Proceedings of the 7th Meeting of Japan CF Research Society

Edited by Hiroshi YAMADA

April 27-28, 2006

Kagoshima University, Japan

Preface

This is Proceedings of the 7th Meeting of Japan CF-Research Society, JCF7, which was held at Kagoshima University, 27-28 April 2006.

Japan CF-Research Society (JCF) was established in March 1999, with its first scientific and general assembly meeting JCF1 at Osaka, aiming at the promotion of CF researches in Japan and sending information to the world. CF researches stand for investigating new kinds of nuclear reactions which are supposed to take place in the environment of condensed matter. In 1999 to 2005, we could successfully organized JCF meetings JCF1 through JCF6, in almost every year. We started to issue the printed and electronic (via internet) versions of Proceedings of JCF meetings since JCF4.

Submitted papers to JCF7 meeting were peer-reviewed by the JCF Editorial Board (Chairman; Professor Hiroshi Yamada, Iwate University). One or two reviewers were offered to review each of submitted papers, who kindly sent back comments, questions, corrections to authors via Editorial Board. After receiving revised versions, papers were accepted to publish.

The book of Proceedings JCF7 does not necessarily contain all of presentations at the JCF7 meeting. Abstracts of all presentations are available at our web-site http://wwwcf.elc.iwate-u.ac.jp/jcf/ . The electronic version of the Proceedings is also available in the same web-site.

CF-Researches in the world is now called as Condensed Matter Nuclear Science (CMNS), since the establishment of the International Society ISCMNS (http://www.iscmns.org/). Accumulation of research efforts by researchers in the world since 1989, especially concrete results obtained in latest reports, has revealed the existence of new nuclear reactions in condensed matter, under strong linkage between nuclear physics and condensed matter physics and chemistry. Clean deuteron-related fusion with ^{4}He ash and cold transmutations of host and added metal nuclei in metal-deuterium and metal-proton systems are actual consequences of latest CMNS studies, both in experiments and theories. JCF has been keeping in touch with linkage and collaboration with ISCMNS and world researchers.

We thank you all participants of JCF7.

Hiroshi Yamada (Prof., Iwate University), Chairman of JCF Editorial Board

September 2006

CONTENTS

THEORY

ENERGY OUTPUT AND MATERIAL BALANCE DURING PLASMA ELECTROLYSIS OF WATER

K. Iizumi, S. Mitsushima, N. Kamiya and K.-I. Ota
Chemical Energy Laboratory, Yokohama National University
79-5, Tokiwadai, Hodogoya-ku, Yokohama 240-3501 JAPAN

Abstract

An accurate heat measurement is needed and difficult during plasma electrolysis, because the large input power must be recovered as the same accuracy as a conventional electrolysis. In this study, a flow calorimetric system has been developed for an accurate measurement. The energy output during plasma electrolysis was ranged from 95 to 101 % of the input power. A clear excess output energy has not been observed during plasma electrolysis with 0.3 mol dm^{-3} K_2CO_3 light water solution and 0.3 mol dm^{-3} Na_2CO_3 light water solution. The current efficiency of 0.3 mol dm^{-3} K_2CO_3 light water solution were from 98 to 107 % and that of 0.3 mol dm^{-3} Na_2CO_3 light water solution were ranged from 115 to 125 %. An excess gaseous generation beyond the Faraday's law was confirmed and the plasma might be related to the excess.

1. Introduction

The excess heat and hydrogen generation were reported during plasma electrolysis [1, 2]. However, the detail of the heat measurement wasn't clarified; hence it's hard to estimate the accuracy of the measurement. Since the input and the output energy of the plasma electrolytic is large and the output energy is the sum of latent and sensible heat, the heat and material balance must be determined carefully.

In this study, in order to obtain an accurate heat balance, we developed a flow calorimetric system using a flow cell system, and measured the energy balance during plasma electrolysis.

2. Experimental

Figure 1 is a schematic drawing of the electrolytic flow cell. The cell was composed of acrylic tubing. It had an internal diameter of 2 cm, an external diameter of 5 cm, and was about 30 cm in length. The anode was a 2 cm diameter hollow cylindrical platinum mesh (99.99% purity, 55 mesh). The cathode was a 1.5 mm diameter tungsten rod (99.95% purity). It was placed at the center of the cylindrical anode. The distance between the electrodes was 1 cm.

The electrolyte was 0.3 M (= mol dm^{-3}) or 0.3 M K_2CO_3 light water solution. The electrolyte circulated in this system, passing through a reservoir. The temperature difference between the inlet and outlet of the electrolyte was measured with Pt resistance thermometers. Hydrogen and oxygen which were generated during electrolysis were collected in a reservoir, and the rate of total gas generation was measured.

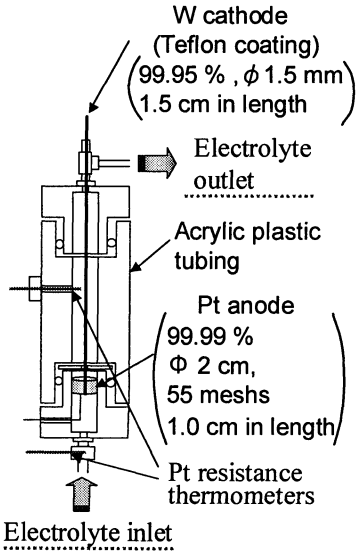

Fig. 1 Schematic drawing of a flow calorimetry cell.

Table 1 shows the experimental conditions.

The run number of h 7 ~ 11 was carried out using 0.3 M Na_2CO_3 light water solution and that of h 12 ~ 14 was performed using 0.3 M K_2CO_3 light water solution.

During electrolysis, the cell voltage and the current, the inlet and outlet temperatures of the electrolyte, room temperature, and the electrolyte flow rate were measured. The heat loss through radiation from our system was negligible, because the inlet temperature was controlled at 26 °C, which is around the room temperature, and the flow rate was controlled at 681 ~ 707 ml min^{-1} so that the outlet temperature was not exceed 5 °C above the room temperature.

The electrolysis was conducted at constant voltage. The energy balances were determined by the experimental operation times of 1 and 2 hours, respectively. The energy balances of the run number h 7 ~ h 10 and h 12 ~ 13 were measured during plasma electrolysis, and that of run number h 11 and h 14 were measured during normal electrolysis.

Table 1 Experimental conditions of energy and material balance measurements.

Run	Operation time / h	Inlet temperature of the electrolyte / °C	Flow rate / ml min^{-1}	Cell voltage / V
h 7	2	26	680	95
h 8	2	26	707	95
h 9	2	26	681	105
h 10	2	26	701	105
h 11	1	26	702	25
h 12	2	26	687	85
h 13	2	26	691	85
h 14	1	26	690	18

The input energy was determined as the product of the cell voltage and the current.

$$W_{in} = U \cdot I \qquad (1)$$

Where, W_{in}, U and I are the input energy, the cell voltage and the cell current, respectively.

The output energy was the sum of sensible and latent energy.

$$W_{out} = H_S + H_L \qquad (2)$$

Where, W_{out}, H_S and H_L represent the output energy, the sensible energy those were obtained from the temperature increase of the electrolyte and the latent energy of the H_2 and O_2 evolution, respectively.

The sensible energy was determined by the product of the electrolyte flow rate and the temperature difference between the outlet and inlet of the electrolyte.

$$H_S = v_E \cdot \Delta T \cdot d \cdot C_p \qquad (3)$$

Where, v_E, ΔT, d and C_p are the electrolyte flow rate, the temperature increase between the inlet and outlet of the electrolyte, the density of the electrolyte and heat capacity of the electrolyte, respectively.

The latent heat was determined from the flow rate of the gaseous product. The energy balances were calculated by the following equations.

$$H_L = v_g \cdot \Delta H \qquad (4)$$

Where, v_g and ΔH represented the generated gas flow rate and the enthalpy change of the water electrolysis, respectively.

Energy balance (= EB) was determined as follows;

$$EB = W_{out} / W_{in} \qquad (5)$$

The current efficiency is the gas generation amount per the theoretical amount by the Faraday's law.

$$f_{th} = n(I/F) \cdot (R \cdot T_{gas}) / (P_{air} - p_{H_2O}) \qquad (6)$$

Here, n, f_{th}, F, R, T_{gas}, P_{air} and p_{H_2O} are gas generation amount per electron, theoretical generated gas flow rate, the Faraday constant, gas constant, temperature of the H_2 and O_2 produced during electrolysis, atmospheric pressure and vapor pressure, respectively.

The current efficiency (η) was follows;

$$\eta = f_g / f_{th} \qquad (7)$$

The theoretical generated gas flow rate was determined from the Faraday's law and the ideal gas equation. The n was determined based on the composition of the generated gas with gas chromatograph. The composition was assumed to be saturated with water. The ratio of hydrogen to oxygen was 2 : 1 theoretically (discussion in 3.2).

The gaseous products were analyzed using a Gas chromatograph equipped with a TCD detector. H_2 was measured with Molecular Sieve 5A column and Ar carrier gas. O_2 was measured with Molecular sieve 5A column and He carrier gas. CO_2 was measured with Porapack Q column and He carrier gas.

3. Results and Discussion

3.1 Typical characteristics of plasma electrolysis

Figure 2 shows the cell voltage and the current at the plasma electrolysis as a function of time in 0.3 M Na_2CO_3 light water solution. In the case, the cell voltage was controlled by a step function which increased the voltage by 10 V at 30-second intervals. At the beginning, the current increased with the voltage from 20 to 80 V. After that, the current decreased with the increase of the voltage from 90 to 120 V. Plasma discharge started in this region. The bright plasma was observed above 130 V. Once bright plasma was formed, it was maintained above 90 V. Plasma discharge stopped if the voltage dropped below 90V, and the current increased from 2 to 10 A at this moment.

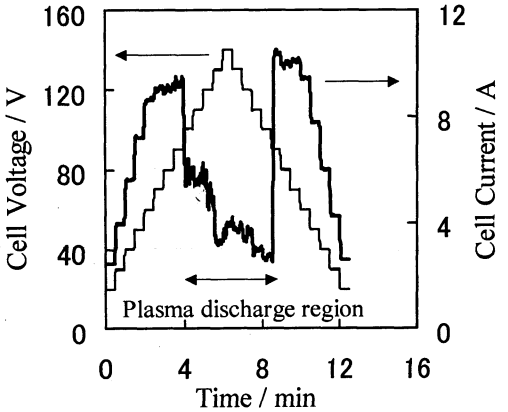

Fig. 2 Trend of input voltage and current during normal and plasma electrolysis in 0.3 M Na_2CO_3 light water solution.

Therefore, the resistance of the cell during plasma discharge was higher than that of normal electrolysis.

3.2 Energy and material balance during plasma electrolysis

Hydrogen, oxygen and trace amount of carbon dioxide were detected with gas chromatograph. The ratio of hydrogen to oxygen was 2 : 1 and the amount of carbon dioxide was below 450 ppm.

Figure 3 and 4 shows the current as a function of time during the normal and plasma electrolysis with 0.3 M Na_2CO_3 and 0.3 M K_2CO_3 light water solution, respectively. The plasma electrolysis of 0.3 M Na_2CO_3 light water solution emitted reddish violet light and that of 0.3 M K_2CO_3 light water solution emitted

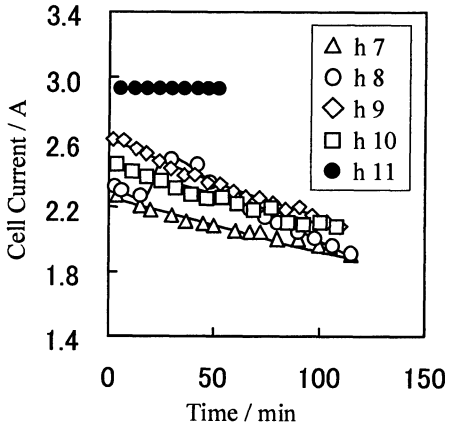

Fig. 3 Cell currents during normal and plasma electrolysis in 0.3 M Na_2CO_3 light water solution.

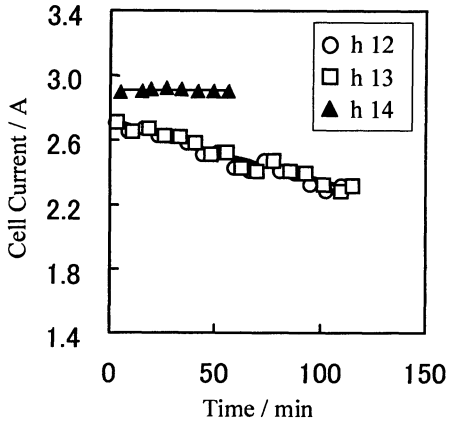

Fig. 4 Cell currents during normal and plasma electrolysis in 0.3 M K_2CO_3 light water solution.

bruise blue light. Before plasma electrolysis at 95 V, the voltage increased to 130 V with a rate of 10 V s^{-1}. After bright plasma formed, the voltage decreased to 95 V by 50 mV s^{-1}, and the measurements were started. A decrease of the current during plasma electrolysis was observed. For h 7 operation, the current was ca. 2.2 A at the beginning of the plasma electrolysis, and the current decreased to 1.9 A after 100 minutes of operation. After the plasma electrolysis, the consumption of the tungsten cathodes was observed. On the other hand, the current was constant with the constant voltage during normal electrolysis without the electrode consumption.

Figure 5 shows the photos of tungsten cathodes before and after plasma electrolysis at 95 V in 0.3 M Na_2CO_3 light water solution. The tungsten cathodes were consumed during plasma electrolysis. After a 2 h operation, the cathode decreased 1.4 mm in length and 0.23 g of the tungsten was consumed. The consumption of a cathode was large, and the electrode surface area decreased during plasma electrolysis.

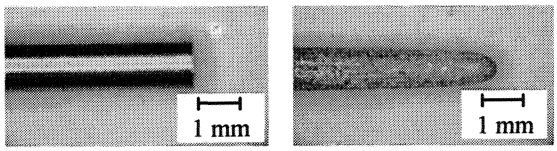

(a) Before electrolysis (b) After h 7 operation

Fig. 5 Photos of tungsten cathode before and after plasma electrolysis.
(a) Before electrolysis (b) After h 7 operation

Figure 6 and 7 show the outlet temperatures of the electrolytes during normal and plasma electrolysis with 0.3 M Na_2CO_3 and 0.3 M K_2CO_3 light water solution, respectively. The inlet temperatures were 26 °C in all cases. The outlet temperatures decreased due to the current decreases during plasma electrolysis. On the other hand, the outlet temperatures were constant due to the constant voltages and currents during normal electrolysis.

Figure 8 and 9 show the current efficiency during normal and plasma electrolysis with 0.3 M Na_2CO_3 and 0.3 M K_2CO_3 light water solution, respectively. The current efficiencies of 0.3 M Na_2CO_3 light water solution were ranged from 115 to 125 % and that of 0.3 M K_2CO_3 light

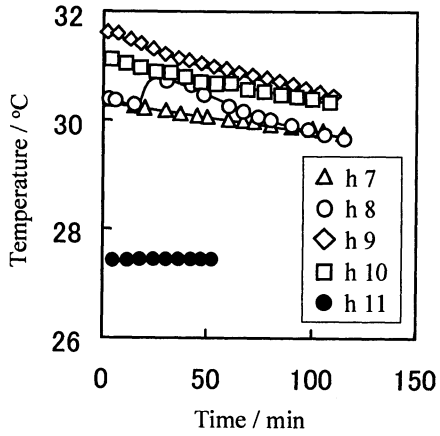

Fig. 6 Outlet temperatures of the electrolyte during normal and plasma electrolysis in 0.3 M Na_2CO_3 light water solution.

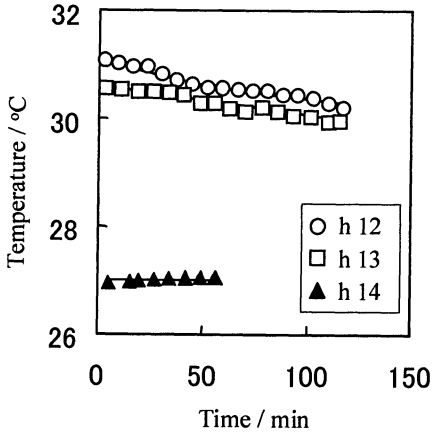

Fig. 7 Outlet temperatures of the electrolyte during normal and plasma electrolysis in 0.3 M K_2CO_3 light water solution.

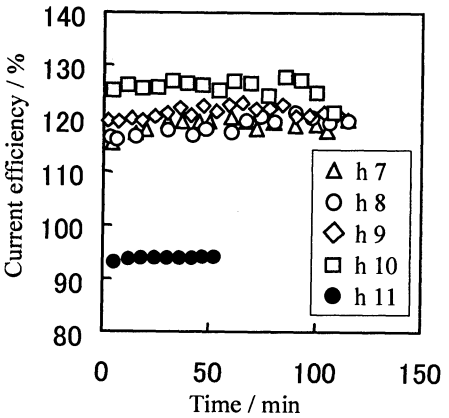

Fig. 8 Current efficiencies during normal and plasma electrolysis in 0.3 M Na_2CO_3 light water solution.

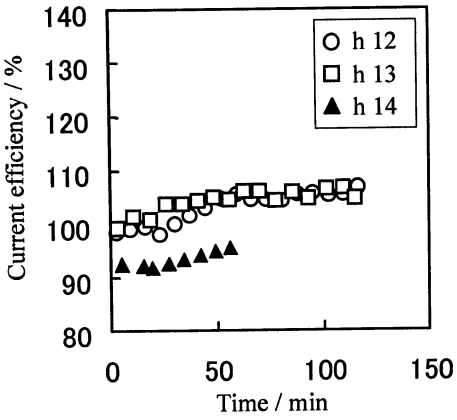

Fig. 9 Current efficiencies during normal and plasma electrolysis in 0.3 M K_2CO_3 light water solution.

water solution were from 98 to 107 % during plasma electrolysis. On the other hand, the current efficiency of 0.3 M Na_2CO_3 light water solution was from 93 to 95 % and that of 0.3 M K_2CO_3 light water solution were from 92 to 94 % during normal electrolysis. During plasma electrolysis, the amount of excess gases of 0.3 M Na_2CO_3 light water solution was larger than that of 0.3 M K_2CO_3 light water solution. No significant difference between the current efficiency of 0.3 M Na_2CO_3 light water solution and 0.3 M K_2CO_3 light water solution.

The excess gas generation could not be explained by the Faraday's law. Therefore, the excess gas might be generated by the plasma process.

Figure 10 and 11 show the energy balances during normal and plasma electrolysis. The energy balances of the plasma electrolysis were

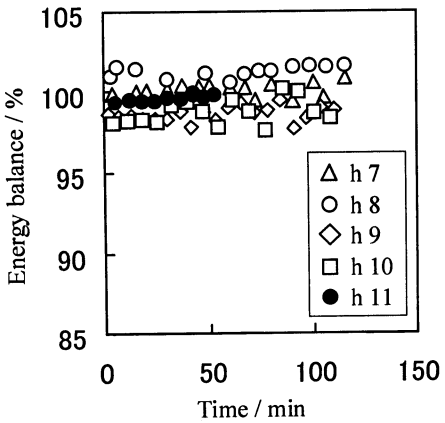

Fig. 10 Energy balances during normal and plasma electrolysis in 0.3 M Na_2CO_3 light water solution.

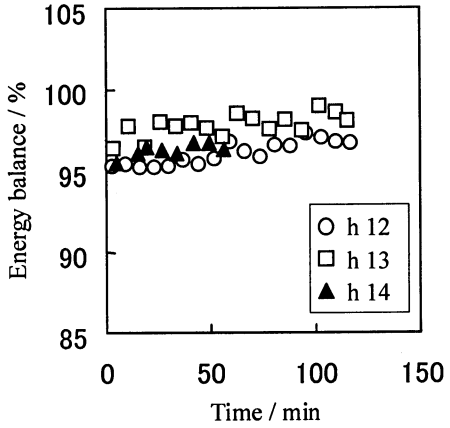

Fig. 11 Energy balances during normal and plasma electrolysis in 0.3 M K_2CO_3 light water solution.

ranged from 95 to 101 % and that of the normal electrolysis were from 95 to 99 %. No significant difference between the energy balance of plasma electrolysis and that of normal electrolysis was observed. Also, a clear excess was not confirmed in both cases.

4. Conclusions

The energy balance during plasma electrolysis was from 95 to 101 %. Clear excess energy could not be detected. The current efficiency of 0.3 mol dm^{-3} K_2CO_3 light water solution were from 98 to 107 % and that of 0.3 mol dm^{-3} Na_2CO_3 light water solution were from 115 to 125 % during plasma electrolysis. An excess gases generation beyond the Faraday's law was confirmed and it might be due to a plasma reaction. During plasma electrolysis, the amount of excess gases of 0.3 mol dm^{-3} Na_2CO_3 light water solution was larger than that of 0.3 mol dm^{-3} K_2CO_3 light water solution. Therefore, the excess gases would have a connection with the type of the electrolyte. A gaseous generation reaction other than the electrochemical process took place during the plasma electrolysis, and generated excess gas.

Reference

1) T. Mizuno, T. Ohmori, T. Akimoto, A. Takahashi, *Jpn J. Appl. Phys.*, **39**, 6055 (2000)

2) T. Mizuno, T. Akimoto, K. Azumi, T. Ohmori, *Jpn J. Appl. Phys.*, **44**, 396 (2005)

Microscopic structural change of Pd during repeated cathodic and anodic electrolysis in glycerin and phosphoric acid

Hiroo Numata [1†] and Masanobu Ban [2] † e-mail: numata.h.aa@m.titech.ac.jp
1 Tokyo Institute of Technology, 2-12-1, O-okayama, Meguro Tokyo 152-8552 Japan
2 Tokyo Metropolitan Leather Technology Center, 3-13-14, Higashi Sumida, Sumida Tokyo 131-0042 Japan

Abstract: Electrochemical hydrogen evolution reaction for well annealed Pd rod (2.0 mm ϕ) in glycerin and phosphoric acid was performed. The physico-chemical properties of hydrogen dissolved in Pd have been studied by *in situ* potentiometric, resistance and dilatometric measurements of repeated hydrogen absorption/desorption electrolysis ($x<0.02$).
During the B applied pulse mode ($x<0.02$) the resistance increased with an increase in the H/Pd ratio and the electrode potentials of the 1st through 4th absorption cycles exhibited Nernstian behavior. For all the cycles except the 1st one, an induction period for the dilation appeared accompanying by a fluctuation, which is attributed to the disorder-order transformation followed by the abrupt ß phase precipitation.

Keywords: electrolytic hydrogen absorption, Pd, phase transition, resistance, dilation, electrode potential

Introduction

Fleischmann and Pons[1)] and Jones et al. [2)] reported the possibility of cold fusion during electrolytic loading of deuterium in Pd at ambient temperatures. They suggested[1-2)] that cold fusion is caused by the absorption of deuterium in a Pd electrode. One of the reasons for this phenomenon might be a nuclear fusion reaction brought about by the dissolution of deuterium within a solid by means of high pressure. However in an equilibrium state, the pressure is no greater than that of several tens atm, and is not sufficient for this case. There has been remained unsolved yet as to what takes place in a non-equilibrium state, e.g., crack and void formations from which miscellaneous phenomena accompanied with cold fusion reaction might originate. It has been shown that prolonged discharge of deuterium on a Pd electrode gave heavily worked features[3-5)], which are different from that obtained in a single absorption run. Since repeated hydrogen absorption followed by desorption (essentially same as deuterium case) might result in an accumulation of the mechanical stress generating miscellaneous structural defects, *in situ* measurements of the electrode potential, dilation and resistance under well controlled hydrogen absorption are of interest in order to evaluate the influence of absorption/desorption cycles on the solid-state properties of Pd.

In this study, the electrochemical behavior, the dilation and resistance of a Pd electrode have been measured *in situ* using a computer-controlled potentiostat connected to the measurement devices. These measurements were made with respect to the microstructure changes induced by hydrogen ingress in a Pd electrode.

Experimental

The absorption and desorption of hydrogen in a Pd electrode (2.0 mm ϕ, 50 mm in length, purity 99.95%) were performed by applying galvanostatic cathodic and anodic pulsed currents at low current densities, $< 2\times10^{-3}$ Acm^{-2}. As received Pd rods were annealed at 800°C for 3h under a flow of helium. After heat treatment the surface of the rods was polished with emery paper upto # 1000 and stored in a desiccator. Before being used annealed samples were maintained in *vacuo* at 300°C overnight to eliminate the influence of residual hydrogen on the measurements. The experiments of *in situ* potentiometric, resistance and dilatometric measurements were performed using a modified three-electrode cell described previously[6-9)]. The electrolyte was composed of glycerin and phosphoric (2:1 in volume ratio). Kirchheim[10)] reported that out-diffusion of hydrogen during electrolysis is very slow when a solution with high viscosity is used, and the hydrogen once, dissolved within the metal, is unlikely to be evolved. The electrolyte was placed in an electrolytic cell with a sintered glass bubbler,

through which dry nitrogen was bubbled for several hours for deoxygenation. A nitrogen atmosphere was maintained by flowing dry nitrogen over the upper side of the solution during measurements. The temperature was kept constant at 40±0.5 °C using a liquid bath.

Electrolysis was performed using the B applied pulse mode of galvanostatic trained pulsed currents as shown in Fig.1. In the B applied pulse mode electrolysis continuous cyclic absorption and desorption (until the 9th cycle) was performed. The saturation of hydrogen is easily detected by the time independent potential, if the potential of the Pd electrode is adopted as an appropriate monitor of the hydrogen concentration. In the B applied pulse mode, desorption was conducted, by supplying a set of inverse anodic pulsed currents with an equivalent coulomb of absorption.

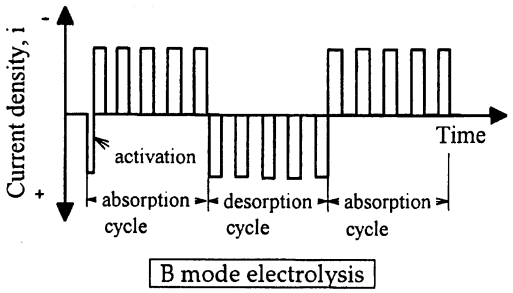

Fig.1 B applied pulse mode patterns of current density-time.

Results and Discussion

1 *In situ* potentiometric, resistance and dilatometric measurements of Pd under the B applied pulse mode

1.1 Hydrogen evolution reaction and absorption in Pd

The hydrogen evolution reaction (HER) on Pd in an acidic solution takes place through the Volmer reaction followed by the Heyrovsky one [Eq.(2)-Eq.(3)] or the Volmer reaction followed by the Tafel one [Eq.(2)- Eq.(4)]:

$2H^+ + 2e^- = H_2$ Total reaction (1)

$H^+ + e^- = H_{ad}$ Volmer reaction (2)

$H_{ad} + H^+ + e^- = H_2$ Heyrovsky reaction (3)

$H_{ad} + H_{ad} = H_2$ Tafel reaction (4)

$H_{ad} \rightarrow H_{ab}$ Ingress (5)

where H_{ad} and H_{ab} denote hydrogen adsorbed on and absorbed in an electrode. From the Tafel slopes obtained by the current interruption method the rate determining step of the HER is the Tafel step Eq.(4) in these experimental conditions[6].

In parallel with the consumption of the adsorbed hydrogen through the recombination reaction (Eq.(3) or Eq.(4)) the adsorbed hydrogen fills interstitial sites forming the α single phase. The electrode potential E of Eq.(1) for Pd is given by the Nernst equation as

$$E = E^\circ - 2.3RT/F \log a_{Had} - 2.3RT/F(pH) \quad (6)$$

$$E = E^\circ - 2.3RT/F \log a_{Had} - 0.248 \quad (7)$$

where a_{Had} is the activity of reduced adsorbed hydrogen on Pd and the other symbols have their usual meanings. For the α single phase (H randomly distributed in octahedral sites) the adsorbed hydrogen equilibrates with that in an electrode, and accordingly, the Nernst equation can be rewritten as

$$E = E^\circ - 2.3RT/F \log a_{Hab} - 0.248 \quad (8)$$

where a_{Hab} represents the activity of hydrogen in a Pd electrode. Thus, the electrode potential E subjected to hydrogen absorption responds to the change of the hydrogen activity in an electrode, where the hydrogen activity can be readily replaced by the hydrogen concentration as long as the concentration is small enough. In the study of EMF of hydrogen on various metals the hydrogen concentration has been determined by the total amount of charges during time of electrolysis assuming that hydrogen is uniformly distributed throughout a specimen. The hydrogen concentration can be conveniently expressed as x: H/Pd (moral ratio) where the absorption efficiency of adsorbed hydrogen is given as 100% for $x < 0.55$ (at 40°C) and almost 80% for $x > 0.6$. On the other hand, when the current density is small, ingress of the adsorbed hydrogen atoms, which are given by Eq. (5), is faster than that of the Tafel reaction (Eq. (4)) and hydrogen loading is performed with a current density of 100 %[11-13].

Figure 2 shows electrode potential E-x isotherm for Pd-H system at 40°C. For $x \leqq 0.01$ it obeys the Nernst equation Eq.(8) showing a straight line with a slope of –2.3RT/F, denoted as α phase, while it exhibits the plateau with the two-phase coexistence region of α and β phases. The observed values of the onset (α_{max}) and the end (β_{min}) concentrations of the two-phase region, and the plateau pressure converted from the two-phase coexistence potential measured (Eq.(11)) are consistent with those obtained from the p_{H2} - x isotherm for Pd-H system obtained by gas equilibrium method. Nevertheless the electrochemical loading can readily attain the desired H/Pd ratio due to a strong gradient of hydrogen concentration, the agreements with these

experimental results obtained by two different methods were quite well. It adds weight to the observation that the average values give the results consistent with a system having a uniform composition between the surface and the bulk. Yet this situation is valid only when the loading was performed in a single absorption.

1.2 Thermodynamics of phase transition of Pd-H system

The chemical potential of hydrogen dissolved among interstices, which is in equilibrium with gaseous hydrogen, can be expressed as[14-15]

$$\mu_H = \mu^\circ_H + RT \ln(r/\beta - r) + \Delta\mu_H \quad (9)$$

where μ°_H is the chemical potential of hydrogen at infinite dilute, r is the fraction of interstices occupied in the f.c.c. structure, β is the number of interstices per metal atom, the second term on the right hand is the configulational term for ideal statistic distribution of the hydrogen atoms among the octahedral sites (r = x, β = 1 for f.c.c. metal), and $\Delta\mu_H$ stands for the deviations from ideal solution behavior. Neglecting the contribution of the electronic property of solute atoms the excess term $\Delta\mu_H$ can be given as

$$\Delta\mu_H = W_I r + W_C r \quad (10)$$

where W_I is a term accounting for the long range attractive H-H interaction (minus sign), and W_C is the constraint energy term. The last term W_C is applied for the specimen constrained by the substrate layer during the phase separation. Both W_I and W_C depend linearly on the concentration[16].

In the frame work of statistic thermodynamics hydrogen in metals can be considered as a lattice gas, which behaves like gaseous atoms residing among non-inoculate host atoms. The 4 typical phase diagrams were predicted on the basis of the gas/liquid transition of a lattice gas, analogous to the van del Waals isotherms of a gas[17]. Figure 3 shows one schematic phase diagram among those ones on μ-ρ plot, where the ρ of an individual phase is equivalent to the concentration of binary alloy systems. This figure resembles that experimentally obtained (Fig. 2) for the same system in the topological features.

As aforementioned the electrode potential E of dissolved hydrogen in equilibrium with hydrogen gas obeys the Nernst equation Eq.(8), and inversely the hydrogen pressure pH_2 in equilibrium with that hydrogen in an electrode can be calculated from the electrode potential under limited conditions[6, 18]:

$$pH_2 = \exp[-(E + E_{SCE})(2F/RT)] \quad (11)$$

where E_{SCE} is the potential of the reference electrode. For example, the equivalent hydrogen pressure pH_2

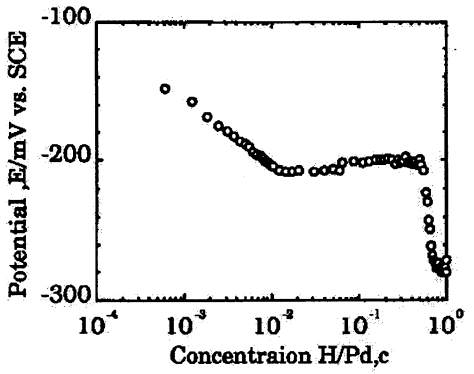

Fig.2 Electrode potential E – x isotherm at 40°C for hydrogen absorption in a Pd electrode.

of the two-phase coexistence, 0.05×10^5 Pa, coincides with that obtained from Pd-H isotherm at 40°C. Furthermore, a quantitative comparison of the characteristic values, e.g., solvus concentrations with the two-phase coexistence region exhibited quite well agreements with those obtained from gas equilibrium method. They reveal that the electrode potential of hydrogen loaded is thermodynamically equivalent to a hydrogen chemical potential with Pd-H isotherm. From the above consideration the electrode potential of hydrogen in Pd can be converted from the proposed chemical potential of hydrogen in Pd (Eq.(9)) where the change of the electrode potential can be calculated from the equation; $E = -\Delta\mu_H / nF$:

$$E = E^\circ + RT/nF \ln(r/1-r) + W_I r/nF + W_C r/nF \quad (12)$$

Since the contribution due to the non-ideal solution on the experimental electrode potential is well defined as the 3rd and 4th terms on the right hand in Eq.(12), more fundamental understanding can be provided in the following sections. Actually, the electrode potential measurement is useful for an evaluation of the non-ideal solution term but an appropriate experimental approach is lacking. In this study the non-ideal solution term of Eqs.(10,

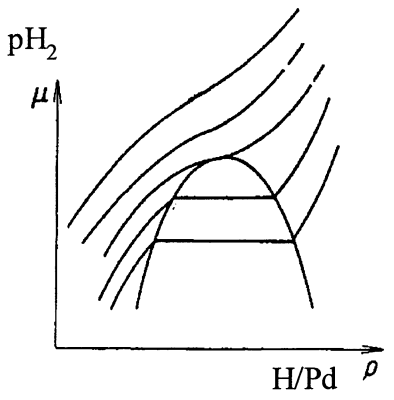

Fig.3 Schematic diagram of the phase diagram for H in Pd.

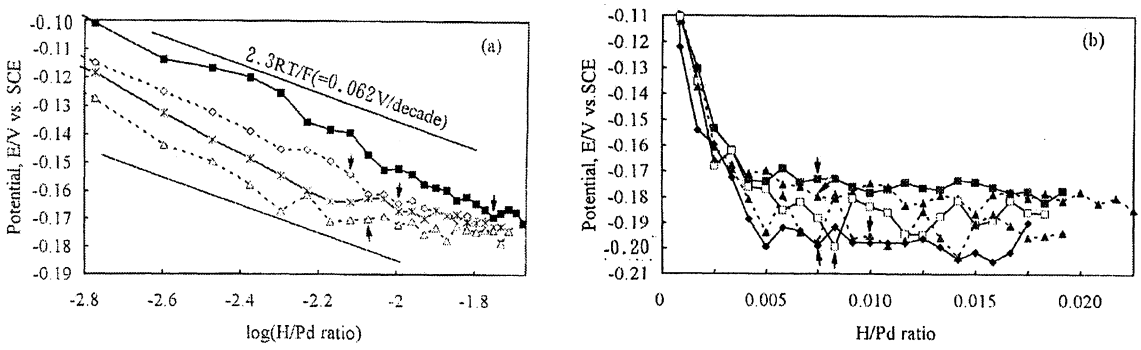

Fig.4 (a) and (b) Effect of number of cycles on B applied pulse mode potential vs. H/Pd ratio(Absorption, x<0.02).

(a) Cycle number 1st-4th, 1st(—■—), 2nd(···○···), 3rd(—✳—), 4th(···△···)

(b) Cycle number 5th-9th, 5th(—■—), 6th(···▲···), 7th(—□—), 8th(···▲···), 9th(—◆—)

12) is first evaluated by analyzing the electrode potentials experimentally obtained.

1.3 Elastic interaction between Pd and absorbed hydrogen

It is known that interaction between dissolved atoms and surrounding materials often bring about lattice strain in materials. This lattice strain introduced by hydrogen doping causes the miscibility gap of the phase transition (spinodal phase separation) and the leaning plateau region in Pd-H isotherm[17]. The molar volume of hydrogen in the metal is given by the following relation[19],

$$V_H = 3V_M\ [d(\Delta l/l_0)/dx] \qquad (13)$$

where V_M and V_H are the molar volumes of the metal and the hydrogen in the metal.

By measuring the slope of the dilation vs. H/Pd ratio, the molar volume of hydrogen in a material can be obtained. Plots of the dilation vs. H/Pd ratio in the α phase are shown in Fig.8 (a), which were measured simultaneously with the case shown in Figs.4 and 8. The dilation is almost in proportion to the increase of H/Pd, and using Eq.(13), the partial molar volume of hydrogen is obtained as V = 1.64cm^{3}mol^{-1} with the supposition that V_{Pd} = 8.87cm^{3}mol^{-1}. The result agrees with values from the literature V_{Pd} = 1.77~1.06cm^{3}mol^{-1} [20].

2 Repeated absorption and desorption of hydrogen in Pd (x<0.02) under the B applied pulse mode

2.1 Effect of absorption and desorption cycles on potential behavior under the B applied pulse mode

For a single absorption, the A applied pulse mode (see Ref.6-9), the potential, resistance and dilation exhibited a well-defined absorption behavior in the single α phase and the resulting phase transition (α → β) within the α + β coexistence region. Repeated absorption and desorption of hydrogen was performed in the B applied pulse mode (x<0.02), where the H/Pd ratio was controlled upto the onset of the (α → β) transition: α_{max}. In this case the hydrogen absorption/desorption cycles were not expected to have any influence; heavy deterioration, on the mechanical properties, because no appreciable (α → β) phase transition occurs.

Figure 4(a) shows that the potential changes as a function of log(H/Pd ratio) during absorption for the 1st through the 4th cycles obey the Nernst equation whose straight lines of a slope -0.062V/decade is plotted as E vs. log(H/Pd). At x >0.01 (log(H/Pd ratio) = -2) these potential changes exhibit roughly straight horizontal lines, although the H/Pd ratios of α_{max} are ambiguous because the irregular potential fluctuations are superimposed on the Nernstian straight line. Moreover, the potential changes as a function of log(H/Pd ratio) shift toward more negative potentials in parallel to the Nernstian straight line (solid lines in Fig.4(a)) as the cycle number increased.

This negative potential shifts during the 1st through 4th cycles can be allocated to the non-ideal terms in Eq.(12) providing that the electrode potential given by Eq.(12) is equivalent to the chemical potential of hydrogen in Pd. Then, there might be negligible disagreement with gaseous hydrogen either in a gas chamber or adsorbed as gaseous molecules on a Pd electrode. In this study, the work due to attractive H-H interaction (minus sign) and that varied by repeated absorption/desorption cycles are evaluated. The interaction energy of H-H W_I in various metal-H systems is calculated based on the mean field approximation[17]. The result shows that the calculated values W_I are in good agreement with those experimentally obtained by the several different methods. Moreover, the phase boundary of (α + α') coexistence; spinodal phase separation in

Nb-H system was fully predicted by the theory of the elastic interaction where an isotropic dipole tensor and lattice compressibility were given[21]. Thus, the values W_I experimentally and theoretically obtained are ranging from 0.19 to 0.25 eV[17, 21]. This interaction energy multiplied by x, i.e., $(W_I)(x)$ is further calculated into E resulting in an order of several mV, $1.90\text{-}2.50\times10^{-3}$V. As a result the deviation of the measured potential due to H-H interaction is evaluated negligible small.

Hence, the major contribution to the non-ideal solution term is the constraint energy term W_C. The hydrogen loading/unloading study for Nb/Pd multi-layer revealed that the W_C term is estimated 65 kJ/mol associated with the stress due to constrained Nb film elasticity by the Pd substrate layer[16]. The model of the Nb/Pd multi-layer indicated that the outer Nb layer expanded and contradicted in bi-axial mode constrained by the substrate on loading/unloading, where the substrate Pd layer stayed unloaded until the Nb layers were saturated. From the fact that the loading behaviors of the multi-layer is very close to this system subjected to the trained pulsed electrochemical charging/discharging the schematic model; the discriminated sub-surface layer and the remaining bulk of the rod Pd; analogous to the multi-layer structure, the outer Nb layer and the substrate correspond to the sub-surface layer and the bulk, respectively, has been proposed.(Fig.7) Therefore, the term of the non-ideal solution corresponds to the constraint energy W_C , that is, the work due to the stress of the sub-surface layer constrained by the bulk, imposed by the hydrogen absorption/desorption cycles.

Figure 5 shows constraint energy W_C and the potential deviation from that of the extrapolated Nernst equation, (the non-ideal term W_I r/nF + W_C r/nF = 0), vs. cycle number, where the values were determined at x 0.00675. For x « 0.01 the term W_Cr/nF should appear negligible small, while at x > 0.01 the potential exhibits the (α +β) coexistence phase. With the exception of high W_C values it tends to decrease with an increase of the cycle number, which leads to the following experimental explanation. Since the stress of the sub-surface layer is imposed by the constraint of the bulk on the absorption/desorption cycles, and accordingly, the values W_C exhibits the dependence on the cycle number, the compression stress of the sub-surface layer develop until the 4th cycle in this system. This conclusion is consistent with the experimental observation shown in the next section. In this case the relaxation of the stress developed during the

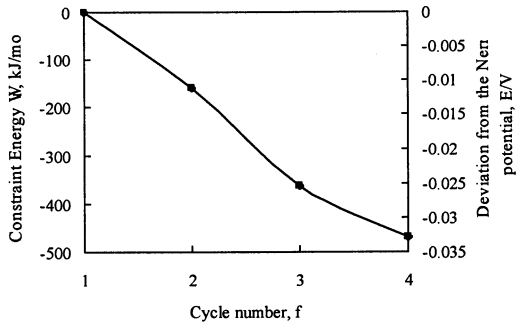

Fig.5 Effect of number of cycles on constraint energy W_I and the deviation from the Nernst potential.

sample preparation is disregarded because of the samples well annealed.

The potential changes as a function of H/Pd ratio (note the H/Pd ratio as linear scale) for the 5th through the 9th cycles are shown in Fig.4 (b). The potentials decrease linearly with an increase of the H/Pd ratio at x<0.005 and take constant values corresponding to the two-phase coexistence region. In the early stage of absorption the appearance of the potential proportionality to the H/Pd ratio is associated with the non-ideal solution terms of hydrogen interaction, as is seen in Eq.(12), along with the invariant compression stress, thus they reasonably seemed to become independent as the cycle number increases. At x > 0.005 the potential changes as a function of H/Pd ratio show flatten straight portions, whose values tend to decrease accompanying the potential fluctuations. This is explained by the gradual increase in the equivalent hydrogen pressure corresponding to the two-phase coexistence region. There have been also observed an evolution of the potential fluctuations accompanied with the increased equivalent hydrogen pressure of the two-phase coexistence region.

A large number of absorption cycles at even low concentrations indicates that the hydrogen ingress occurs through the sub-surface layer containing the formerly formed phases, and hence the coexistence region was attained at a relatively low H/Pd ratio compared with that of the A applied pulse mode. An evolution of the axial compression stress during absorption-desorption cycles or the prolonged discharge of hydrogen was reported[8, 22], which have shown that a rectangular foil became a spherical shape due to contractions in the width and length and an increase in the thickness. In Figs.4 (a) and (b) the arrows indicate the H/Pd ratios corresponding to the on-set of the dilation, whose values change to lower H/Pd ratios for the 2nd

through the 9th cycles. Thus, the on-set of the (α → β) phase transition proceeds at a much smaller H/Pd ratio than that of the 1st run. The potential change exhibiting Nernstian behavior is associated with an evolution of the compression stress, however the resistance ratio R/Ro as a function of H/Pd ratio showed no dependence on the cycle number, as shown in the next section. This inconsistency of two *in situ* measured values is explained taking into account hydrogen absorption in the sub-surface layer. Kandasamy et al.[23] reported that there has been remained hydrogen trapped in the sub-surface layer even after annealing at 1100 °C. Hence, these consecutive potential shifts are attributed to the progressively enhanced compression stress of the sub-surface layer, which subsequently diminished after a few absorption/desorption cycles. It should be noted that the resistance change as a function of H/Pd ratio was independent on the cycle number because it predominantly responds not to surface but to bulk volume.

Figure 6 shows plots of the potential changes as a function of H/Pd ratio during desorption subsequent to absorption, where desorption was conducted by applying anodic pulsed currents. The potentials of the 1st and 2nd cycles tend to depart from the coexistence region exhibiting ca. -0.17V at relatively low H/Pd ratios and stay at 0.025V corresponding to the fully desorbed phase. The charge required to reach the β phase was ca. 0.005 in H/Pd ratio for the 1st and 2nd, and 0.0075~0.009 for the 3rd through the 9th cycles. The potentials for the 3rd through the 9th cycles hold the coexistence region at -0.17V and then increase to 0.025V corresponding to the fully desorbed phase, less dependently on cycle number.

This first recovery of the potentials for the 1st and 2nd cycles is consistent with not large enough dilation during the H/Pd ratio increases, which suggests the primary stage of the sub-surface layer development during absorption. Thus, the incomplete sub-surface layer somewhat retards the dilation changes during absorption and also makes desorption proceed easily. In other words, the sub-surface layer behavior does not respond directly to the bulk one (the core side volume compared to the surface shown in Fig.7), which might be termed a "dashpot effect". Figure 7 shows the schematic of the sub-surface layer and remaining bulk of a rod Pd where the former is preferentially subjected to heavy strain under the increased compression stresses during the early stage of absorption/desorption cycles. Further apparent and consistent explanation with respect to Dashpot effect,

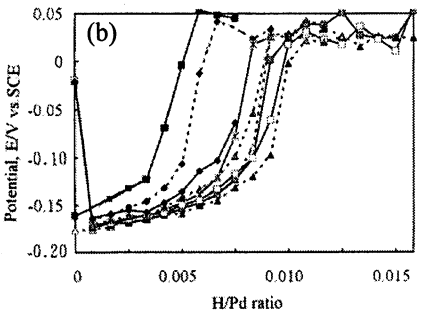

1st(—■—), 2nd(·✦··), 3rd(—✕—), 4th(·△··), 5th(—●—), 6th(·▲··), 7th(—□—), 8th(·▲··), 9th(—◆—)

Fig.6 Effect of number of cycles on B applied pulse mode potential vs. H/Pd ratio(Desorption, x<0.02).

i.e., the sub-surface layer elasticity constrained by the bulk, related with the induction period of the dilation will be presented in the next issue.

It is of significant to note that the anodic pulsed current facilitates the recovery of the fully desorbed phase, occasionally accompanied with a non-equilibrium process, e.g., the sub-surface layer formation.

2.2 Effect of absorption and desorption cycles on dilation behavior under the B applied pulse mode

The dilation changes as a function of H/Pd ratio during absorption are shown in Fig.8 (a), where the slopes of the dilation vs. H/Pd ratio for the 1st through the 3rd cycles increase progressively; most of the slopes after the 4th cycle tend to converge into one line close to the solid line indicating the first absorption under the A applied pulse mode.

For all the cycles during absorption except the 1st, an induction period for the dilation appeared, whereupon the α single phase might exist. Everret et al.[24] have studied the hydrogen absorption-desorption process of Pd blacks, where evolutions of the α and β phases were identified by

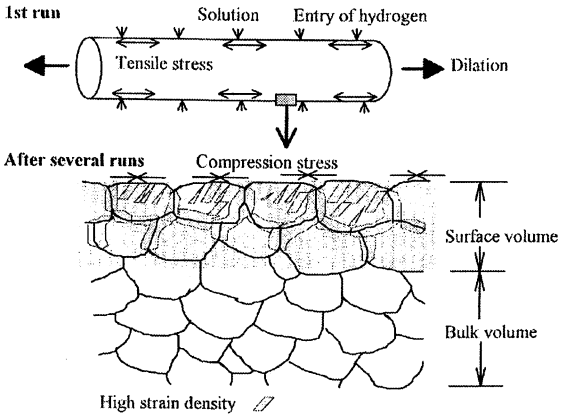

Fig.7 Schematic of the discrimination of surface and bulk volumes and state of surface stress during hydrogen absorption and desorption cycles.

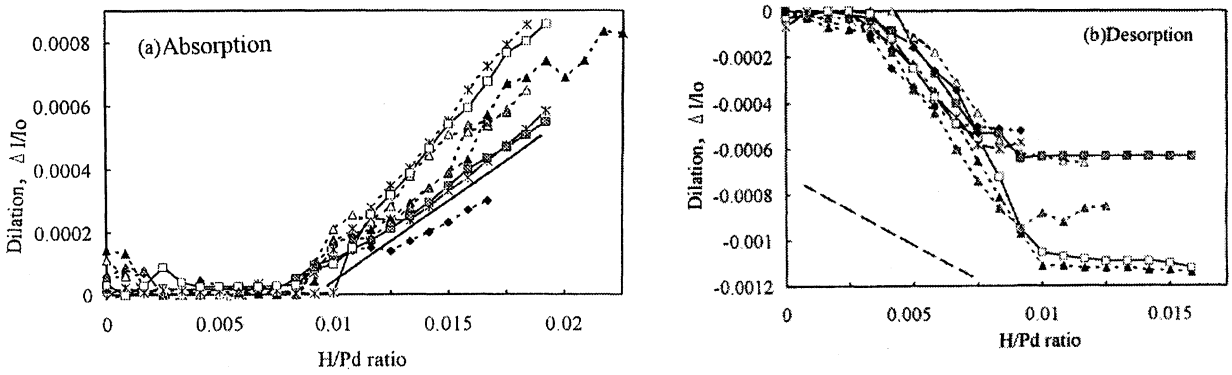

(a)Absorption (b) Desorption 2nd(··◆··), 3rd(—×—), 4th(·☆·), 5th(—■—), 6th(·▲··), 7th(—□—), 8th(·▲··), 9th(—●—)

Fig.8 (a) and (b) Effect of number of cycles on B applied pulse mode dilation vs. H/Pd ratio(x<0.02).

XRD peak ratios of the α and the β phases along with equilibrium hydrogen pressure measurement. They observed that during absorption the peak intensity of the α phase once diminished at a considerably lower pressure than that of the α + β coexistence region followed by an abrupt increase of the α phase intensity. This non-equilibrium phenomenon was explained by introducing the transition of the order-disorder α phase and the progressive spreading of strain volume: α phase with hydrogens orderly distributed.

In our study an induction period can be seen such that the dilation did not occur even though the resistance ratio steadily increased, which means that the average H/Pd ratio continues to increase, whereas at a certain H/Pd ratio well defined dilation occurred. Until x = 0.005~0.008 the transformation of the α disordered phase to the ordered phase proceeds accompanying strain volume, and then the β phase precipitation occurred concurrently with random hydrogen absorption in the remaining α phase.

Thus, the process of hydrogen absorption in the remaining α phase gives rise to the dilation subsequent to an induction period. Additionally it is shown that the formation of non-equilibrium α phase was saturated at ca. 80% (corresponding to x = 0.008) in volume percent.

The slopes of the dilation vs. H/Pd ratios are almost consistent with that obtained by the first A applied pulse mode (see solid line in Fig.8(a)), although the dilation curves during absorption exhibit somewhat modulated one with a fluctuation. Inspecting these curves and taking into account the uncertainty in the experiment, it is reasonable to assume that the dilation (Δl/lo) is comprised of a linear term in the lattice expansion and a constant term as follows,

$$\Delta l/lo = a\,x + b \qquad (14)$$

where the first term on the right hand corresponds to the change of dilation due to lattice expansion and the second term is attributable to sporadic dilation (discontinuous to H/Pd ratio and time). The latter is also observed under work hardening on a single crystal. Although it is questionable that a Pd rod under repeated absorption and desorption behaves like a heavily strained crystal, we often observe such sporadic and stepwise dilation under electrochemical loading.

Meanwhile the dilation changes as a function of H/Pd ratio during desorption (see Fig.8(b)) show approximately reverse behavior; the short non-contradiction period and the steady decrease in dilation. At the α + β coexistence potential -0.17V the β phase transfers to the ordered α phase, simultaneously converts to the disordered one (diminishing of strain volume), and the desorption of the α phase proceeds smoothly along with a decrease in dilation. It is inferred that the formation and decomposition of the ordered α phase and hence strain volume are representative not of the electrode potential and resistance but to the dilation, based on the implicit idea that the dilation exhibits the 1:1 correlation to the hydrogen absorption-desorption cycles only when the phase of the bulk (not the sub-surface layer) absorbs hydrogen randomly.

2.3 Effect of absorption and desorption cycles on resistance behavior under the B applied pulse mode

Figures 9 (a) and (b) show plots of the resistance ratio changes as a function of H/Pd ratio during absorption and desorption, where both an increase and decrease in the resistance are proportional to the H/Pd ratio; the effect of the cycle number lies within a maximum experimental uncertainty. In Fig.9(b) the resistance curves as a function of H/Pd ratio are almost straight lines with the same slope and progressively shift toward higher H/Pd ratios. However, these straight lines do not seem to vary systematically with cycle number. Since the resistance ratio follows the last cathodic

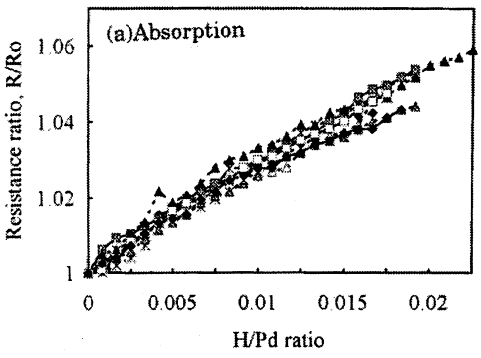

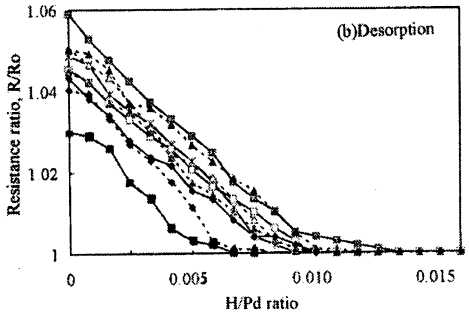

(a) Absorption 2nd(- ◆-), 3rd(—×—), 4th(- △-), 5th(—■—), 6th(- ▲-), 7th(—□—), 8th(- ▲-), 9th(—●—)
(b) Desorption 1st (—□—), 2nd(- ◆-), 3rd(—×—), 4th(- ☆-), 5th(—■—), 6th(- ▲-), 7th(—□—), 8th(- ▲-), 9th(—●—)

Fig.9 (a) and (b) Effect of number of cycles on B applied pulse mode resistance vs. H/Pd ratio(x<0.02).

pulsed current during absorption was used for the initial one on desorption, these initial values are rather scattered due to the uncontrollable initial condition of the absorption. In the figure the absorbed hydrogen is mostly desorbed at x = 0.008~0.013 when the resistance ratio reaches the initial value (R/Ro = 1) exhibiting the potential 0.025V (see also Fig.6).

These results indicate that the resistance maintains absorption and desorption, while the changes of the potential and dilation are sensitive to a non-equilibrium process, as mentioned above. This is also consistent with the resistance due to the scattering of conduction electrons by interstitial hydrogen causing a resistance increase with an increase of the H/Pd ratio, and electron scattering due to phonons, which might not be influenced by the slightly deformed lattice corresponding to x = 0.002. Hence, the resistance in this experiment does not respond to the formation of non-equilibrium α phase and absorption in the sub-surface layer, or similarly during desorption.

2.4 Sequential microstructure changes during absorption and desorption in the α phase

Let us examine the processes of electrochemical hydrogen absorption and desorption in Pd. During absorption the following reaction take place;

(1) Discharge of protium ion is controlled by a cathodic overpotential between electrode/electrolyte interface,

(2) Adsorbed H atoms are transported through in-fusion and finally diffusion into octahedral sites of Pd lattice: H_{ab}

From thermodynamic aspect the chemical potential energy of H_{ab} was derived in Eq.(9), where the 3rd and 4th terms stand for the deviation of ideal solution[14, 22]. With respect to the deviation term the contribution originates from the electronic interaction of hydrogens with surrounding Pd atoms and protonated hydrogen ions' (H) elastic interaction with screening electrons distributed on the octahedron of adjacent Pd atoms. The former is unlikely to be given rise under a given concentration range. Hence, the major part of the non-ideal solution term appeared during absorption/desorption cycles is understood as due to the elastic interaction of protons with the surrounding expanded Pd lattice. Provided that the non-ideal solution term is corresponding to the elastic strain energy, the dilation change correlates more to the potential change, which is consistent with good correlations between the potential and the dilation changes plots as shown in Figs.10 (a) and (b).

On the other hand, during desorption the reaction inversely proceeds by a anodic overpotential where H_{ab} changes to protinium ion through inverse diffusion and anodic reaction. On this occasion the elastic strain energy would be released (probably as heat) unless otherwise must be accumulated as the local plastic strain energy (e.g., forming a domain rich in defects). It is suggested that such accumulated local strain energy tends to be released by triggering, independently on repeated absorption/desorption performance.

Next the sequential dilation changes of Pd due to the (α → β) phase transition is presented by comparing the results of the dilation and the potential changes as a function of H/Pd. Figures 10 (a) and (b) show typical hydrogen absorption and desorption data. Firstly, the value of the dilation at the end of the desorption is lower than that of the initial one of the absorption, which is consistent with the observation by Krause et al.[22] The earlier work[5] also showed that thick rod Pd (9mm ϕ, 35mm in

length) expanded diamentally during long-term deuterium evolution, simultaneously the length shrank. The ratio taken from these data; - ($\Delta l/l_o$(in length)/increment of H/Pd ratio) / ($\Delta d/d_o$(in lateral)/increment of H/Pd ratio, d diameter) is defined as the Poison ratio assuming the conservation of volume. The present data don't support such a calculation because of an inaccurate measurement of lateral specimen dimension. Secondly, among every absorption and desorption curve the slope of the dilation vs. H/Pd ratio during desorption appeared to be higher than that during absorption. Further experimental and theoretical study is needed for a reasonable explanation of this issue.

In Figs.10 (a) and (b) when the H/Pd ratio reaches at x = 0.008, the potential becomes the $\alpha + \beta$ coexistence region with the potential fluctuations and the dilation exhibits an abrupt increase (similarly to the first dilation during the A applied pulse mode) subsequent to an induction period. On the reverse desorption the potential stays at the potential -0.17V, during which the dilation terminates for a short period, and then a decrease of the dilation occurs accompanied with the transition of a potential from -0.17 to 0.025V. The contraction finishes, simultaneously reaching at 0.025V of the fully desorbed phase. Apart from the cycle effect of absorption/desorption process, the clearly defined feature of the potential and dilation plots as a function of H/Pd ratio is seen in distinct correlation of these behaviors (refer dotted lines in Figs.10 (a) and (b)). Hence, it is demonstrated that the irregular behaviors concerning the dilation and the potential changes during the absorption/desorption cycles are really the results of non-equilibrium processes, undoubtedly not instrumental artifacts.

Conclusion

The main conclusions to come from this work are as follows:

1. For $x < 0.01$ in the α single phase the electrode potential obeyed the Nernst equation, and it exhibited a constant value within the coexistence region

2. During the B applied pulse mode ($x<0.02$), the electrode potentials of the 1st through the 4th cycles shifted to a less-noble direction, while those of the 5th through the 9th cycles showed steep straight lines, i.e., non-Nernstian behavior. The slopes of the dilation vs. H/Pd ratio increased progressively, and most of the slopes after the 5th cycle converged into one line.

3. An induction period of the dilation during absorption was appeared, whereupon the hydrogen behavior is related to the transition of the disordered-ordered phase, subsequently to delayed remaining the α phase absorption.

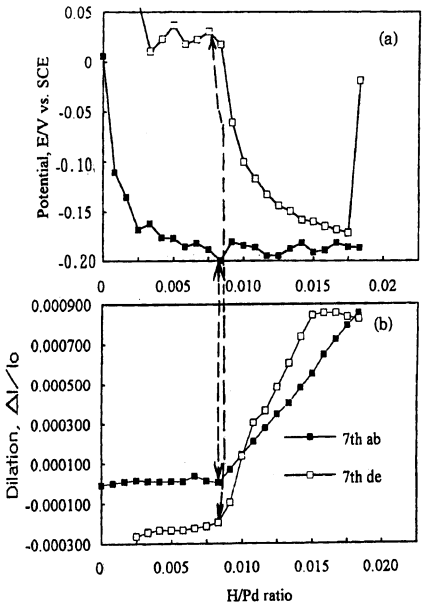

Fig.10 (a) and (b) Comparison of B mode potential vs. H/Pd ratio curve with that of B mode dilation($\Delta l/l_o$) vs. H/Pd ratio.

Acknowledgment

This study was funded by the New Hydrogen Energy Project, NEDO and the Institute of Applied Energy, Japan. The author (H.N.) would like to express sincere thanks to Prof. M. Enyo at Hokkaido University and Prof. I. Ohno at Tokyo Institute of Technology for their valuable discussions.

References

1) M. Fleischmann and S. Pons, J. Electroanal. Chem., **261**(1989)301.

2) S. E. Jones et al., Nature, **338**(1989)737.

3) H. Numata, R. Takagi, I. Ohno, K. Kawamura and S. Haruyama, Proc. Conf. Science of Cold Fusion, Vol.33, p.71, T.BRESSANI,E.DEL GIUDICE, and G.PREPARATA eds., SIF, Bologna, Italy(1991).

4) R. Takagi, H. Numata, I. Ohno, K. Kawamura and S. Haruyama, Fusion Technol., **19**(1991)2135.

5) H. Numata, R. Takagi, I. Ohno, K. Kawamura and S. Haruyama, Proc. of Mini Symp. on Cold Fusion , Tokyo Metro. Univ. pp.129(1990).

6) T. Ooi, H. Numata and I. Ohno, Denki Kagaku, **61**(1993)324.

7) H. Numata, T. Ooi and I. Ohno, Extended Abst. Electrochem. Soc. Spring Mtg., Vol.**93-1**, Honolulu, 1993, p.2419, Electrochem.Soc.Inc., (1993).

8) H. Numata and I. Ohno, Proc. of the 6th Int. Conf.

on Cold Fusion, " Prog. in New Hydrogen Energy", Toya, Japan, October 13, 1996, Vol.1, p.213, NEDO, The Inst. of Appl. Energy, (1997).
9) H. Numata and I. Ohno, Fusion Technol., **38**(2000)206.
10) R. Kirchheim, Acta Metal., **29**(1981)835.
11) T.B. Flanagan and F.A. Lewis, Trans. Faraday Soc., **55**(1959)1400.
12) T.B. Flanagan and F.A. Lewis, Trans. Faraday Soc., **55**(1959)1409.
13) R.T. Fallon and G.W. Castellan, J. Phys. Chem., **64**(1960)4.
14) C. Wagner, Z.Physik.Chem. A **193**(1944)386, 407.
15) W.A. Oates and T.B. Flanagan, J..Mater.Sci., **16**(1981)3235.
16) Q.M. Yang, G. Schmitz, S. Fähler, H.U. Krebs and R. Kirchheim, Phys.Rev. B, **54**(1996)9131.
17) G. Alefeld, Ber. Bunsenges.Physik.Chem., **76**(1972)746.
18) H. Züchner and H.G. Schöneich, J. Less-Common Metals, **101**(1984)363.
19) H. Peisl, "Lattice Strains due to Hydrogen in Metals", Hydrogen in Metals, Eds. G. Alfeld and J. Völkl, Vol.1, Springer, Berlin, p.53(1978).
20) R. Feenstra, R. Griessen and D.G.de Groot, J. Phys. F: Met. Phys., **16**(1986)1933.
21) H. Wagner, "Elastic Interaction and Phase Transition in Coherent Metal-Hydrogen Alloys", Hydrogen in Metals I, Eds. G. Alefeld and J. Völkl, Vol.1, Springer, Berlin, p.5(1978).
22) W. Krause and L. Kahlenberg, Trans. Electrochem. Soc., 68 pp.449(1935).
23) K. Kandasamy, F.A. Lewis and S.G. McKee, Surface and Coating Technol., **35**(1988)93.
24) D.H. Everett and P.A. Sermon, Z. Phy. Chem. Neue Folge, **114**,S. (1979)109.

ANALYSIS OF NUCLEAR TRANSMUTATION YIELDS FOR Pd-H SYSTEMS BY SCS MODEL

Yu TORIYABE[1], Tadahiko MIZUNO[2], Tadayoshi OHMORI[3], Yoshiaki AOKI[4]

[1]*Division of Quantum Science and Engineering, Graduate School of Engineering, Hokkaido University*
[2]*Division of Energy and Environmental System, Hokkaido University*
North 13, West 8, Kita-ku, Sapporo 060-8628, Japan
E-mail: torigoya@pop.qe.eng.hokudai.ac.jp

[3]*Advanced Technology, Inc., Hokkaido Institute of Technology*

[4]*Technology and Electronics College of Hokkaido*

Nuclear transmutation yields for Pd-H systems were theoretically analyzed. An innovative model to predict fission yield with a concept of channel dependant fission barriers, which is referred to as Selective Channel Scission Model: SCS Model, was improved on macro-terms of energy balance in the nucleus. The channel dependant fission barriers were estimated by not deformed shape geometrically but the energy balance between surface and coulomb energy in the Pd nucleus. The results were compared with the experimental results in the viewpoints of observation frequency of detected elements and isotopic ratio change. In consequence predicted fission products of Pd electrode can explain the observation frequency of nuclear transmutations. Changes of isotopic ratio can also agree with experimental values qualitatively. And an excitation source to induce fission is very likely to be not neutron but photon at this study.

1. Introduction

Anomalous nuclear reactions are occurred in not only deuterium but also hydrogen loaded metals[1)]. We have already conducted a number of light water electrolysis experiments with several electrodes and some elements that could not be detected before the experiments and nowhere in the cell as contamination were detected on the cathode surface after the experiments[2-5)]. The results strongly suggest these elements were signs that unknown nuclear reactions must be occurred in the solid state.

In H/ordinary-water systems the preliminary reaction is low energy nuclear transmutation[1)] because $H(p,e^{+}\nu)D$ reaction can be ignored due to weak interaction with extremely small S-value. Although the reaction mechanism is still unknown, the detected elements are distributed as if they were fission products.

Incidentally, an innovative model to predict fission products yield deterministically has already been proposed by Takahashi and Ohta[6-8)]. Through this model, fission barriers that are considered to be same for all fission channels in the past, are determined as channel dependant. This model can be applied for almost all host elements, including Pd, Au, W, and Ni.

In this study, we have improved this SCS Model at some points and applied to Pd-H systems, which we have conducted for a few years. The theoretical results will be compared with the experiment with referring some papers.

2. SCS Model

The liquid drop model is a quite suitable model to treat the nuclear fission. That mechanism has already theoretical studied in the early era of nuclear science[9)].

Figure 1 shows a deformation process and potential change with the liquid drop model through the nuclear fission. If the heavy nucleus is excited sufficiently high as a result of nuclear reaction, such as the absorption of a thermal neutron, that will transform into dumbbell shape with oscillating. At a certain point, various forces within the nucleus are momentarily in balance. This point is referred to as the saddle point.

If it stretches a little more, coulomb repulsive force will be stronger than nuclear strong interaction. Hence the nuclear fission is induced. Finally two fission products fly apart in opposite directions because of the coulomb repulsion.

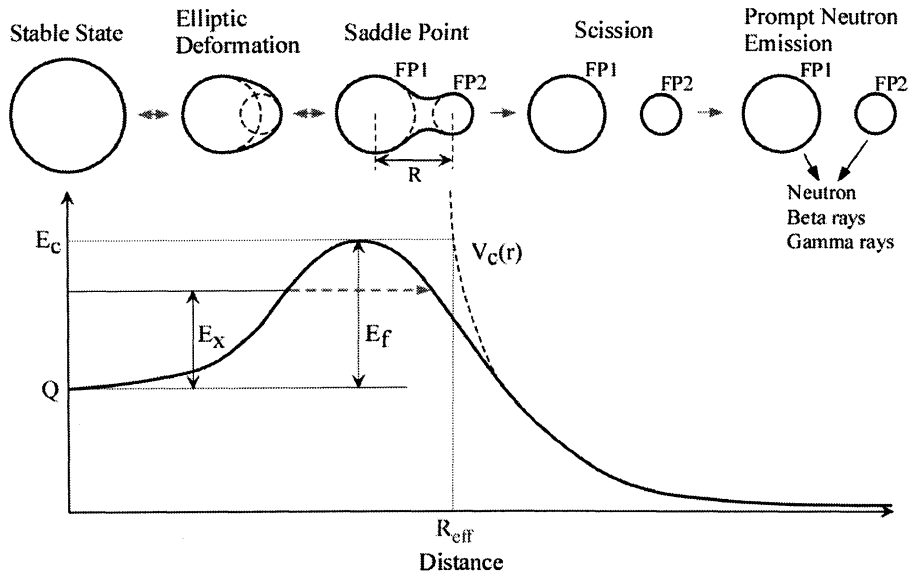

Figure 1. Nuclear fission process and potential with liquid drop model. Fission barrier is estimated by assuming an effective scission distance R_{eff} from the bare coulomb potential between two FPs.

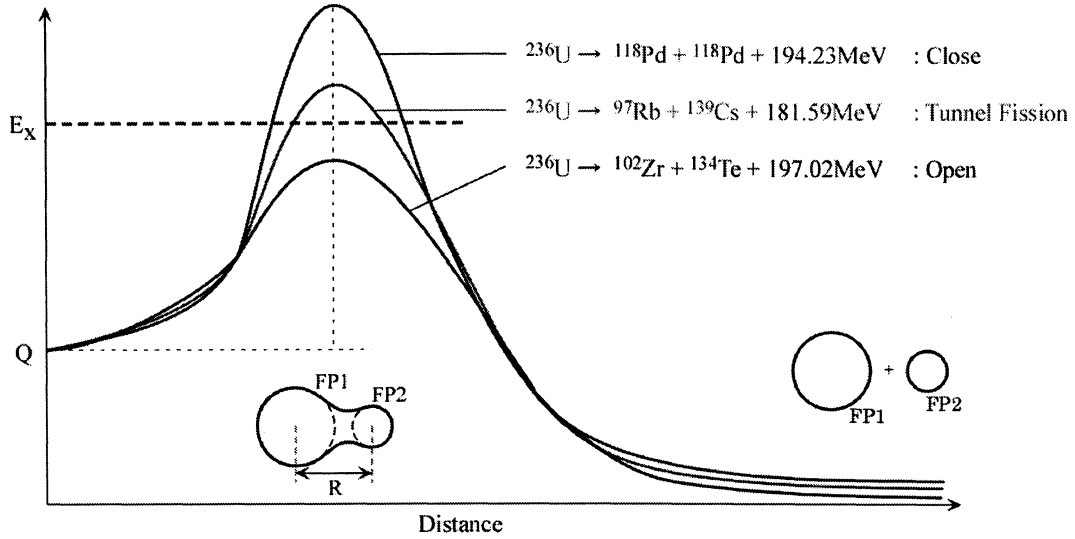

Figure 2. Concept of channel dependant fission barriers. Typical three channels are illustrated. The channels whose barriers are lower than the excitation level can be selectively opened.

The fission barriers that are energy width between the stable state and the saddle point are different for each fission channel in the SCS analysis[6-8] as illustrated in Fig. 2. It is the concept of channel-dependant fission barriers that makes the SCS model innovative.

At the present stage of SCS Model study, these barriers are estimated by the bare coulomb potential between two FPs after the fission, given as

$$V_c(r) = 1.44\frac{Z_1 Z_2}{r},$$

in MeV and fm units. If we can estimate E_c properly, then the fission barrier is defined by

$$E_f = E_c - Q.$$

In order to calculate E_c level, we suppose the virtual scission distance R_{eff}, where the bare coulomb potential is equal to E_c. Precision of the fission yield depends on that of R_{eff} value. Since the correct estimation of R_{eff}, however, has not been constructed, it has approximated by the geometrical shape of deformed nucleus.

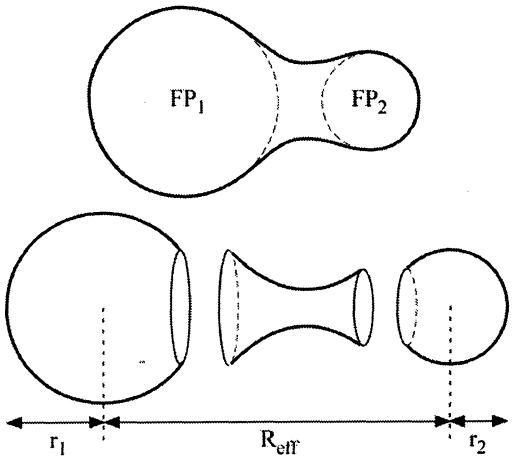

$r = 1.3 \times A^{\frac{1}{3}}[\mathrm{fm}]$: Radius of a nucleus

$O = 0.56[\mathrm{MeV/fm^2}]$: Surface tension

$E_s = 4\pi r^2 O[\mathrm{MeV}]$: Surface energy of a nucleus

$E_c = \frac{3}{5}\frac{Z^2 e^2}{r}[\mathrm{MeV}]$: Coulomb energy in a nucleus

Figure 3. R_{eff} estimation by spheres and hyperbolic curve. R_{eff} is given when a ratio of coulomb energy to surface energy is equal to a certain value.

In this study, we have investigated a new method to obtain more proper R_{eff}. Essentially, the saddle point should be estimated by the energy balance in the nucleus. Thus we calculated the macro terms, namely, surface energy and coulomb energy change through the deformation process.

Volume of the deformed nucleus is constant, because it is considered as constant density liquid drop. To obtain the exact surface area and coulomb energy change, Monte Carlo method should apply to determine a distribution of nucleon. A neck of the deformed nucleus is, however, approximated by a hyperbolic curve,

$$\frac{x^2}{a^2} - \frac{y^2}{b^2} = -1,$$

for the sake of convenience as illustrated in Fig.3.

The coefficients a and b are determined by constant volume condition and contact condition with the two virtual FP spheres. Then the surface area is defined in unique depending on R_{eff} value. Since the surface tension has already been studied[10], we set this parameter as 0.54MeV/fm^2 for U and 0.55MeV/fm^2 for Pd.

On the other hand, calculation method of coulomb energy has still some problems. We assumed that the nucleon concentrate in the two virtual FP spheres and not exist in the middle section, because we did not applied Monte Carlo method to determine the nucleon distribution in the deformed nucleus. In general, coulomb energy in a spherical nucleus is given as,

$$E = 0.86\frac{Z^2}{r},$$

in MeV and fm units. In this study, all coulomb energy is estimated with a summation of those of FP1 and FP2, and that between two FPs, approximately as,

$$E_{Coulomb} = 0.86\left(\frac{Z_1^{\,2}}{R_1} + \frac{Z_2^{\,2}}{R_2}\right) + 2 \times 1.44\frac{Z_1 Z_2}{R_{eff}}.$$

Then the ratio: $E_{Surface}$ / $E_{Coulomb}$ is a judgment factor to induce fission.

3. Results

3.1. U fission

First of all, we applied to this improved SCS Model to the uranium fission to confirm the validity. Although Bohr et al. claimed fission to just same two FPs is occurred when the surface/coulomb energy ratio is equal to 2.0[9], we assumed the R_{eff} is given when that ratio is equal to 1.5 in the uranium fission process, because R_{eff} is estimated by the bare coulomb potential after the fission. Then the channel dependant fission barriers for ^{236}U compound nucleus are calculated as shown in Fig. 4.

The uranium compound nucleus is excited 6.5MeV on the average by thermal neutron incident. Therefore the channels above the 6.5MeV line can be selectively opened. Those below that line also can be opened due to the tunneling effects, whose probabilities are estimated by following WKB formula for each

channel.

$$P(E_x) \propto \exp\left[-0.436\sqrt{\mu}\int_a^b \sqrt{V(r)-E_x}\,dr\right]$$
$$\propto \exp\left[-0.218(b-a)\sqrt{\mu(E_f-E_x)}\right],$$

in MeV and fm units, where μ and b-a, are reduced mass and tunnel distance, respectively. Although the tunnel distance depends for each channel, we set this parameter as 2.5fm. Because this tunneling effect is very small, this assumption cannot give an effective difference for the fission yield.

After the scission, two FPs emit prompt neutrons. The number of them is a function of mass number of FPs[11].

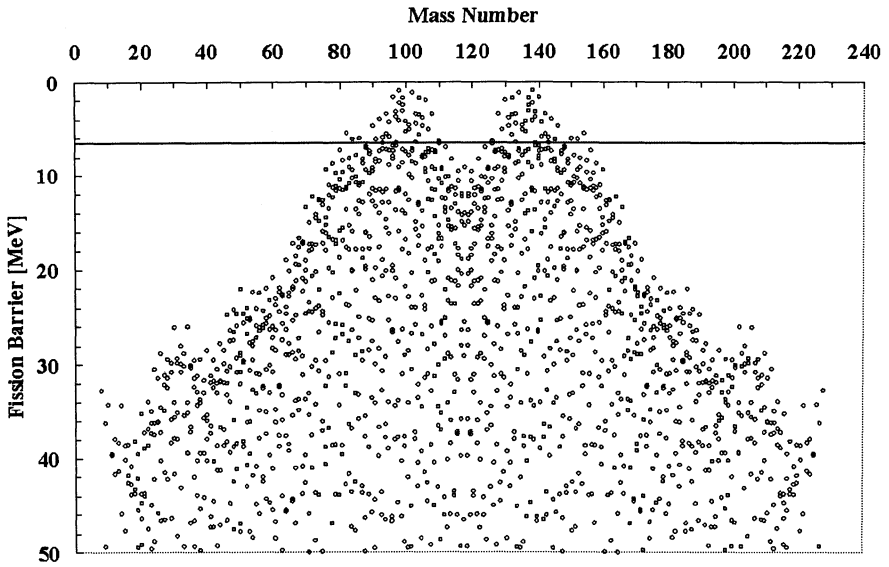

Figure 4. Pattern of channel dependant fission barriers for ^{236}U. The excitation level is 6.5MeV by thermal neutron incident.

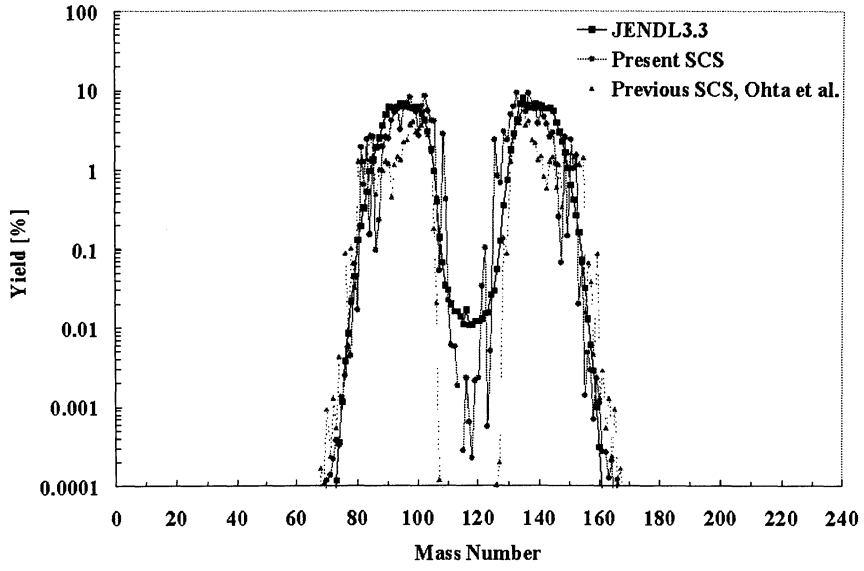

Figure 5. Mass distribution of FP yield for thermal neutron fission of ^{235}U. The result (●) is compared with the independent yield from JENDL 3.3. (■) and previous SCS Model (▲).

Finally, the yield is compared with the Japanese evaluated nuclear data library, JENDL3.3[12]. As shown in Fig. 5, the improved SCS Model can give a better agreement than the previous estimation[7], especially in the center range, therefore it is more suitable to analysis the Pd fission.

3.2. *Pd fission*

In H/ordinary-water systems the low energy nuclear transmutation products are distributed as if they were fission products[1]. Although there are various theories to induce the Pd fission, we limited excitation sources to photon or neutron in this study.

In the photon case, we assume very low incident energy for each photon, but the fission would be induced if a large number of photons interacted with Pd nucleus in sub-pico sec order[6]. The excitation levels for 6 stable Pd isotopes are same on the average.

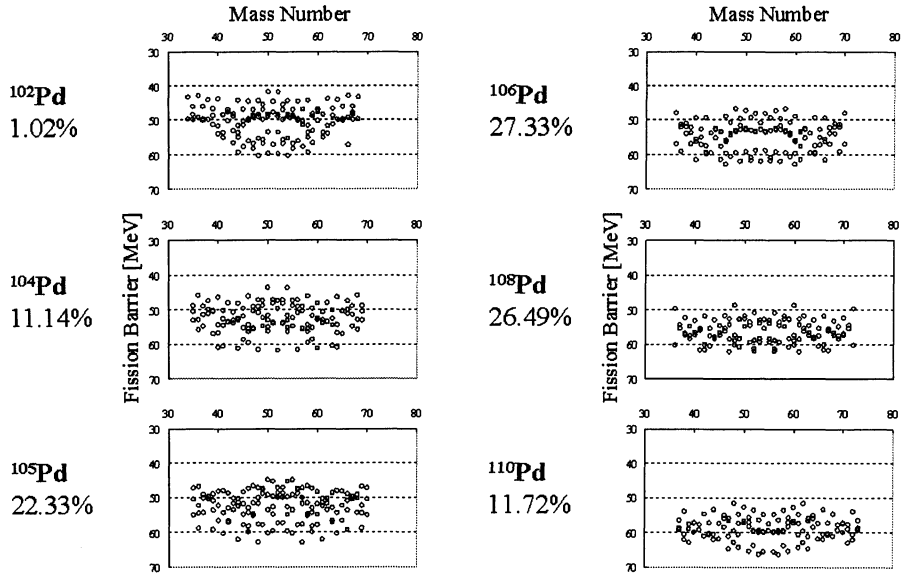

Figure 6. Pattern of channel dependant fission barriers for 6 stable Pd isotopes in the case of photon excitation. Isotopic contents are shown below each nuclide.

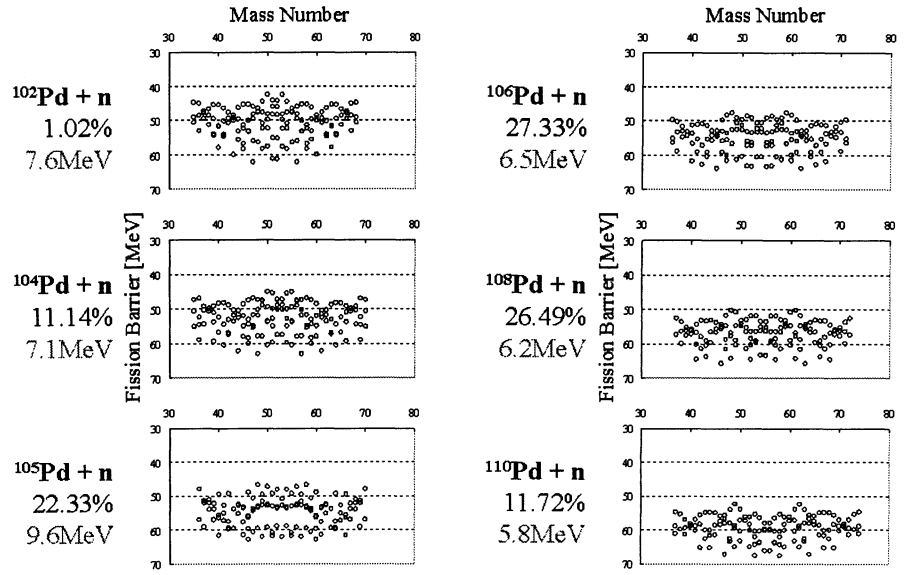

Figure 7. Pattern of channel dependant fission barriers for 6 compound Pd nuclei in the case of thermal neutron excitation. Isotopic contents and excitation energies are shown below each nuclide.

In the neutron case, we assume the single neutron that can exist in the condensed matter lattice at stable[13] while polyneutron theory[14] was ignored. Since the energy of neutron is supposed thermal, the excitation levels are different for the 6 compound nuclei because binding energies are determined for each nucleus.

The surface/coulomb energy ratio to give R_{eff} is assumed to be 1.0 in Pd fission. Calculated fission barriers in the center section of the mass number are plotted in Fig. 6 and 7, in the case of photon and neutron fission, respectively. The excitation energies by thermal neutrons are shown in Fig. 7.

It is obvious that lighter Pd isotopes have lower barriers. This result predicts that content of ^{110}Pd should increase while that of ^{102}Pd should decrease through the nuclear fission process and, at the same time, supports the experimental results reported by Ohmori et al[15].

After the fission a certain nuclide emit β rays. However, the nuclei whose half life is longer than 1 month are ignored and considered as stable isotopes. Finally we obtained the atomic distributions of fission products for natural abundant Pd, which are shown in Fig. 8.

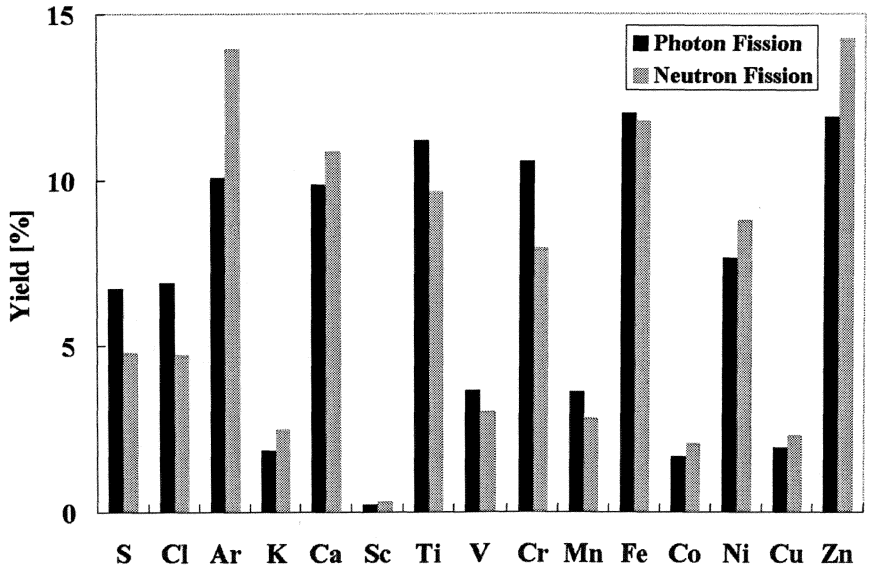

Figure 8. Atomic distribution of FP for photon fission and neutron fission of natural abundant Pd. The results are plotted with limiting the atomic number from 16 to 30.

4. Discussion

4.1. Observation Frequency

We compare the results with the experimental results in H/ordinary water system reviewed by Miley[1] at the viewpoint of observation frequency and summarized in Table I.

The experimental values agree better with the photon excited case, relatively. Furthermore, the neutron related theories have some fatal problems, interaction between some neutrons, stability in solid state, scattering and so on[16]. Therefore the excitation source is considered very likely to be photon at this moment.

Table I Observation frequencies of elements comparing the experiments and theory.

No	Review[1]	Photon	Neutron	Exp[4]
1	Fe	Fe	Zn	Fe
2	Cu	Zn	Fe	(Zn)
3	Ca, Cr, Zn	Ti	Ca	(Cu)
4	Ni, K	Cr	Ti	Mn
5	Ag, Cl, Ti	Ca	Ni	Cr
6	Mg, Mn, Co, Pb	Ni	Cr	Ni
7	Li, Ba, Al, Os, C, Si	S	S	Ti

4.2. Isotopic Yield

Isotopic yields for typical elements, namely, Ti, Cr and Fe were also calculated and compared

with experimental values through H_2 permeation process with Pd bulk conducted Yamada et al[17] in Table II.

Table II Change of isotopic ratio for Ti, Cr and Fe comparing experiment and theory.

Ratio	Natural	Yamada[16]	Photon
$^{49}Ti/^{47}Ti$	0.727	0.943 (+30%)	1.371 (+89%)
$^{53}Cr/^{52}Cr$	0.113	0.145 (+28%)	0.812 (+618%)
$^{57}Fe/^{56}Fe$	0.024	□	0.645 (+2590%)

Although the theoretical yields cannot agree quantitatively, SCS Model can explain the tendency of increase of $^{49}Ti/^{47}Ti$ and $^{53}Cr/^{52}Cr$ ratios. Because $^{57}Fe/^{56}Fe$ ratio does not be mentioned in Ref. 16, we referred other reports in heavy water system. Some researchers still have claimed that ratio increased due to the nuclear transmutation. The SCS Model also predicts this isotopic ratio change, qualitatively.

At the present stage of the CMNS study, the experimental results of isotopic yields are of uneven quality. Evaluated nuclear transmutation data library has not been prepared. If the reproducible conditions became clear and a margin of error reduced, these comparisons would be more worthwhile. Moreover, the proper barrier estimation is strongly required to obtain better agreement.

5. Conclusion

The nuclear transmutation yields induced in the Pd-H systems are theoretically predicted by the improved SCS Model. The channel dependant fission barriers were calculated by the macro energy balance in the nucleus, namely, surface and coulomb energy.

This estimation was firstly applied for U fission with thermal neutron incident. The result agrees much better with the JENDL3.3 than the conventional geometrical estimation of the deformed nucleus, especially in the center section of the mass number.

The improved SCS Model was applied for two types of Pd-H systems, photon excite and neutron excite fission in Pd. The simulated results were compared with the experimental values at the viewpoint of observation frequency and isotopic yield of the detected elements. The excitation source is very likely to be photon, because the result in the photon case can explain the experimental values, qualitatively.

This study strongly suggests the nuclear transmutation reactions in the Pd-H systems are originated from not proton related fusion but nuclear fission.

If the more precise experiment were conducted and more proper barrier estimation were developed, an excellent agreement would be achieved.

Acknowledgement

The SCS Model was originally proposed by Professor emeritus Akito Takahashi, Osaka University and Dr. Masayuki Ohta, Japan Atomic Energy Agency. This study is fully based on their work.

The authors would like to thank Dr. Ohta for his helpful comments about the SCS Model.

References

1. G. H. Miley, *Proc. ICCF12*, 2006
2. T. Ohmori and T. Mizuno, *Curr. Top. Electrochem.*, **5**, 37, 1997
3. T. Ohmori, *Curr. Top. Electrochem.*, **7**, 102, 2000
4. Y. Toriyabe et al., *Proc. ICCF12*, 2006
5. T. Mizuno and Y. Toriyabe, *Proc. ICCF12*, 2006
6. A. Takahashi et al., *Jpn. J. Appl. Phys.*, **40**, 7031, 2001
7. M. Ohta et al., *Jpn. J. Appl. Phys.*, **40**, 7047, 2001
8. M. Ohta and A. Takahashi, *Jpn. J. Appl. Phys.*, **42**, 645, 2003
9. N. Bohr and J. A. Wheeler, *Phys. Rev.*, **56**, 426, 1939
10. E, Feenberg, *Phys. Rev.*, **55**, 504, 1939
11. *The New Encyclopaedia Britannica 15th ed.*, **13**, 301, 1974
12. K. Shibata et al., *JENDL-3.3, J. Nucl. Sci. Technol.*, **39**, 1152, 2002
13. H. Kojima et al., *J. New Energy*, **7**, 81, 2002
14. J. C. Fischer, *Proc. ICCF12*, 2006
15. T. Ohmori et al., *Proc. JCF5*, 36, 2004
16. A. Takahashi, *Proc. ICCF12*, 2006
17. H. Yamada et al., *Proc JCF5*, 69, 2004

Reproduction of Nuclear Transmutation in CaO/Sr/Pd Samples by Deuterium Gas Permeation

H. Iwai*, R. Satoh, R. Nishio, A. Taniike, Y. Furuyama and A. Kitamura

Division of Environmental Energy Science, Graduate School of Science and Technology,
Kobe University
5-1-1 Fukaeminami-machi, Higashinada-ku, Kobe 6580022, Japan

Abstract: Results of preliminary experiments presented at ICCF12 have implied nuclear transmutation from Sr to Mo. In the present work, for the purpose of increasing the amount of transmutation products, the another method of Sr deposition has been employed. During the deuterium permeation, the sample was diagnosed to identify the transmutation elements and measure the deuterium distribution by *in situ* and simultaneous PIXE, RBS and NRA methods

Keywords: nuclear transmutation, CaO/Sr/Pd samples, D_2 permeation, PIXE, NRA

1. Introduction

It has been claimed [1-3] that forced permeation of deuterium through Cs-doped Pd/(CaO+Pd)/Pd samples induced nuclear transmutations from ^{133}Cs to ^{141}Pr, from ^{88}Sr to ^{96}Mo, from ^{138}Ba to ^{150}Sm and from ^{137}Ba to ^{149}Sm. The diagnostic methods they mainly used were X-ray photoelectron spectroscopy (XPS), time-of-flight secondary-ion mass spectroscopy (TOF-SIMS) and X-ray fluorescence (XRF). To confirm and investigate the phenomena, it is essential that the same results are obtained in different laboratories with different analytical methods.

We have constructed an experimental system, with which accelerator analyses of the samples including particle induced X-ray emission (PIXE), elastic recoil detection analysis (ERDA), nuclear reaction analysis (NRA) and Rutherford backscattering spectroscopy (RBS) can be made *in situ* and simultaneously with gas permeation through the samples.

Preliminary results of experiments on the permeation based on the XPS characterization have suggested the transmutation from Sr to Mo. Areal densities of Sr before deuterium permeation and Mo after the permeation were calculated to be 1.3×10^{14} cm^{-2} and 6.6×10^{13} cm^{-2}, respectively [4]. The sample was prepared by means of electroplating method. In the present work, the samples are prepared by means of ion beam sputtering for the purpose of enhancing the transmutation yield, and the advanced diagnostic system mentioned above is employed.

2. Experimental procedure

A schematic of the experimental setup is shown in Fig. 1. The sample structure used in the

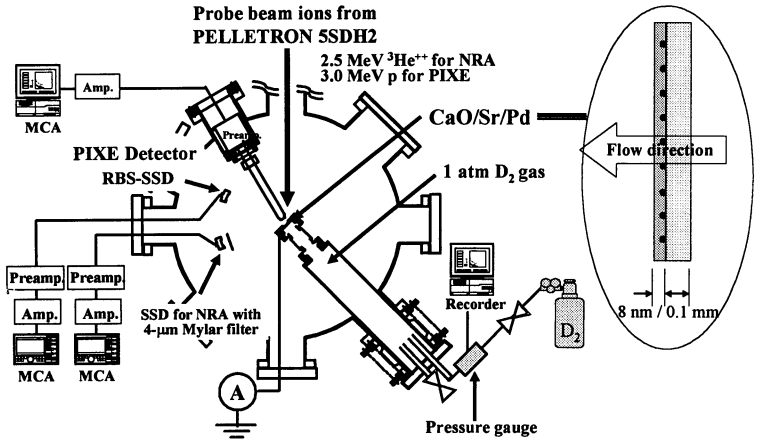

Fig. 1. Schematic of deuterium permeation and *in situ* accelerator analyses system.

present work is basically the same as before [4] except that Sr atoms were deposited on one side of the Pd surface using the ion beam sputtering: 5-keV Ar^+ ion beam was used to bombard the Sr target for about 1 hour. Thereby, a layer containing Sr atoms with an areal density of 3.2×10^{15} cm^{-2} as measured with the XPS method was formed on the Pd bulk.

The sample with the CaO/Sr/Pd structure on the surface is placed in a vacuum chamber, and its rear surface is exposed to D_2 gas at a pressure of 0.1 MPa typically. The deuterium permeation condition is somewhat different from that used in refs. [1] through [3]; the Sr doped Pd/CaO interface is exposed to the flow of deuterium purified by permeation through the Pd bulk. The sample surface is diagnosed with probe beam ions to emit characteristic X-rays which are analyzed either with a CdTe detector or a Si-PIN-type X-ray detector positioned at 150 degree relative to the probe beam direction. Additional solid-state charged-particle detectors are provided for RBS and NRA characterization of the sample.

3. Results and discussion

During deuterium gas permeation, the CaO/Sr/Pd samples were occasionally analyzed by means of PIXE, RBS and NRA methods using 3-MeV p or 2.5-MeV $^3He^{++}$ beams. Here, the RBS spectra were used to monitor the number of incident probe beam ions.

A typical energy spectrum of NRA at about 300 h after initiation of deuterium permeation is shown in Fig. 2(a). The continuum below 1.6 MeV in the spectrum originates in the ^3He particles scattered by the bulk Pd atoms, while the continuum below 3.8 MeV originates in α particles produced by the $D(^3He, \alpha)p$ nuclear reaction. The reduction of α particle energy below 3.8 MeV from 4.2 MeV, which is expected for α particles produced by the reaction taking place just on the surface, is due to passage through a 4-μm-thick Mylar foil.

The deuterium depth profile is shown in Fig. 2(b), which is calculated from the energy spectrum mentioned above. The deuterium density of 4.4×10^{22} cm^{-3} averaged over the surface region up to the depth of 1.8 μm corresponds to the composition of $PdD_{0.65}$.

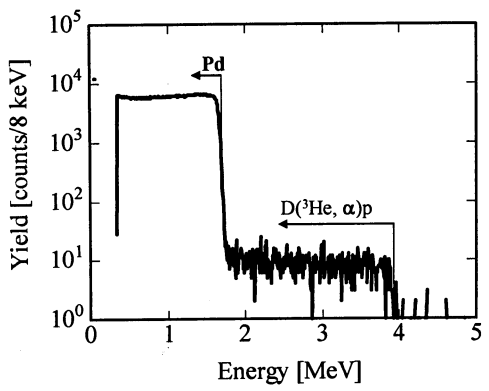

(a)

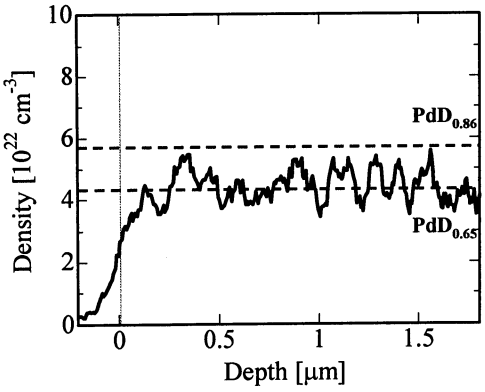

(b)

Fig. 2. (a) Energy spectrum recorded on the NRA-SSD, and (b) evolution of the depth profile of the D density in the CaO/Sr/Pd sample at about 300 h after initiation of D permeation.

Variation of the D_2 gas pressure after its introduction into the reservoir was monitored to give the number of deuterium atoms absorbed in and/or transmitted through the sample as shown in Fig. 3. Deuterium absorption up to the uniform composition of $PdD_{0.65}$ mentioned above requires 2.3×10^{21} deuterium atoms, which was lost from the reservoir by at least 100 h after initiation of deuterium permeation. This means that the D_2 gas was permeating through the sample into vacuum after the saturation at about 100 h. Then the deuterium flux through the sample is calculated to be about 2.7×10^{15} $cm^{-2}s^{-1}$ from the slope of the pressure decrease shown in Fig. 3. This corresponds to a flow rate of 0.02 sccm, which is smaller by a factor of about 1/50 than that realized in ref. [2].

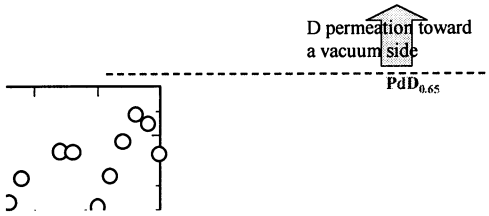

Fig. 3. Number of D atoms absorbed and/or transmitted during permeation.

Typical X-ray energy spectra before and after deuterium permeation are shown in Fig. 4(a). The Sr K-α line is clearly identified in all spectra. However, we could not confirm the transmutation from Sr to Mo, because of interference by unexpected signals of unknown origin appearing in the neighborhood of the Mo K-α line.

The density N of any target element can be calculated from the X-ray yield Y_X during irradiation with Q projectiles;

$$Y_X = QN\frac{\sigma_i(E)}{4\pi}\Delta\Omega\omega_K k_\alpha T\varepsilon\cdot\frac{\cos\theta}{\mu}\left[1-\exp\left(-\frac{\mu\Delta t}{\cos\theta}\right)\right],$$

where $\sigma_i(E)$, ω_K, k_α and $\Delta\Omega$ denote the ionization cross section at a colliding energy of E, fluorescence yield for the K-shell, fractional transition probability of the K_α-line to all K-lines

and the solid angle of the detector, respectively. And then, μ, θ, T and ε are the X-ray absorption coefficient of the target itself, the detection angle, X-ray transmittance of the absorbers in front of the detector and the detection efficiency of the detector, respectively. Here homogeneous distribution of the element throughout the thickness Δt is assumed.

The areal densities $N\Delta t$ of the target materials can be evaluated from the above equation. The temporal variation of the areal density of Sr during the permeation process is shown in Fig. 4(b). The areal density of Sr decreases during the permeation by about 7.0×10^{11} $cm^{-2}h^{-1}$, which is of the same order of magnitude as that of 2.9×10^{11} $cm^{-2}h^{-1}$ obtained earlier [4] using the electroplating method.

The detection limit of areal densities of Sr and Mo for PIXE analysis is estimated using the 3σ criterion to be 1.2×10^{14} cm^{-2} and 1.9×10^{14} cm^{-2} for 10.6-μC/3-MeV proton probing. These are compared in Table 1 with that given in the specification sheet of the XPS method.

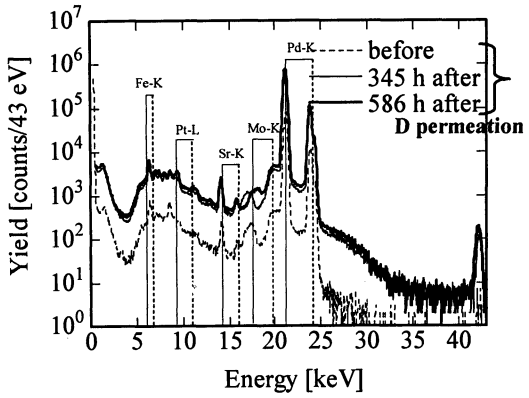

(a)

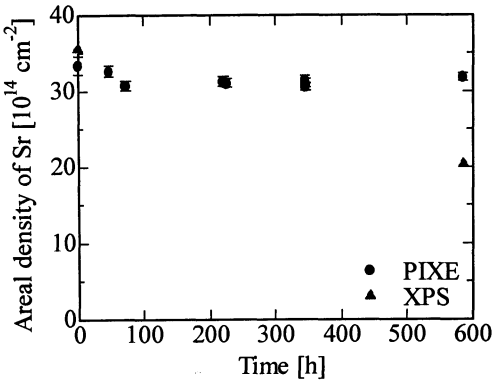

(b)

Fig. 4. (a) PIXE spectra before and after deuterium permeation, (b) temporal variation of the areal density of Sr during the permeation process.

Table 1. The detection limit of areal densities of Sr and Mo for PIXE analysis and XPS.

Method of analysis		PIXE (Si-PIN)	XPS
Filter		Al 90μm	-
Probe		3MeV-p(10.6μC)	Mg-Kα
Incident angle		45 deg	0 deg
Detection limit [cm^{-2}]	Sr	1.2×10^{14}	6.7×10^{12}
	Mo	1.9×10^{14}	1.1×10^{13}

Figure 5(a) shows an example of XPS spectra in the energy range of Sr-3d photoelectrons for the sample before deuterium permeation. This and the corresponding spectrum after the permeation give the triangles shown in Fig. 4(b). However, we can hardly observe the corresponding increase in the Mo signal even after permeation lasting for 600 hours. The XPS spectrum in the energy range of Sr-3d photoelectrons is shown in Fig. 5(b).

In the present work the amount of atoms transmuted to Mo was below the detection limit in the XPS characterization. A possible reason for this negative result would be the low flow rate, or the low deuterium flux. Another reason might be the abundance of Sr itself. Although the areal

density of Sr is of the order of one monolayer, the density might have been too high for the transformation to take place. This might suggest that the transmutation elements should be dispersed in the Pd bulk with a relatively low density.

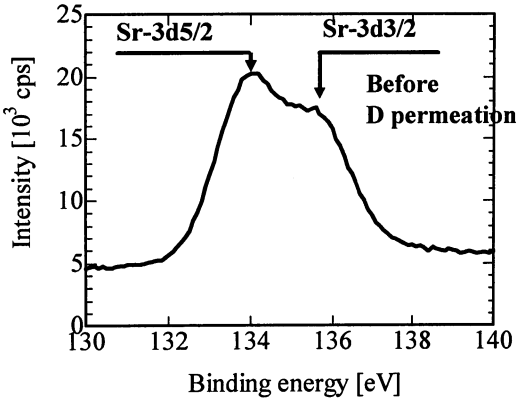

(a)

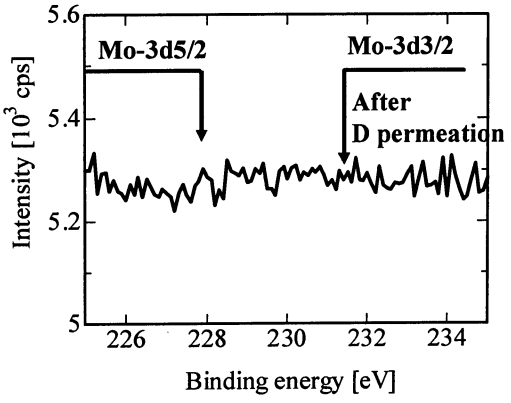

(b)

Fig. 5. (a) Sr photoelectron spectrum in the XPS for the sample before D permeation, (b) the spectrum in the energy range of Mo photoelectrons for the sample after D permeation.

4. Summary

In situ PIXE, RBS and NRA methods for measurements of areal densities of elements and deuterium distribution have been performed simultaneously with deuterium permeation to induce nuclear transmutation. For the purpose of increasing the amount of transmutation products, Sr atoms as the element to be transmuted were deposited using ion beam sputtering instead of the method similar to electroplating used in the first stage experiments reported earlier.

Unfortunately, we could not reproduce and confirm the transmutation from Sr to Mo. It has been suggested that a higher flow rate of deuterium and/or a lower density of the transmutation element might be preferable for a high efficiency of transmutation.

We are going to investigate systematically the dependence of the transmutation efficiency on various parameters including the flow rate and the multilayered sample structure.

References

1. Y. Iwamura *et al.*; Jpn. J. Appl. Phys. 41 (2002) 4642-4650.
2. Y. Iwamura *et al.*; Proc. ICCF10, Cambridge, USA, 2003 (World Scientific, 2006).
3. Y. Iwamura *et al.*; Proc. ICCF11, Marseilles, France, 2004 (World Scientific, 2006).
4. A. Kitamura *et al.*; Proc. ICCF12, 2005, Yokohama, Japan.

PRODUCING AN ELEMENT OF MASS NUMBER 137 ON MULTI-LAYERED Pd SAMPLE WITH SMALL AMOUNT OF Cs BY DEUTERIUM PERMEATION

H. YAMADA, S. NARITA, S. TANIGUCHI, T. USHIROZAWA, S. KURIHARA, M. HIGASHIZAWA, H. SAWADA and M. ITAGAKI

Department of Electrical and Electronic Engineering, Iwate University, Ueda 4-3-5, Morioka, 020-8551 Japan *yamadahi@iwate-u.ac.jp*

Abstract: Elemental analysis on the Pd samples was performed after deuterium permeation experiment and for control Pd samples using TOF-SIMS. The TOF-SIMS has provided the marked count peaks at mass numbers 135 and 137 in spectra after deuterium permeation at 70℃, only when the multilayered Pd sample with a small amount of Cs was used. The substance with mass number 137 could be ^{137}La or ^{137}Ba produced during deuterium permeation by some nuclear transmutation occurring on/in the uppermost of multi-layered Pd sample. The single couple of Pd/CaO thin films on Pd foil might contribute to induce production of an element with mass number 137. This would imply a transmutation of 4 mass number increasing before ^{141}Pr production.

Keywords: Pd-deuteride, Deuterium permeation, Transmutation, TOF-SIMS, Surface analysis

1. Introduction

The phenomena on nuclear reactions at low temperature in solid-state have been widely investigated for these 17 years. Among several experimental methods for the reaction, the gas permeation method is one of the promising methods. Iwamura et al.[1] have studied using this method with Pd film complexes and have reported a low energy nuclear reaction such as the transmutation of Cs into Pr.

While, we have been taking account of the possibility of nuclear transmutation not only in such Pd film complexes but also in plain Pd foil by hydrogen gas permeation at room temperature[2]. The results obtained have suggested that several elements were produced by a nuclear transmutation and the reaction could occur in hydrogen system as some researchers have claimed in various experiments [3-5].

The aforementioned results caused us to study the phenomena systematically by the permeation experiment for deuterium as well as hydrogen using multi-layered Pd samples. Thus, in this present investigation, we have performed a deuterium permeation experiment using a multi-layered sample consisting of single couple of CaO and Pd thin films and a bulk Pd foil.

On the basis of the reports on transmutation of ^{133}Cs into ^{141}Pr, production of elements with mass number ranging between 133 and 141 could be expected before Pr production. Therefore, we have focused our attention to this mass number range to search for the elements produced by low energy nuclear reaction.

2. Experimental

The multi-layered sample consisted of a couple of CaO and Pd thin films on the base Pd foil of $0.1 \times 12.5 \times 12.5$mm in size. The CaO and Pd thin films were formed on the Pd foil by Ar ion beam sputtering. After forming the thin films, small amount of Cs was deposited on the multi-layered Pd sample by an electrochemical method. The thickness of CaO and Pd films formed were 2 and 40 nm, respectively. No deuterium gas was loaded to the samples before deuterium permeation experiment.

Figure 1 shows the deuterium permeation system to investigate the transmutation of Cs into other elements of larger mass number. The vacuum chamber and the sample holder were baked at 200℃ sufficiently before setting the sample. The chamber is usually filled with N_2 gas under non-experiment condition.

Just before the permeation experiment,

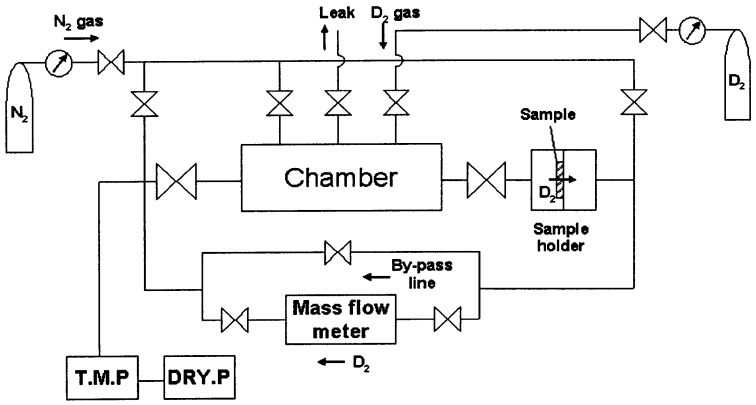

Fig. 1 Apparatus for cold transmutation.

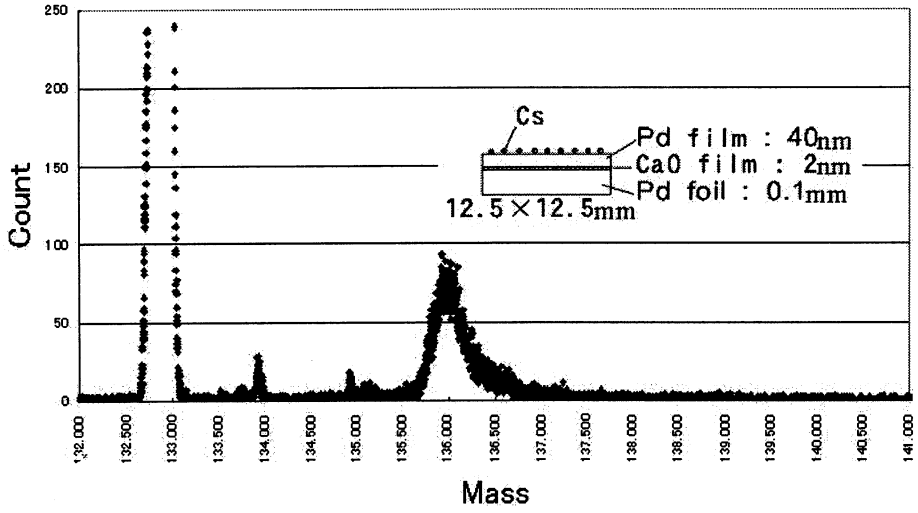

Fig. 2 TOF-SIMS spectrum of mass number range 132-141 before sputter cleaning for control sample.

the Pd samples were set into the sample holder in an air environment and it was placed at the vacuum chamber.

Then, the chamber was filled with deuterium gas at a pressure 0.1 MPa; the thin Pd film side of multi-layered Pd sample was exposed to D_2 gas. The other side of sample was evacuated by a turbo molecular pump. The deuterium permeated from the chamber through the Pd sample to the evacuated side by the pressure gradient for about 1 month. A heater was employed to keep the temperature of the chamber at 70℃ during the experiment.

After the permeation experiment, the heater is turned off and the chamber was filled with N_2 gas, then the sample ("Permeation sample") was taken out from the holder. Before the elemental analysis, the sample was not treated for purging the deuteron atoms remaining in. The sample surface of gas-filled side was analyzed by TOF-SIMS (ULVAC-PHI: TFS-2100).

The primary ion in TOF-SIMS was Ga^+ and we measured three randomly selected areas of 40×40 micron square. The spectra were obtained before and after a sputter cleaning of the uppermost surfaces of samples by the Ga^+ for 10 sec. In order to take into account the contamination from the environment, we prepared the control sample ("Control sample") without flowing the

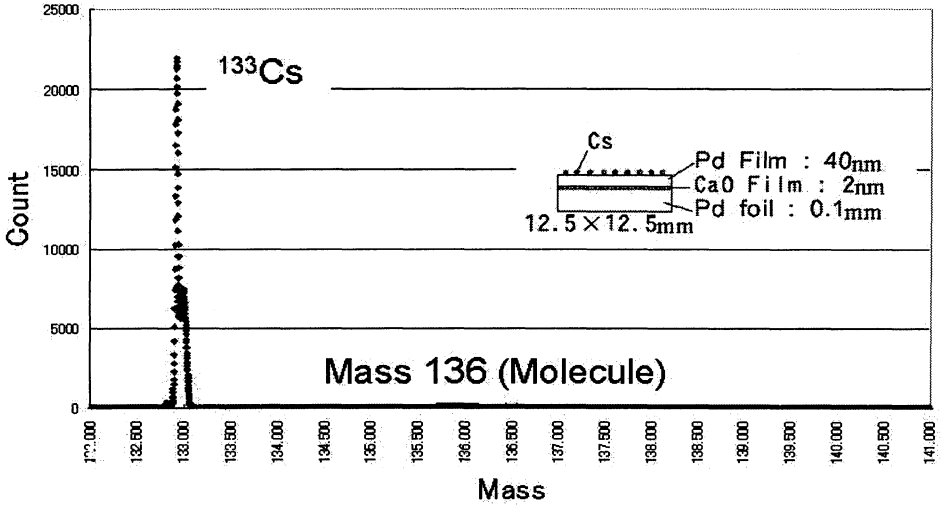

Fig. 3 TOF-SIMS spectrum of mass number range 132-141 after sputter cleaning for control sample.

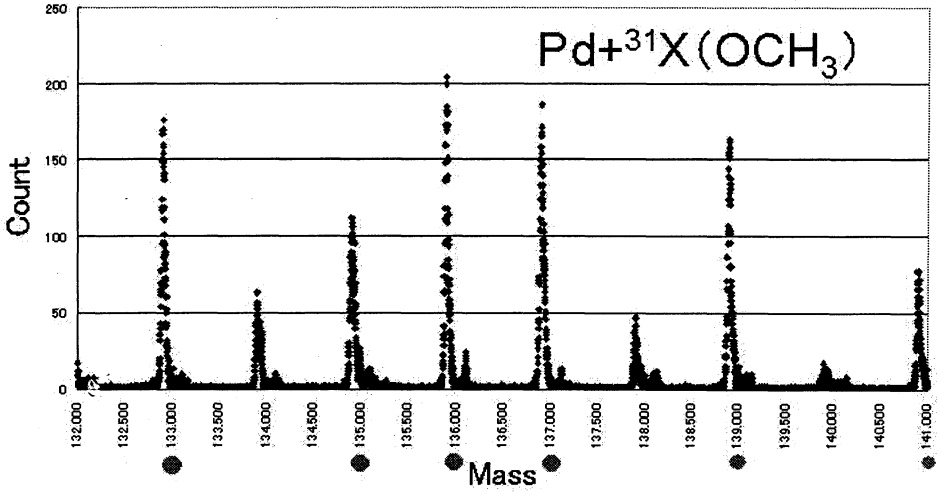

Fig. 4 TOF-SIMS spectrum of mass number range 132-141 before sputter cleaning for permeation sample without Cs deposition.

deuterium gas, which was prepared by the same procedure for the permeation samples.

3. Result and Discussion

TOF-SIMS spectrum of mass number range 132-141 before sputter cleaning for a control sample is presented in Fig. 2. The schematic view of sample is shown in this figure. The peak at mass number 136 in this figure would correspond to a molecule deposited on the upper most of the sample. No other marked peak, except that at mass number 133 corresponding to Cs, is seen in the figure.

Similar spectrum after sputter cleaning for control sample is shown in Fig. 3. No marked count, except that corresponding to ^{133}Cs, was again observed. However, one can realize a few count due to a molecule contaminant at mass number 136. It implies that the depositing substance with mass number 136 is hard to be removed from the

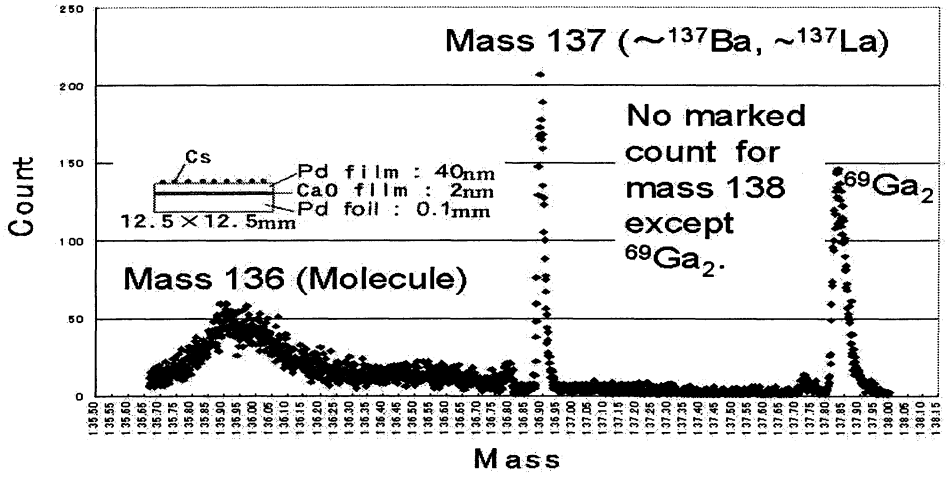

Fig. 5 TOF-SIMS spectrum around mass number 137 after sputter cleaning for permeation sample with Cs deposition.

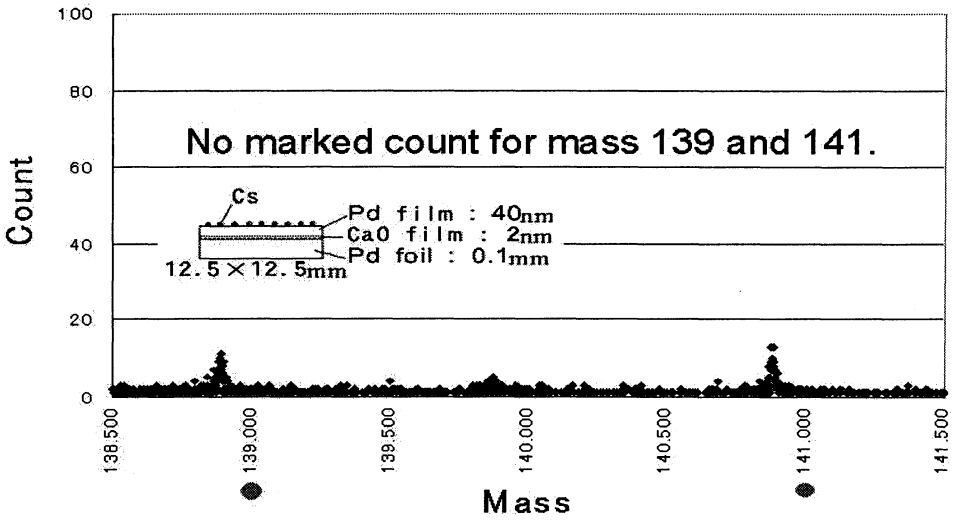

Fig. 6 TOF-SIMS spectrum of mass number range 139-141 after sputter cleaning permeation sample with Cs deposition.

sample surface by the sputter cleaning. This substance may be introduced during the procedure of Cs deposition.

Fig. 4 gives a similar spectrum before sputter cleaning for a permeation sample without Cs deposition. Several larger peaks are seen, which are indicated by the symbols ● under each mass number. These mass numbers are larger than those of Pd isotopes by 31. In other words, the substance corresponding these peaks could be Pd compounds; the candidate molecule can be $Pd(OCH_3)$. The result means that the deuterium permeation caused the formation of Pd compounds and contamination of the uppermost surface of sample by the compounds.

Next, we have performed the deuterium permeation test using the multi-layered Pd sample with Cs deposition. We have found anomalous peak at mass

number 137, as shown in Fig. 5. Similar anomalous peak was also observed at mass 135, even though the count intensity was lower than that of the mass number 137. The substance with this mass number may be molecule CsD or an element such as ^{135}Ba.The substance, corresponding to mass number 136 in Fig. 5 is considered to be a molecule, which would be the same kind of molecule mentioned above.

It should be noticed that the count intensity seen at mass number 137 is higher than that at mass number 135. This is the characteristic commonly observed in all the three measured areas. In general, amount of CsD formed is much more than that of CsD_2 during the deuterium permeation experiment. Accordingly, the substance corresponding to mass number 137 cannot be CsD_2.

TOF-SIMS spectrum of mass number range 139-141 after sputter cleaning for a permeation sample with Cs deposition is shown in Fig. 6. When the substance with mass number 137 was $^{106}Pd^{31}X$, marked count due to $^{108}Pd^{31}X$ should have been seen at mass number 139 in Fig. 6. However, almost no marked count was detected in this mass number range. Further, no peak appeared at mass numbers 134 and 138 after sputter cleaning for the permeation sample. Considering the fact that Pd has large natural isotopic abundance in mass number 105, 106 and 108, the compounds of Pd isotopes cannot account for the anomalous count at mass number 137. Thus, the substance with mass number 137 observed after deuterium permeation is unlikely to be contaminant but would be an element such as ^{137}La or ^{137}Ba. The results suggest an important role of alpha cluster in the transmutation process of 8 and 12 mass number increasing.

4. Conclusion

Time-of-flight secondary ion mass spectroscopy (TOF-SIMS) was employed for elemental analysis of surface of multi-layered palladium sample with a small amount of Cs. The TOF-SIMS has provided the marked count peaks at mass numbers 135 and 137 in spectra after deuterium permeation at 70℃, when the multilayered Pd sample with a small amount of Cs was used. The result suggests production of an element with mass number 137 which would be produced from Cs. The substance with mass number 137 could be ^{137}La or ^{137}Ba produced during deuterium permeation by some nuclear transmutation occurring on/in the uppermost of multi-layered Pd sample. The single couple of Pd/CaO thin films on Pd foil might contribute to induce production of an element with mass number 137. This would imply a transmutation of 4 mass number increasing before ^{141}Pr production.

References

1) Y. Iwamura, T. Itoh and, M. Sakano, Jpn. J. Appl. Phys., **41**, 4642 (2002).
2) H. Yamada, S. Narita, H. Onodera, H. Suzuki, N. Tanaka, T. Nyui and T. Ushirozawa, Proc. 5th Meeting of Japan CF Research Society, p. 69 (2004).
3) G. H. Miley, H. Hora, A. Lipson, S. Kim, N. Luo, C. H. G. Castano G and T. Woo, Proc. 9th International Conference on Cold Fusion, p. 255 (2002).
4) T. Ohmori, H. Yamada, S. Narita and T. Mizuno, Proc. 9th International Conference on Cold Fusion, p. 284 (2002).
5) J. Tian, B. Liu, X. Z. Li, W. Z. Yu, M. Y. Mei, D. X. Cao, A. L. Li, Jing Li, Y. G. Zhao and C. Zhang, Proc. 9th International Conference on Cold Fusion, p. 360 (2002).
6) H. Yamada, S. Narita, S. Taniguchi, T. Ushirozawa, S. Kurihara, M. Higashizawa, H. Sawada, M. Itagaki and T. Odashima, Proc. 6th Meeting of Japan CF Research Society, pp. 48 (2005)

Possibility of Inducing Selective Transmutation in Discharge Experiment

S.Narita*, H.Yamada, D.Takahashi, Y.Wagatsuma, M.Itagaki, S.Taniguchi

Department of Electrical and Electronic Engineering, Iwate University

Morioka, Iwate, 020-8551, JAPAN

* narita@iwate-u.ac.jp

ABSTRACT

In the condensed matter nuclear science, it is one of the most interesting topics to clarify the mechanism of selective transmutation just as Cs to Pr observed in deuterium permeation experiments with Pd/CaO multi-layered samples. For establishing the reaction model theoretically, it is quite important to reproduce the phenomenon with various methods and evaluate it quantitatively. Several researchers have independently tried to confirm the reaction and some positive results have been already reported. We have also attempted to induce selective transmutation in discharge experiment with deuterium gas, taking into account the key items mentioned in the permeation method (e.g. multi-layered sample structure, deuterium fluence, and so on). Although clear evidence for the selective transmutation has not been found up to now, some phenomena supposed to be a symptom of nuclear reaction has been observed in our experiments.

Keywords : Glow discharge, Corona discharge Multi-layered sample, Pd/CaO, Selective Transmutation

1. Introduction

We have performed discharge experiments in which Pd or Pd deuteride electrodes were exposed in high purity deuterium gas under various conditions; the pressure of deuterium in the chamber, electrode shape, duration time and so on. In such experiments, we have observed the nuclear products and anomalous gamma radiation with energy around ~100 keV, and it was suggested that some short-lived radio isotopes was produced [1,2]. However, the reproducibility of the phenomena was rather poor and we have not specified the origin of the radiations.

Besides the discharge experiments, there is a well-established technique for the study of low energy transmutation in condensed matter, that is, deuterium permeation method using multi-layered Pd/CaO complex sample. In the method, the transmutation from Cs to Pr, Sr to Mo and Ba to Sm were observed with good reproducibility [3,4]. Although the reaction mechanism has not been clarified theoretically, it has been claimed that sufficient D flux in the permeation through the sample and Pd/CaO multi-layered structure of the sample, especially existence of the CaO layer, are necessary for triggering the phenomenon in the method.

In the present study, considering those experimental results, we performed transmutation test using deuterium gas with a Pd/CaO multi-layered cathode on which Cs atoms are deposited, and searched for peculiar phenomena which suggest occurrence of nuclear reactions especially for Pr production by the transmutation from Cs. In addition, the possibility of other elements production as the evidence of a nuclear reaction was investigated. According to recent reports, laser irradiation of a deuterated metal sample is supposed to initiate and/or amplify the nuclear effect in condensed matter, although the power is just a few 10 mW [5,6]. Then, we also tested the effect of laser irradiation of the cathode sample during discharge.

2. Experiment

In the present experiments, we tested two discharge conditions; the glow discharge under low deuterium pressure with a foil type anode and the corona discharge under higher pressure with a needle type anode. The samples used in each experiment were of different types from each other. One is the sample with Pd and CaO thin layers on the Pd substrate (type-1). The other is 5 alternate thin layers of Pd and CaO on the Pd substrate (type-2), which has the same structure as that used in the permeation experiment by Iwamura *et al.* [3]. The type-1 and type-2 samples were used for the glow discharge

Run #	Cathode	Anode	D_2 pressure	Voltage	Current	Time [hour]	Laser
1	Type-1	Au foil	1 Torr	400-600V	~1mA	~170	ON
2						~170	OFF
3	Type-2	Pd wire	1 atm	~10000V	~4mA	~70	ON
4						~70	OFF

Table 1: Experimental conditions

experiment and the corona discharge experiment, respectively.

The sample was prepared in the following procedure. The Pd foil (12.5mm x 12.5mm x 0.1mm) was washed with acetone and aqua regia. For the type-1 sample, 10-nm CaO and 40-nm Pd layers were formed on the Pd foil by Ar ion beam sputtering. As the type-2 sample, five-fold alternate layers of 2-nm thick CaO and 20-nm thick Pd were formed on a Pd substrate by sputtering. The fifth, uppermost, Pd layer was made thicker: it was 40 nm. The thickness of CaO and Pd layers was adjusted by sputtering time. Onto the sample, Cs was deposited by an electrochemical method with Cs_2CO_3 solution.

For the discharge, the sample was placed in the cell as the cathode. The cell made of Pyrex glass has a spherical shape with a volume of ~1500 cm^3. The thickness of the glass is 5 mm. The cell is connected to a vacuum system through the port so that we can drive out the gaseous impurities in the cell and control the pressure inside the vessel. A Au foil (0.1 mm in thickness) for the glow discharge experiment or a Pd needle (0.2 mm in diameter) for the corona discharge was used as the anode.

Under the discharge, it is possible that the elements on the cathode surface are scattered by sputtering, so that small amount of elements produced by the nuclear reactions (if it happens) would be lost. In order to detect such elements, a highly pure Au foil (5mm x 10mm x 0.1mm) was placed 2 cm away from the cathode. One of the surfaces of each foil faced to the cathode to receive the elements sputtered. The Au foil is called "Au side-foil" hereafter.

After the discharge, the elemental composition of the cathode sample was analyzed by the inductively coupled plasma mass spectrometry (ICP-MS) and atomic emission spectrometry (ICP-AES). These are used for measuring Cs and Pr density on the sample and identifying other elements. The sensitivity of ICP-MS is so high that it can detect the element with a density as small as 0.1 ppb. The ICP-AES is less sensitive and it was mainly used for checking qualitatively the elements to be analyzed by ICP-MS in qualitative analysis. In pre-processing for ICP-MS and ICP-AES analyses, the multi-layered cathode sample was immersed in 1 cc of ultra pure nitric acid for 30 s, and the elements on/in the sample were dissolved in it. Then it was diluted by adding pure water to become totally 50 cc. This sample solution was analyzed by ICP-MS and ICP-AES. We evaluated the quantity of each element by the density of the elements measured in this solution

The composition of Au side-foil was analyzed by time-of-flight secondary ion mass spectroscopy (TOF-SIMS). In the analysis, we checked Pr signal and any other elements detected by ICP-MS and ICP-AES. Moreover, we searched for all elements and investigated the anomaly in the isotopic abundance.

For investigating the effect of laser irradiation, we utilized a semiconductor laser (690 nm in wave length and ~20 mW in output power) placed outside of the discharge cell. The whole area of cathode was irradiated during the discharge. Taking account of the reflection and absorption of photons by the glass cell, the power at the cathode surface was supposed to be a few mW.

Table 1 shows the summary of run conditions. Four types of condition were tested in this study. The run #1 and #2 were glow discharge, and run #3 and #4 were corona discharge.

From the results of permeation experiments, the conversion rate of Cs to Pr is thought to be determined by the deuterium flux: a sufficient deuterium flux is an important factor to obtain a significant yield. Here we assume that the current is dominated by D ions and the discharge area on the sample is ~1 cm^2, about 10^{22} D ions were incident on the cathode during the discharge. From the results of the permeation experiment, Iwamura *et al.* has estimated the cross section of Cs-to-Pr transmutation and its conversion rate assuming the flux of deuterium permeating through the sample being equivalent to deuterium irradiation current [7]. They found that the conversion rate is proportional to the

average flow rate and is ~0.3 for irradiating ~$3x10^{23}$ deuterium atoms. Considering our experimental conditions (Table 1), roughly speaking, the fluence estimated in our case is comparable to the value which gives ~10 % conversion rate of Cs to Pr in permeation experiment. By ICP-MS analysis, we found that the Cs concentration deposited onto the sample with the electrolysis was normally 10-100 ppb (the uniformity can not be controlled in the present method and varied run by run), then we may expect the Pr density of 1-10 ppb if it is transmuted with a conversion rate of ~0.1.

3. Results

3.1 Cs- to-Pr Transmutation

The Cs and Pr density of cathode samples were quantitatively measured by ICP-MS. No Pr signal was found in any run. Also Cs signal was not appreciable either or very small. They might be lost due to the sputtering in the discharge. No Pr signal was found in ICP-AES results, and this was expected because the Pr density should be below its sensitivity, when we take into account of the initial density of Cs on the sample and the conversion rate deduced from the D fluence.

The Au-side foils were analyzed by TOF-SIMS. Figure 1 and Figure 2 show the spectra obtained under each discharge condition. No clear signal at the mass number 141 corresponding to Pr mass was found. For the most samples, sputtered Cs signals were observed at the mass number 133. The peaks observed at the mass numbers mentioned above are possibly due to molecular ions and/or their fragments.

3.2 Production of other elements

In qualitative analysis of ICP-MS and ICP-AES, we found some candidates of elements produced during the corona discharge as shown in Table 2. In the table, the elements which are not detected in the reference sample are only listed. On/in the sample subjected to the corona discharge without laser irradiation, traces of Ga, Ag, Sn, and Ba atoms were recognized in ICP-MS and Te was found in ICP-AES. Since the sensitivity of ICP-MS is much better than that of ICP-AES, Te signal should have appeared also in ICP-MS analysis if it really existed. However, it might be the case that the element really existed only on/in the sample where the element was recorded: the inconsistency might only be a result of a poor reproducibility. So, it is kept in the list as a possible product here. For laser-on run, Ga, Ag, Sn, I, and Ba were found.

The existence of these elements was checked by TOF-SIMS analysis for the Au-side foil. Note that Ga cannot be checked in this analysis because a Ga^+ ion beam is used as the incident beam in TOF-SIMS. For

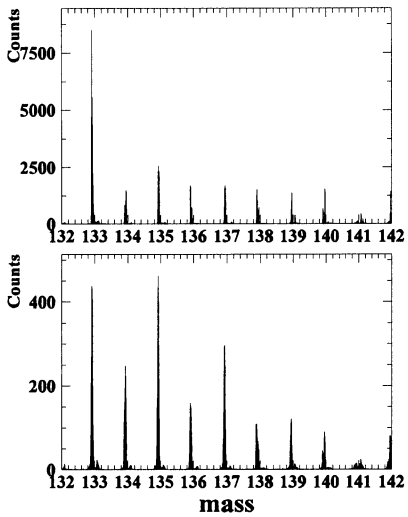

Figure 1: Mass spectrum measured by TOF-SIMS for Au-side foil used in glow discharge experiment. Laser-OFF (TOP) and Laser-ON (BOTTOM)

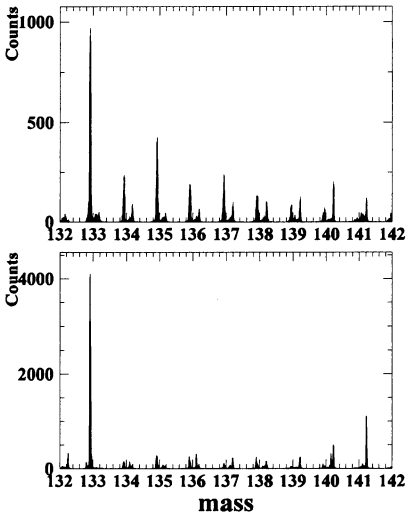

Figure 2: Mass spectrum measured by TOF-SIMS for Au-side foil used in corona discharge experiment. Laser-OFF (TOP) and Laser-ON (BOTTOM)

Laser	Corresponding element	
	ICP-MS	ICP-AES
OFF	Ga, Ag, Sn, Ba	Te
ON	Ga, Ag, Sn, I, Ba	---

Table 2: Elements corresponding to the signals detected by ICP-MS and ICP-AES for the sample used in corona discharge.

	Discharge	Permeation
Particle emission	Detecting prompt n, p, alpha. by DD(D...) reaction, possibly. Emission of X-ray or low energy gamma.	No clear signal for high energy particle emission.
Transmutation	Producing various nuclides. by fusion/fission reactions.	Selective transmutation with a certain rule. e.g. Cs to Pr, Sr to Mo, Ba to Sm. Other foreign elements not identified.
Excess heat	Observed.	Not measured precisely yet.
Multi-layered structure	Effective	

Table 3: Comparison of results of experiments using the discharge and the permeation method.

the laser-off run, isotopes of Ag (^{107}Ag and ^{109}Ag), Sn (^{112}Sn, ^{116}Sn, ^{117}Sn, ^{118}Sn and ^{119}Sn), Te (^{120}Te and ^{130}Te) and Ba (^{130}Ba and ^{132}Ba) were identified. Ag isotopes were detected with natural abundance, and it is possible that the peaks are overlapped by those of ^{106}PdH and ^{108}PdH compounds. As for S, Te and Ba isotopes, the abundances are quite different from natural ones. For the laser-on run, Ag (^{107}Ag and ^{109}Ag) was found with natural abundance and S (^{112}Sn, ^{116}Sn and ^{118}Sn) and Ba (^{130}Ba, ^{134}Ba, ^{135}Ba, ^{136}Ba and ^{138}Ba) were found with anomalous abundances. The signal of Iodine was not identified. We have observed apparent anomaly in isotopic abundance of some elements. However, taking into account of the fact that the signals at large mass number are affected by fragmentation of molecule ions, we should still examine the possibility of miss-identification and/or miss-counting.

4. Discussion

In the present study, clear evidence of Cs-to-Pr selective transmutation was not obtained. In order to clarify the conditions which can induce the Cs-to-Pr selective transmutation, we consider the difference in the experimental conditions between the discharge and the permeation experiments. There are some items; D fluence to the sample, the D energy, temperature of the sample, the discharge characteristics, and others related to the techniques employed in our method.

We assumed that the D fluence to the cathode was sufficient to induce the transmutation, comparing with the result in the previous permeation experiment, as discussed above. However, it is not obvious how much D ions contribute to the electric current, and the fluence might be less than we expected in practice. The energy of incident D ions/atoms widely distributes up to ~1 keV in discharge, while it is thermal in permeation. The sample temperature is usually kept at ~70 degree Celsius in the permeation experiment, but it is much higher in the discharge. The phase state of the Pd is determined by its temperature and the dynamics. The difference in the fluence, the incident particle energy and target temperature could be extremely important. Besides these items, there are problems in our method. The elements on the cathode sample can be sputtered by discharge and the Cs concentration, and therefore the transmutation products, were decreased substantially during the discharge. It was possible that we could not get much Pr yields due to these problems.

We have regarded these as the possible reasons why the Cs-to-Pr transmutation was not induced significantly in our method. Meanwhile, several kinds of nuclear phenomena have been reported even in the discharge method by many researchers. The phenomena are supposed to be resulting from some types of nuclear reactions. So, we review the phenomena observed for each method.

In the discharge method, especially in gas phase, the emission of neutrons and/or protons has been observed and it is supposed to be resulting from both conventional DD fusion at the low energy and multi-body D fusion. In fact, discharge method has been used for the systematic study of low energy DD fusion (<10 keV) [8]. Also, low energy gamma rays or X-rays emission has been observed [9,10]. It may suggest the production of short-lived radio-isotopes. As for the transmutation, the generation of various nuclides has been observed, which suggests both fusion and fission like reactions are taking place in the discharge [1,10,11]. However the selectivity in the transmutation has not been clarified.

In the permeation experiment, any radiation or the evidence of DD reaction has not been reported. However, the selective transmutation with some rule has been observed with good reproducibility, without producing a variety of nuclides. The effectiveness of using multi-layered sample is commonly claimed in both discharge and permeation.

The summary of experimental results reported for the discharge and the permeation methods is shown in Table 3, and we found that the phenomena observed in each method were clearly characterized. Here, we assume a scenario that there are at least two types of nuclear reactions. At first, DD fusion and/or multi-body D fusion occurs, then a fusion/fission reaction or a selective transmutation is initiated by the products of the primary reaction. For the primary reaction, a kind of conventional DD fusion with hard radiation is likely to be induced in the discharge rather than in the permeation, while multi-body fusion without radiation is more likely to happen in the permeation. As the result, the secondary reaction in each method is different. In the discharge, nuclear reactions with a variety of products can occur, while, specified transmutation can be induced in the permeation. We should accumulate and sort out the experimental results, then discuss applicability of this assumption as well as some theoretical models proposed so far[12-14], in the future study.

5. Summary

We have attempted to induce a selective transmutation of Cs-to-Pr in deuterium gas discharge using multi-layered Pd/CaO cathode of the same structure as that used successfully in the gas permeation experiments, but we have not found the evidence of Pr production.

Identification of some element production was obtained in corona discharge. Further studies are necessary to identify such candidates correctly by various methods. Irradiating the deuterated metal with a laser is an interesting method for enhancing the reaction rate of the low energy nuclear reaction in condensed matter. We made the first trial to investigate the effect of irradiating the cathode sample with the semiconductor laser in the discharge experiment, but without positive symptom showing the effect.

The experimental results for the discharge and permeation methods were characterized, and we found that the selective transmutation like Cs-to-Pr is more easily induced in the permeation conditions.

In the future study, we will continue to investigate the possibility to induce Cs-to-Pr selective transmutation using the discharge method with a modified/improved experimental arrangement. Some problems inherent in out experimental configuration should be solved. Then, we will get the answer to the question whether the Cs-to-Pr transmutation can be induced even in the discharge. Furthermore, we will clarify the mechanism of the nuclear reactions induced in the discharge.

References

1. A. Arapi et al., Jpn. J. Appl. Phys. (2002) L1181.
2. S. Narita et al., Proc. of JCF5 (2004) 14.
3. Y. Iwamura et al., Jpn. J. Appl. Phys. (2002) 4642.
4. Y. Iwamura et al., Proc. of ICCF11 (2006) 339.
5. D. Letts, Proc. of ICCF10 (2006) 159.
6. V. Violante et al., Proc. of ICCF12, in press.
7. Y. Iwamura et al., Proc. of JCF5 (2004) 60.
8. A.G. Lipson et al., Proc. of ICCF10 (2006) 635.
9. A.B. Karabut et al., Proc. of ICCF11 (2006) 253.
10. A.B. Karabut et al., Proc. of ICCF10 (2006) 99.
11. I.B. Savvatimova et al., Proc of ICCF11 (2006) 438.
12. A. Takahashi et al., Jpn. J. Appl. Phys. (2000) 7031.
13. A. Takahashi, Proc. of JCF6 (2005) 61.
14. A. Takahashi, Proc, of JCF6 (2005) 66.

Electrochemical Compression of Hydrogen inside a Pd-Ag Thin Wall Tube, by Alcohol-Water Electrolyte

FRANCESCO CELANI[1*], A. SPALLONE[1], P. MARINI[2], V. DI STEFANO[2], M. NAKAMURA[2], V. ANDREASSI[1], A. MANCINI[3], E. RIGHI[1], G. TRENTA[1], E. PURCHI[2], U. MASTROMATTEO[7], E. CELIA[6], F. FALCIONI[6], M. MARCHESINI[6], E. NOVARO[6], F. FONTANA[5], L. GAMBERALE[5], D. GARBELLI[5], P.G. SONA[4], F. TODARELLO[2], G. D'AGOSTARO[1], P. QUERCIA[1],
1 INFN-LNF Via E. Fermi 40, 00044 Frascati, Rome, Italy * francesco.celani@lnf.infn.it
2 EURESYS, Via Lero 30, 00129 Rome, Italy
3 ORIM SpA, Via Concordia 65, 62100 Piediripa, Macerata, Italy
4 Via S. Carlo 12, 20090 Segrate, Milan, Italy
5 Pirelli Labs SpA, Viale Sarca 222, 20126 Milan, Italy
6 CSM SpA, Via di Castel Romano 100, 00129 Rome, Italy
7 STMicroelectronics, Via Tolomeo 1, 20010 Cornaredo, Milan, Italy

Abstract.

Yoshiaki Arata (Osaka University) has since 1955 developed and on 1994 patented in Japan (also USA, N° 5647970, 1997) a procedure for producing ultrahigh pressure H/D gas, based on the electrolytic loading of a hollow cathode made of a Hydrogen and/or Deuterium absorbing material (Pd).
The truthfulness of Arata's results and even the real existence of Arata's device have been recently challenged by an influent Italian scientist and suspected to be merely a *"computer simulation experiment"*.
Accordingly, we decided to replicate the Arata experiment in order to confirm his results. A further reason for such a replication is due to the consideration that the electrolytic compression of Deuterium (D) is the basic for most of the Cold Fusion experiments. Moreover, the experiment allows for a direct evaluation of the D_2 (or H_2) pressure inside the hollow cathode, without making use of indirect measurements, like those based on the well-known "Baranowsky curve" (change of the Pd electrical resistance, versus D or H absorption).
The cathode was a Pd-Ag (75%-25%) tube, closed at one end (diameter 10mm, total length 10cm, useful length exposed to electrolyte 9cm) with a very thin wall (thickness about 50μm), previously used as a Hydrogen purifier (home-made by Dr. Silvano Tosti: ENEA, Frascati, Italy).
The effective volume of the Pd-Ag tube (partially filled with a porous ceramic tube, in order to avoid the vacuum collapse of the Pd-Ag tube), pipes, valves and pressure gauges was about 18ml.
The anode was a Pt (purity >99.99%) wire (diameter 0.25mm) wounded as a pseudo-cylindrical spiral of radius about 4cm. The total length of the Pt wire was about 200cm, number of turns about 5.
The volume of the electrolyte was about 2000ml. The cell was commercial glass (Pyrex type). The solution, according to our long experience in this field, was alcohol-water type (C_2H_5OH 85-90%, H_2O 15-10%) electrolyte. $Th(NO_3)_4$ (in 5% wt HNO_3), $SrCl_2$ and Hg_2SO_4 salts were added. Th and Sr salts were added at an amount of some tens of micromoles, and the Hg ion at an amount of only a few micromoles. The electrolytic current density was as low as 2-10mA/cm^2. The anode-cathode voltage was 20-136Volts. During the experiment the cell temperature ranged between 20 and 60°C.
The Pd-Ag tube surface was previously mechanically cleaned (by fine, silica based, sandy soap), acetone rinsed, washed several times with distilled water, and finally treated at a temperature of about 450°C for a complete degassing.
Before the cathodic H loading operations, the surface was "activated" by proper cycles of anodic oxidation. Vacuum was made inside the tube cavity, connecting pipes, pressure gauges and valves.
We reached a maximum value of pressure inside the hollow cathode of about 8.5atm (absolute 9.5). The maximum value of 8.5atm was imposed by the mechanical strength limit of the 50μm wall of the tube.
We would like to note that the faradic efficiency, i.e. the amount of hydrogen gas produced by the electrolytic current (collected and pressurised inside the tube) reached values as large as 15--20%; the efficiency strongly depends on the Pd surface conditions, type of electrolyte, current density, and temperature.
In comparison, the device invented by Arata (using usual D_2O - LiOH 0.1M electrolyte, tube 2.5mm thick) had efficiency on the order of 0.5--2.5%.
Arata was able to reach pressures as high as several hundred atmospheres; up to now, we can't say anything regarding the capability of our electrolyte in obtaining such a high pressures.
In a further set of experiments we are going to use a thicker (0.250mm) ultra-pure (99.99%) Pd tube, specially developed for this purpose by ORIM SpA Company (Italy).
In conclusion:

1) The effectiveness of the original device developed by Yoshiaki Arata since 1955 was fully confirmed;
2) The surprisingly high Faradic yield for H-D loading in hydro-alcoholic electrolyte might open some ways toward practical applications;
3) The measurement of H_2 pressure in the hollow cathode directly confirms our previous results (H/Pd-D/Pd close to one, measured by the change in resistivity of the Pd cathode, and high faradic efficiency), obtained by electrochemical loading of long (typically 60cm) and thin (diameter 50μm) Pd wires in C_2H_5OH-H_2O or C_2H_5OD-D_2O electrolytes.

Following the positive results of our experiment we received the acknowledgement of a large part of the Italian scientific community formerly sceptical about all that concerns Cold Fusion.
Moreover, one of the most diffuse and influential (in Italy) INTERNET blog about environment & clean energy (http://www.vglobale.it) has adopted, as front page for 3 months, the photo of the experimental apparatus build at INFN-LNF. The number of down-loads of such photo (and 2 pages of explanations/comments) was quite large (increases of over 500 access/day of the blog, up to now). Such blog is certified by "spazio RP" and was established about 9 years ago.

1 Introduction and Motivations

It is well known that any kind of experiment, based on the anomalous effects (the so called "Cold Fusion") in Condensed Matter Nuclear Science (CMNS) has, as a pre-requisite, the forced absorption of Deuterium (D) and or Hydrogen (H) inside or at the surface of some specific metals at values well over the thermodynamic equilibrium limits. Such metals (M) are usually: (for D loading) Palladium (Pd) and Titanium (Ti); (for H loading) Nickel (Ni).
The most diffuse method for H or D overloading is the electrolytic one.
* The term "overloading" is used to point out that the value of the H-D/M ratio is larger than that is allowed at the normal equilibrium conditions. Consequently, the extra H or D forced inside the M is in a meta-stable condition, i.e. they were in general rapidly released when the loading driving force is removed.

1.1 The Baranowsky curve

In the case of Pd loading, by adopting a proper wire geometry, it is possible to evaluate the amount of H or D absorbed into the bulk of the metal through the relationship between the H-D/Pd ratio and the value of the resistivity of the actual (H-D)–Pd system ("Baranowsky curve").
We remark that Prof. B. Baranowsky developed such curve since 1969 (further elaborated in 1982 and 1990) by measuring the H_2-D_2 absorption in Pd rods (up to 50,000 bar), at a temperature close to ambient one. Because of the low diffusion speed due to the relatively large thickness of the used Pd samples, each set of experiment, from vacuum up to 50,000 bar, takes over 100 days of measurements.
It's noteworthy that the gas pressure method is an experiment performed in *static equilibrium condition*, i.e. the Pressure-Concentration-Temperature relationships are always satisfied.
Recently (ICCF12) Dr. Mike McKubre (Ref.1) has performed a comprehensive review of such an argument.

1.2 Electrolytic loading

As previously remarked, the electrochemical Pd loading is the most frequently adopted technique to achieve high (H-D)/Pd ratios; in fact, the cathodic discharge of H-D ions on the Pd surface generally requires a certain over-voltage (with respect to the thermodynamic value for the water decomposition) that can be considered equivalent to a very high H-D pressure; in an open electrolytic cell. It is therefore possible to achieve in a simple way (H-D)/Pd loading ratios similar to that obtained in sealed cell operating at a very high H-D pressure. In this case open-cell means that the pressure inside the electrolytic cell is controlled as to maintain a small over-pressure (usually less then 0.1 bar) needed to avoid that the light water humidity (always present in the air) may contaminate the heavy water (or others deuterated compounds) of the electrolyte.

1.3 The Arata experiments

Very recently, during ICCF12 (November 27--December 2, 2005, Yokohama-Japan), Prof. Yoshiaki Arata (Osaka University), Ref. 2, explained in some details about his recent experiments: high-temperature & high-pressure diffusion of D_2 through a thick Pd rod with a closed "reaction chamber" inside and, for sake of comparison, the previous experimental set-up (based on the forced diffusion of D_2 through a thick Pd rod using an usual electrolytic open-cell).
* We recall that the experimental set-up developed by Arata and co-workers was named "Double-Structures Cathode" (D-S Cathode) and in some experiments, after very long time (some months) of electrolysis at high current density (about 500mA/cm^2) he measured, inside the thick wall reaction chamber, that the pressure was very large (1000 bar and over); excess heat was detected as well as traces of ^{4}He. No photo of the experimental set up, type and position of the pressure gauges are unfortunately available (1990-2004).
Mike McKubre, another well known researcher in the field of CMNS, claimed to have reproduced in USA, in 1999-2000, some of the anomalous effects found by Arata using a Pd cathode lent to him by Arata himself. Unfortunately, no gauge pressure was installed in the D-S Cathode, so no direct measurement was possible.
During ICCF12, Arata made known to everybody that the D-S Cathode experimental set-up was developed by himself since 1955, in the framework of Hot Fusion studies (at Osaka University), and later world-wide-patented in 1994 (Ref. 3). Moreover, at the beginning of the talk, he further specified that he developed such a "high pressure deuterium generator" because in 1954-1955, after the second World War, it was not possible to buy pressurised deuterium gas in Japan even for small amount needed for scientific Hot Fusion experiments. Likely, the Arata devices worked well enough to first observe D-D Hot Plasma Fusion in Japan in 1955 and he was (and still is) very proud of both such scientific and technological achievements.
We arbitrarily named the "work of high pressure deuterium generator" as the *"Arata_1955 experiment"*.
* The experimental results presented by Arata at ICCF12 were particularly impressive; he showed that it was possible to get continuous excess heat in a pressurised (about 70bar) Pd cell, where few grams of nano-particles of Pd dispersed in a matrix

of ZrO_2 are located. The estimated excess heat, by comparison with blanks, was on the order of 10W, at about 190°C. Despite the starting-up from the ambient temperature in somewhat heat-leaking condition, net input power to the reactor was not necessary to maintain excess heat production.

1.3.1 Distribution-in-Italy of Arata's experimental reports and reactions

The experimental results, together with the full patent of 1994, were immediately reported and diffused in Italy through a mailing-list (over 130 addresses, F. Celani is the manager) of people interested in Condensed Matter Nuclear Science. Obviously, most of the people inserted in the mailing-list judged the Arata results very interesting, although some criticized the CMNS experiments in-toto.

* One of the Researchers interested in critics is an important and very influent Nuclear Chemist: Prof. Camillo Franchini. He was Director (over 20 years), of the Laboratory of Nuclear Chemistry and of the Nuclear Reactor installed at the "**C**entre for **M**ilitary **A**pplications of **N**uclear **E**nergy", (CAMEN) S. Piero a Grado (near Pisa), Italy. Later, the CAMEN was renamed CISAM.

* At present, he is the manager of another mailing-list whose main aim is to disprove most of the very innovative results coming out from several advanced fields of research, in Chemistry, Physics and Biology in particular.
BTW, he is one of the strongest opponents to the so-called "Italy-Japan Project" for a physical remediation of nuclear wastes (Ref.4). Aim of this project is to evaluate the effectiveness of the method developed (since 2001 and continuously improved) by Yasuhiro Iwamura (Mitsubishi Heavy Industries, Yokohama, Japan), using natural Sr and Cs (Ref. 5), also for the remediation of the radioactive ashes (i.e. ^{90}Sr, ^{134}Cs, ^{137}Cs) coming out from nuclear power plant as fission products.
We recall that Iwamura showed transmutation with some amounts (of the order of 10^{15} Atoms/cm^2) of natural strontium (transmuted to stable molybdenum) and caesium (transmuted to stable praseodymium) using pressurised deuterium gas, permeating through a sophisticated multilayered sample of Pd-CaO-Pd, for about 2 weeks.
We remark that the mailing list of Prof. Franchini includes, among others, several politicians, editors of journals/newspapers, makers of scientific TV programs.

* Prof. Franchini, together with other important University teachers, claimed (and, de-facto, shared such opinion to several thousand people) that both the Iwamura experiment (the transmutation of natural Sr and Cs) and the Arata one (compression of H, D by electrolysis) are just "*computer simulation experiments*" because they violate the rules of nature. In other words, both Iwamura and Arata, according to Prof. Franchini, deceived the whole scientific community and specially the Italians. In particular, Franchini and his colleagues claimed that it was impossible to get inside a hollowed and closed Pd cathode, using an open cell configuration (i.e. at 1 bar of external pressure), a pressure larger then few bars. If such situation would have happened, it means that Arata has invented the "Maxwell devil" and as a consequence he, and/or whoever else could reproduce the experiment, have to get immediately the Nobel Price. Because of such critics several doubts/ironies grew in Italy coming from researchers/opinion-makers/industrialists. The meaning was: ***all*** the experiments, about Cold Fusion, were performed by incompetent or even cheating scientists.

1.3.2 Planning replication of the Arata_1955 experiment

As a consequence, we decided, at the end of February 2006 to start, as soon as possible, at Frascati National Laboratory of INFN, a scientific rush-program, in order to reproduce the Arata_1955 claims, at least with a pressure inside the cell not larger than some bars.

* At that time, the only Pd tube immediately available was a Pd-Ag alloy (Pd at 75%) tube with a very thin wall (only 50μm) and 10mm of diameter: it was manufactured by a cold-rolling and diffusion welding procedure, which is patented (Ref. 6). It was used, for long time, as high temperature (300-400°C) membrane for gas (hydrogen) separation-purification and was developed by Dr. Silano Tosti at ENEA-Frascati (Ref. 7, Ref. 8).

* Moreover, thanks to long time lasting scientific collaboration, among CMNS, with ORIM SpA, we asked to prepare an extruded tube of ultra-pure Pd (>99.99%). ORIM is one of the few Companies, in Italy, having long experience about melting and purification of precious metals, specifically Ag, Pd and Pt.
The reasons about the use of ultra-pure Pd tube are essentially:
- to compare the results with respect to the Pd-Ag tube;
- to get higher values of pressures due to thicker wall (250μm instead of 50μm) and reduced diameter (8mm instead of 10mm).
The expected disadvantages of pure Pd tube, with respect to the Pd-Ag one are:
- worse mechanical performances (due to lower tensile strength and higher hydrogen embrittlement behaviour);
- lower diffusion speed.

2. Experimental Considerations and Set-up

According to our scientific rush-program, we built an experimental apparatus as simple as possible. In Fig.1, 2 and 3 are shown photographs, respectively, of Pd-Ag tube before use, an overview of the whole set-up, the Pd-Ag tube at the end of the 3 months experiments.

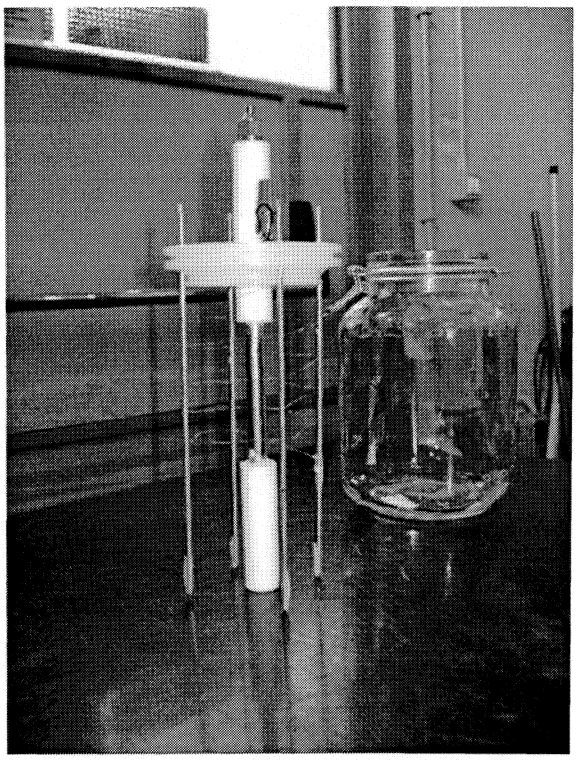

Fig.1 Photo of the Pd-Pt cell. At the centre there is the Pd–Ag tube, with 2 PTFE tube (top and bottom) to avoid contamination (to electrolyte) from SS connections. The anode is 250μm Pt wire, rounded on 4 Cu sticks covered by PTFE sheaths. The cell is just a commercial, Pyrex-type, bottle.

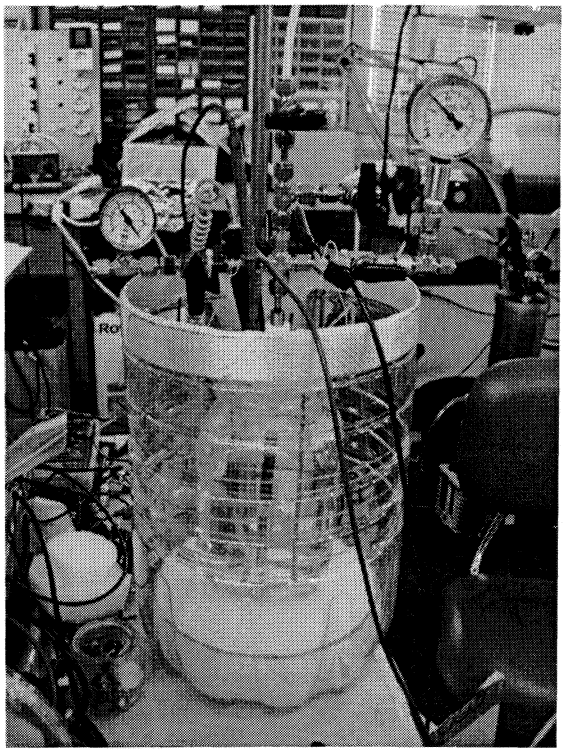

Fig. 2. Photo of the very simple experimental set-up in the first series of experiment (without electronic pressure gauge); The second vessel around the electrolytic cell, transparent plastic (0.5mm tick PET with some fibre –glass reinforcing tape) is filled with tap water and is used for safety reasons in the case of the Pd-Ag tube explosion.

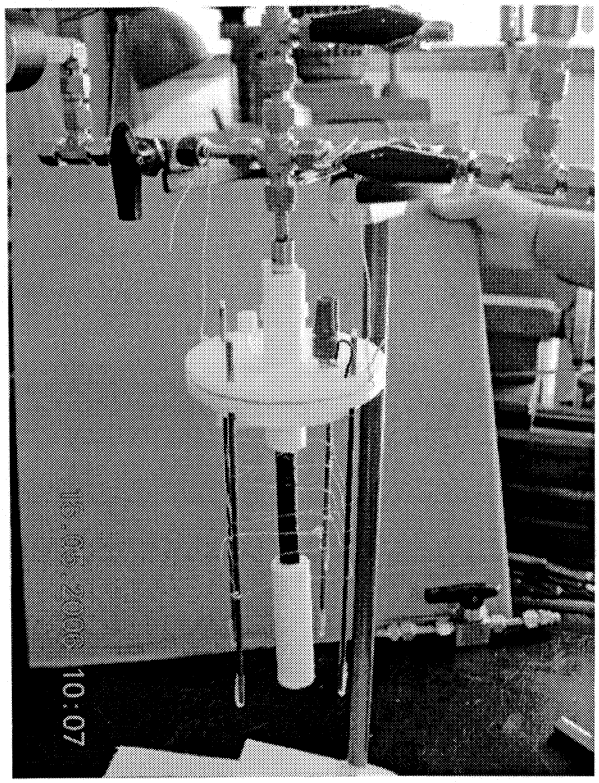

Fig.3. Photo of the Pd-Ag tube after second series of experiments; The cathode, from silver colour, changed to dark one due to salts deposited at its surface.

For pressure measurement, we used both mechanical (needle) gauges and electronic sensors (in the second series of experiments). The gas accumulated inside the tube, cf. Fig.2, can be collected into a very light, rubber balloon: it flies! This confines really full of hydrogen.

2.1 Mechanical characteristics of Pd and Pd-Ag

The maximum pressure allowable, taking into account the tube dimension and the tensile strength of the Pd-Ag, alloy can be evaluated according to the formula:

$$P=(t*\sigma)/r \qquad (1)$$

Where P is the pressure (Pa), r is the tube radius (m), t is the tube thickness (m) and σ is the tangential stress (Pa) in the metal tube, respectively.

In Table-1 are reported, according to Ref. 11 and 15 quoted in Ref. 4, the tensile strength data of annealed and cold worked Pd and Pd(75%)-Ag(25%), at ambient and 400°C temperatures. The positive effect of Ag alloying and worsening of mechanical characteristics (for both Pd and Pd-Ag) due to large temperatures, are evident.

Material	Tensile strength (MPa), T=ambient	Tensile strength (MPa), T=ambient	Tensile strength (MPa), T=400°C
Treatments →	Annealed	Cold-worked	Cold-worked
Pd	150	380	150
Pd(75%)-Ag(25%)	380	690	380

Table-1 Tensile strength data of Pd and Pd-Ag, annealed or cold-worked, at ambient and 400°C

* About the rupture pressure, P_r (MPa), for a 10 mm diameter tube, the calculated (Ref. 4) values, for a fully annealed and heavily cold worked tube, at ambient and 400°C, are reported in Table-2.

	P_r, annealed	P_r, annealed	P_r, cold-worked	P_r, cold-worked
Temperature →	Ambient	400°C	Ambient	400°C
Pd, 50μm	1.50	0.67	3.78	1.68
Pd, 70μm	2.1	0.93	5.29	2.35
Pd-Ag, 50μm	3.79	1.68	6.84	3.04
Pd-Ag, 70μm	5.30	2.36	9.58	4.25

Table-2: Calculated rupture pressure, in MPa, for 10mm diameter tubes (wall thickness of 50μm and 70μm), Pd (100%) and 25%Ag alloy, at ambient and 400°C

* Taking into consideration that Pd-Ag in our usage worked for long time (over 6 months) at very different operating conditions (pressure, thermal stresses, embrittlement due to hydrogenation and thermal cycles), and adopting the usual safety factor (3) about pressurised devices, we decided that never we would allow a pressure larger than 9 bar (10 absolute).

2.2 H_2 Production and absorption

About the evaluation of hydrogen collected into the hollow cathode, we have to consider as follows:

a) As a proton (H) inside the Pd lattice;
b) As H_2 inside the cathode cavity.

a) H absorbed inside Pd lattice:
Pd-Ag tube dimension: radius (R) 5mm; wall thickness 50μm; length (l) 10cm.
The amount of Pd gram atoms is:

$$\text{Pd (gram atoms)} = ((\pi*(R^2-r^2)*l)*\delta)/M_w \quad (2)$$

Where: δ =Pd density (12 g/cc); M_w= atomic weight (106 Amu)

$$\text{Pd (gram-atoms)} =(3.14*(0.500^2-0.495^2)*10)*12)/106=0.01769$$

By considering that the effective amount of Pd is 75% and that the expected H/Pd at 10 bar is about 0.80, the real amount of H gram-atoms in the Pd lattice are: 0.01769*.75*.80=0.0106
As a consequence, the moles of H_2 gas are 0.0106/2=0.0053

b) Moles of H_2 inside the hollow cathode (filled with porous ceramic, because mechanical strength reasons), pressure gauges, valves, connections:
Total measured Volume=18cm^3.
For each bar of H_2 pressure the moles present in the cavity are (at NPT conditions)

$$18/22410=8.032*10^{-4} \text{ Moles of } H_2 \quad (3)$$

The Moles of H_2 gas produced during the electrolysis are proportional to the total amount of charge Q (Coulomb, C) involved: Q = It, if I is constant.
Generally, Q=integral, over time t, of I.
In the formula I is the electrolytic current in Ampere (A), t is the time in seconds (s).
The formula about Moles H_2 produced is:

$$\text{Moles } H_2 \text{ produced}=Q/(2*F) \quad (4)$$

In Formula #4, F is the Faraday constant (96480 C/Moles); the factor 2 is due to the fact the molecule of Hydrogen is H_2.

* The efficiency of the total hydrogen collection (η) is evaluated by the ratio between the sum of H gram-atoms (calculated as H_2) present in the Pd lattice (formula #2) plus the moles present in the cathode cavity (formula #3) over the gas produced during the electrolysis (formula #4).
Separately, it is given the efficiency about the "useful" gas produced, i.e. neglecting the contribution of H-atoms absorbed by the Pd lattice. Such value of η is, obviously, lower than the total one. In our experiments we compare only such, very conservative, values.

3 The cell, electrolytes and experimental results

* The cell was just a commercial glass, Pyrex type. All the other materials used inside the cell were protected by PTFE tube or sheath.

The cell was completely open to environment through a hole for gas escaping.

* Following our long experience (Ref. 9, Ref. 10) on unconventional electrolytes that were able to load thin Pd wires at high value of H, D/Pd, within enough short time, we decided to use our "standard" receipt (ethyl alcohol-water mixtures, concentrations respectively 85-90% and 15-10%) with some amounts of salts of $Th(NO_3)_4$ in 5%wt HNO_3, $SrCl_2$, Hg_2SO_4 at some micro-molar concentrations. The Hg_2SO_4 was added at a concentration about ten times lower than Th and Sr. The only important variation, in respect to our usual salt addition using 50μm tick, 60cm long wire (about $1cm^2$ of surface) was to increase by about a factor 10 of the amounts of salts in order to compensate (partially) for larger surface (exposed area about $27cm^2$) of Pd-Ag tube. Moreover, the total amount of liquid solution was about 2000cc in respect to usual 750-1100cc. The pH was adjusted to about 3 adding, *slowly*, some amounts of, diluted in H_2O, HNO_3.

The anode was a pure (99.99%) Pt wire (diameter 250μm, length about 200cm) rounded on the cathode, see Fig. 1 and Fig. 3. The anode-cathode distance was about 4cm.

* Before starting cathodic regime on Pd-Ag, there were made several cycles of anodic-cathodic conditions in order to activate the Pd-Ag surface.

We make experiments with current density between 2 and (about) $10mA/cm^2$.

The temperature ranged from 20 up to 60°C, depending on current density and conductivity of the solution.

*We experienced a "conversion factor efficiency" of H_2 gas stored inside the tube (see discussion of § 2.2, points a) and b)), in respect of that produced (because electrolysis, see Formula #4) typically of 6-8% (Fig.4).

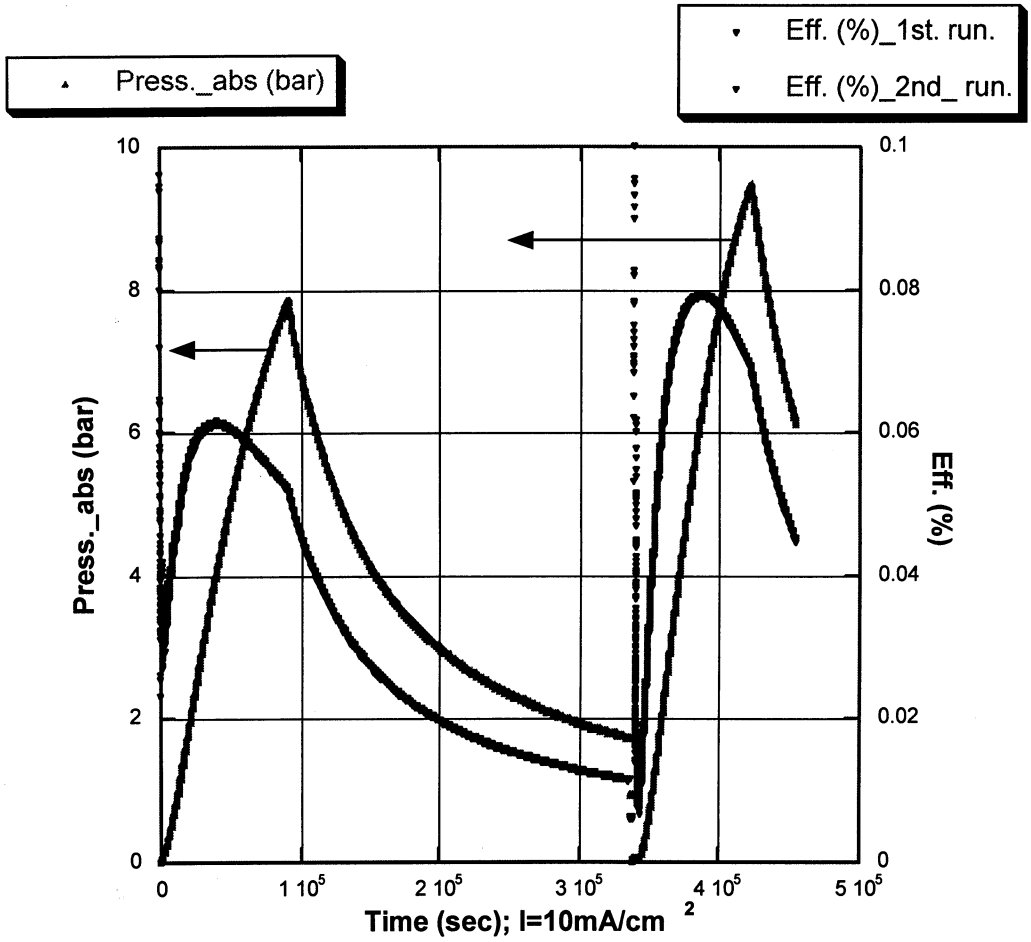

Fig.4. Second series of experiment: electronic gauge pressure (apart the usual mechanical "needle" gauge in parallel). Behaviours of pressure and H_2 gas efficiency, versus time. At time 95000sec the electrolysis was interrupted and the tube was allowed to degas for over 2 days. The second loading cycle, at the same current density, gave better results about pressure and gas loading efficiency (improved from 5.5% at 7.8bar to about 7.5% at 9.5bar). At time 420000sec the electrolysis was interrupted and was studied, again, the degassing behaviour.

Observing in some details the behaviour of second spontaneous degassing, Fig. 4, at time 420000 (current removed), we can easily understand that the Pd-Ag is very permeable even at room temperature: between 6 and 9.5bar in absolute values, the loading and de-loading times are quite similar.
As a consequence, in order to further increase the gas collection efficiency, it can be enough to increase the current density, now at only 10mA/cm^2.

* The best value up to now obtained, about η, was larger than 18% (Fig. 5) at the beginning of the experiment when the cathode was just cleaned and properly activated. At that time we were very prudent about pressure increase: we stopped the electrolysis when the pressure reached a value of over 3.8bar relative to ambient.

* The pressure value of 3.8bar was judged sufficient to demonstrate that ***Arata*** was a ***fully honest Scientist*** and that ***Franchini*** (together with some of his University Colleagues) ***made completely wrong assertions***.

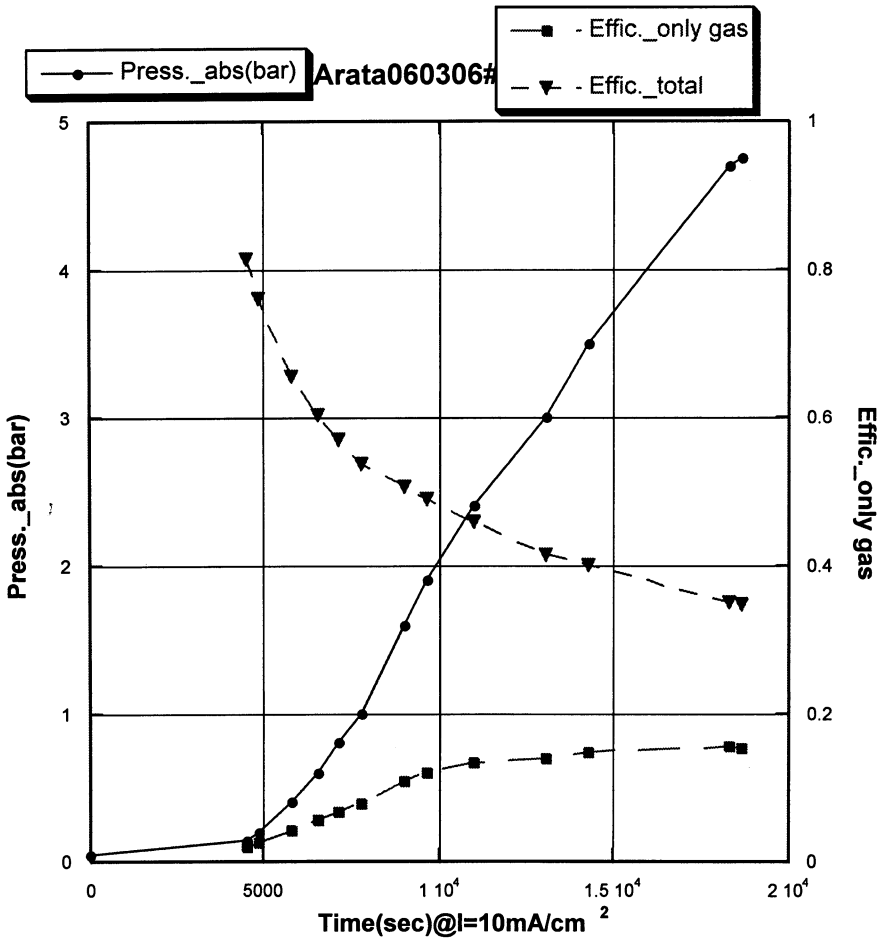

Fig. 5. Behaviour of pressure increasing, from vacuum, at the beginning of the experiment; The current density was 10mA/cm^2. They were shown also the efficiencies of absorption, considering both the total amounts of hydrogen dissolved in the Pd lattice and the only gas in the chamber (the so called η_useful).

* We realised that the efficiency depended strongly on: electrolyte compositions, surface conditions of Pd-Ag, current density, and temperature. Such conditions are very similar to what we found using thin and long Pd wires.
As a comparison, the efficiency of original Arata device, using D_2O and LiOH 0.1Molar, was of the order of 0.5-2.5%. Anyway, Arata was able to get pressure as high as 1000bar (using very tick Pd, several mm) and, up to now, we get a maximum pressure of only 8.5bar (value due to mechanical limits of 50μm Pd-Ag tube).

4 Conclusions

1) The effectiveness of Arata procedure was fully proven by an experimental set-up, which was done by Researchers/Country completely different from original one.

2) Within the limits of pressure up to now explored (up to 9.5bar in absolute value), we have found a conversion efficiency, of H_2 collected inside the hollow cathode, about 5-10 times larger than that reported by Arata in his experiments.

3) The method of gas collection inside a hole is a powerful method to demonstrate directly (and without further questions) that also the electrolysis is able to load, at large amounts (over the thermodynamic limit) of Hydrogen or Deuterium inside proper materials. In other words, also the original claim of M Fleischman and S. Pons about possible nuclear fusion using Pd rods that underwent electrolysis, in D_2O-LiOD solution for long time, can be reinforced by this experiment.

4) The next experiment, now in the calibration state, with ultra-pure (>99.99%) Pd, will add very precious information on the peculiarity of H, D forced absorption (and spontaneous de-sorption) by electrolysis.

5) We have to thank Prof. Camillo Franchini, and his University Colleagues (at Rome and Pisa), that, de-facto, forced us to reproduce the Arata_1955 experiment: we learn, by experiments, very precious information (some of them not written in the text books) that we are happy to share between the world wide CMNS Researchers.

5 Acknowledgements.

We are indebted to Prof. Yoshiaki Arata (Osaka University) that gave us some useful information to avoid "closed ways" about such experiment.

We are glad to Prof. Akito Takahashi (Osaka University) for his continuous scientific advices and strong encouragements.

We can't forget to thank, very deeply, Dr. Silvano Tosti (ENEA-Frascati) that lent us the Pd-Ag tube without hesitations and conditions.

We are glad to Dr. Vincenzo Valenzi (Univ. Roma "La Sapienza") that introduced our work, and problematic, to the Director of INTERNET blog (about environment and clean energy) "Il Villaggio Globale".

References:

1) M.C.H. McKubre, F.L. Tanzella: *Using resistivity to measure H/Pd and D/Pd loading: method and significance,* Invited Paper at ICCF12, Nov.27-Dec.2, 2005, Yokohama, Japan, to be published by World Scientific Publ. Co., 2006.

2) Yoshiaki Arata, Yue-Chang Zhang: *Development of "DS-Reactor" as the practical reactor of "Cold Fusion" based on the "DS-cell" with "DS-Cathode",* Invited Paper at ICCF12, Nov.27-Dec.2, 2005, Yokohama, Japan, to be published by World Scientific Publ., 2006.

3) Yoshiaki Arata: *Method of producing ultrahigh pressure gas,* Japan Patent 6-324459, December 27, 1994, United States Patent: 5,647,970. July 15, 1997.

4) A. Takahashi, F. Celani, Y. Iwamura: *The Italy-Japan Project: fundamental research on cold transmutation process for treatment of nuclear wastes,* Invited Paper at ICCF12, Nov.27-Dec.2, 2005, Yokohama, Japan, to be published by World Scientific Publ., 2006.

5) Y. Iwamura, T. Itoh, M. Sakano, S. Sakai, S. Kuribayashi: *Low energy nuclear transmutation in condensed matter induced by D2 gas permeation through Pd complexes: correlation between deuterium flux and nuclear product,* ICCF10 Conference Proceedings, 2003. pp. 435-446, World Scientific Publ., ISBN 981-256-564-7 .

6) Tosti S, Bettinali L, Lecci D, Marini F, Violante V: *Method of bonding thin foils made of metal alloys selectively permeable to Hydrogen, particularly providing membrane devices, and apparatus for carrying out the same,* Italian Patent IT20RM00412, 25 July 2000, European Patent 1184125 A1, 12 July 2001.

7) S.Tosti, L. Bettinali, V. Violante: *Rolled thin Pd and Pd-Ag membranes for hydrogen separation and production,* International Journal of Hydrogen Energy 25 (2000) 319-325.

8) S. Tosti: *Supported and laminated Pd-based metallic membranes,* International Journal of Hydrogen Energy 28 (2003) 1445-1454.

9) F. Celani, A. Spallone et al: *"Innovative procedure for the, in situ, measurements of the resistive thermal coefficient of H(D)/Pd during electrolysis; cross-comparison of new elements detected in the Th-Hg-Pd-D(H) electrolytic cells"* ICCF11 Conference Proceedings 2004, pp. 108-112. World Scientific Publ., ISBN 981-256-640-6.

10) F. Celani, A. Spallone et al.: *"New procedures to make active, fractal like, surfaces on thin Pd wires."* Invited Paper at ICCF12, Nov.27-Dec.2, 2005, Yokohama, Japan, to be published by World Scientific Publ., 2006.

Possibility of Control on Coulomb Potential

Shigeru Sasabe
Tokyo Metropolitan University (Science and Engineering)
E-Mail: ssasabe@cc.tmit.ac.jp

The largest obstacle for a realization of the nuclear fusion is Coulomb potential. It is found that Coulomb potential may be weakend in some region. The particle called 'electron' in this paper stands for charged particles in general.

1. Lorentz-Dirac Equation

P.A.M. Dirac established the equation of motion for a radiating charged particle in 1938*), that is called Lorentz-Dirac (L-D) equation[1]:

$$mc\frac{\mathrm{d}u_\mu}{\mathrm{d}s} = F_\mu^{\mathrm{ext}} + \frac{2e^2}{3c}u_\nu\left(-u_\nu\frac{\mathrm{d}^2u_\mu}{\mathrm{d}s^2} + u_\mu\frac{\mathrm{d}^2u_\nu}{\mathrm{d}s^2}\right), \quad (1)$$

where s is the four-distance, c the speed of light, m and e are rest mass and charge of the electron, respectively.

In this equation, we should note that

(a) The electron is a charged point particle with no size.

(b) L-D equation is in agreement with the principle of the special relativity, and expressed in covariant form.

Nobody doubts the validity of his equation in the present day.

The energy balance of L-D equation was derived by Plass [2] in 1961:

$$\frac{\mathrm{d}}{\mathrm{d}\tau}\left\{mc^2\left(1+\frac{u^2}{c^2}\right)^{\frac{1}{2}} + V(\boldsymbol{r}) - \frac{2e^2}{3c^3}u^k\frac{\mathrm{d}u_k}{\mathrm{d}\tau}\left(1+\frac{u^2}{c^2}\right)^{-\frac{1}{2}}\right\} = -\frac{2e^2}{3c^3}\left(1+\frac{u^2}{c^2}\right)^{-\frac{1}{2}}\left\{\frac{\mathrm{d}u^k}{\mathrm{d}\tau}\frac{\mathrm{d}u_k}{\mathrm{d}\tau} + \frac{1}{c^2}\left(\boldsymbol{u}\times\frac{\mathrm{d}\boldsymbol{u}}{\mathrm{d}\tau}\right)^2\right\}, \quad (2)$$

where τ is the proper time, and $u^2 = u^k u_k = u_1^2 + u_2^2 + u_3^2$ with $u^k = \mathrm{d}x^k/\mathrm{d}\tau$. Equation (2) means the conservation law of energy:

$$E_{\mathrm{tot}} = K + V - \tau_0\left(\frac{\mathrm{d}K}{\mathrm{d}\tau}\right) + R = \mathrm{const.}, \quad (3)$$

where $K = mc^2\sqrt{1+u^2/c^2}$ $= mc^2(1-v^2/c^2)^{-1/2}$ is kinetic energy, v is the usual velocity, and R denotes the energy of

(*) Dirac considered the divergence problem in quantum field theory, and derived L-D equation in order to avoid the difficulty caused from a point model of the electron.

radiation emission which is equal to time integral of the right hand side of eq.(2). We define r_c as 2/3 times 'Classical electron radius' $r_0 = e^2/mc^2$, then $\tau_0 = 2e^2/3mc^3 = r_c/c$ means the time that the light goes across the radius $r_c = 2r_0/3$.

The nonrelativistic form of L-D eq. is known as Abraham-Lorentz (A-L) equation:

$$m\frac{d\boldsymbol{v}}{dt} = \boldsymbol{F}^{\text{ext}} + \frac{2e^2}{3c^3}\frac{d^2\boldsymbol{v}}{dt^2} \ . \qquad (4)$$

Equation (4) has strange solutions called 'Runaway solution' or 'Violation of micro causality'. Dirac said in his paper [1] that the electron behaves as if it has finite size when interaction works, but whole theory holds the Lorentz invariant in spite of this departure from ordinary relativistic idea.

2. Quantization of A-L Equation

A-L eq. was quantized [3] in order to confirm what happened when the above strange property was introduced into the world of quantum mechanics. In this case, we obtain Hamiltonian from eq.(3).

$$H = K + V + H_{IR} \quad (R \simeq 0) \ , \qquad (5)$$

where $K = -\hbar^2\nabla^2/2m$, and $H_{IR} = -\tau_0\,(dK/dt) = (i\tau_0/\hbar)[K,H]$, in which the Heisenberg equation of motion is used. No radiation emission (or nearly equal zero emission) is supposed in eq.(5). New energy term H_{IR} in the right hand side of eq.(5) has a form of recursion formula:

$$H_{IR} = \frac{i\tau_0}{\hbar}[K,V] + \left(\frac{i\tau_0}{\hbar}\right)^2[K,[K,V]] + \cdots + \left(\frac{i\tau_0}{\hbar}\right)^n[K,[K,\cdots,[K,V]]\cdots] + \cdots \ . \quad (6)$$

Schroedinger equation which we should solve is then

$$\left[-\frac{\hbar^2}{2m}\Delta + V(\boldsymbol{r}) + H_{IR}\right]\psi(\boldsymbol{r},t) = i\hbar\frac{\partial\psi(\boldsymbol{r},t)}{\partial t} \ . \qquad (7)$$

We note that $H_{IR} = 0$ if $V(\boldsymbol{r}) = 0$ or constant. New energy term H_{IR} then arise only when interaction works.

CASE 1: $V(r) = \dfrac{e^2}{r}$ (Electron in fixed Coulomb potential)

We have

$$U(r) \equiv V(r) + H_{IR} = \frac{e^2}{2\pi^2}\int d^3\boldsymbol{k}\frac{\exp(ikr)}{k^2+\varepsilon^2}F(k) \quad (\varepsilon \to +0) \ . \qquad (8)$$

Effective potential $U(r)$ involves a form factor $F(k)$ which means introducing some structure to ordinary Coulomb potential, or to the electron. The form factor

$$F(k) = \frac{1}{1 - iR_c^2k^2} \qquad (9)$$

includes characteristic length R_c, which is defined as geometric mean value of 'Classical electron radius' r_c and 'Compton wavelength' λ of the electron:

$$R_c \equiv \sqrt{\frac{r_c\lambda}{2}} \simeq \sqrt{\frac{e^2}{\hbar c}}\left(\frac{\hbar}{mc}\right) = \sqrt{a}\,\lambda \ , \quad (10)$$

where $a = e^2/\hbar c$ is the fine structure constant. Classical electrodynamics and quantum mechanics, the characteristic constants of both world are fused into the length R_c. We notice the

numerical value of $R_c \simeq \sqrt{\alpha}\,\lambda = \lambda/\sqrt{137}$ in vacuum. We finally obtain[4]

$$U(r) = \frac{e^2}{r}\left[1 - \exp\left(-\frac{r}{\sqrt{2}\,R_c}\right)\cos\left(\frac{r}{\sqrt{2}\,R_c}\right)\right]$$

$$(\text{except for } 0 < \frac{r}{R_c} \ll 1). \qquad (11)$$

We find in the above equation that ordinary Coulomb potential is weakened by H_{IR} energy.

CASE 2: $V(|\boldsymbol{r}_1 - \boldsymbol{r}_2|) = \dfrac{e^2}{|\boldsymbol{r}_1 - \boldsymbol{r}_2|}$ (Two electrons)

Each electron has kinetic energy, respectively; $K_1 = -\hbar^2\nabla_1^2/2m$, $K_2 = -\hbar^2\nabla_2^2/2m$. Their coordinates are $\boldsymbol{r}_1$ and $\boldsymbol{r}_2$, respectively. Effective potential in this case is [4]

$$U(|\boldsymbol{r}_1 - \boldsymbol{r}_2|) \equiv V(|\boldsymbol{r}_1 - \boldsymbol{r}_2|) + H_{IR} = \frac{e^2}{|\boldsymbol{r}_1 - \boldsymbol{r}_2|}\left[1 - \exp\left(-\frac{|\boldsymbol{r}_1 - \boldsymbol{r}_2|}{2R_c}\right)\cos\left(\frac{|\boldsymbol{r}_1 - \boldsymbol{r}_2|}{2R_c}\right)\right] \quad (12)$$

except for $0 < |\boldsymbol{r}_1 - \boldsymbol{r}_2|/2R_c \ll 1$, where H_{IR} is given by

$$H_{IR} = \sum_{n=1}^{\infty}\left(\frac{i\tau_0}{\hbar}\right)^n [K_1 + K_2, [K_1 + K_2, \cdots, [K_1 + K_2, V(|\boldsymbol{r}_1 - \boldsymbol{r}_2|)]]\cdots]. \qquad (13)$$

When two electron are at distance $2R_c$, the bracket in eq.(12) gives

$[1 - \exp(-1)\cos(1)] = 0.8$. Then ordinary Coulomb potential weakens by 80%.

At distance $|\boldsymbol{r}_1 - \boldsymbol{r}_2|/2R_c = 0.1$, the factor $[1 - \exp(-0.1)\cos(0.1)] = 0.1$ gives rapid decrease of Coulomb potential.

CASE 3: $V(r) = \kappa e\,\delta^3(\boldsymbol{r})$ (δ-functional potential)

We consider the interaction of an electron with δ-functional potential. This potential works only at the origin of the coordinate. Sum of $V(r)$ and H_{IR} becomes an extended potential with action radius R_c. If we interpret the interaction between a point electron and the extended potential is equal to the interaction between extended electron with radius R_c and the ordinary δ-functional potential,

---

we can obtain a virtual charge distribution operator $\rho(r)$ of the electron[5]:

$$\rho(r) = \frac{e}{4\pi\sqrt{2}\,R_c^3}\frac{\sin\eta}{\eta}\exp(-\eta)$$

$$\left(\eta = \frac{r}{\sqrt{2}\,R_c}\right) \qquad (14)$$

except for $0 < r/\sqrt{2}\,R_c \ll 1$.

Effective action radius of $\rho(r)$ can be obtained such as

$$< r >= \frac{\int \mathrm{d}^3\boldsymbol{r}\, r\rho(r)}{\int \mathrm{d}^3\boldsymbol{r}\,\rho(r)} = \sqrt{2}\,R_c \simeq R_c\,. \quad (15)$$

Thus the electron has virtual size with action radius R_c when it interacts with others. The present author assures that this is a realization of Dirac's conjecture described in his paper[1].

CASE 4: $V(\boldsymbol{r}) = \dfrac{e^2}{(2\pi)^3}\int \mathrm{d}^3\boldsymbol{q}\,\beta(\boldsymbol{q})\exp(i\boldsymbol{q}\boldsymbol{r})$

(Any potentials expressed by Fourier integral)

In this case, we find [6]

$$U(\boldsymbol{r}) = V(\boldsymbol{r}) + H_{IR}$$
$$= \frac{1}{e}\int \mathrm{d}^3\boldsymbol{r}'\,\rho(\boldsymbol{r}-\boldsymbol{r}')V(\boldsymbol{r}'), \quad (16)$$

where $\rho(\boldsymbol{r})$ is virtual charge distribution operator given by eq.(14). Factor $(1/e)$ is multiplied because $\rho(\boldsymbol{r})$ is normalized as

$$\int \mathrm{d}^3\boldsymbol{r}\,\rho(\boldsymbol{r}) = e. \quad (17)$$

Equation (16) means that the virtual charge distribution $\rho(\boldsymbol{r})$ is always useful to obtain effective potential energy $U(\boldsymbol{r})$ for any ordinary potential $V(\boldsymbol{r})$.

3. Other remarkes

Weisskopf described his interesting point of view in 1939.[7] He said that a particle which obeys Bose statistics requires much larger radius that is

$$a = (\hbar c/e^2)^{-1/2}\cdot(\hbar/mc). \quad (18)$$

We surprise that this is exactly in agreement with R_c of eq.(10). The electron which we used here is a nonrelativistic particle, then it must obey Bose statistics. Weisskopf said also that a theory of particles obeying Bose statictics must involve new features at this length.[7] The results obtained here agree to his conjecture.

The numerical value of R_c are

$$R_c = 1.9\times10^{-12}\mathrm{cm} \text{ for an electron}$$
$$= 1.0\times10^{-15}\mathrm{cm} \text{ for a proton}$$

in vacuum.

Virtual size R_c for the electron is small but is sufficient to overcome the divergence problem of self-mass, and to obtain finite mass change[3]. R_c for the proton is too small to advance nuclear fusion in vacuum. However, R_c may change the value in material. This implies the possibility that we can control Coulomb potential in material.

References

[1] P.A.M.Dirac; "Classical theory of radiating electrons", Proc. Roy. Soc. (London) Vol.A167, 148 (1938).

[2] G.N.Plass; "Classical electrodynamic equation of motion with radiative reaction", Rev. Mod. Phys. Vol.33, 37 (1961).

[3] S.Sasabe; "Finite mass change of electron in altered self-field approach", J. Phys. Soc. Jpn, Vol.59, 449 (1990).

[4] S.Sasabe; "Coulomb potential weakened by self-field of electron", J. Phys. Soc. Jpn, Vol.61, 812 (1992).

[5] S.Sasabe, Y.Okunaga; "Virtual charge distribution of nonrelativistic electron with bound self-field", J. Phys. Soc. Jpn, Vol.64, 1034 (1995).

[6] Y.Okunaga, S.Sasabe, M.Arai; "Virtual charge distribution of the electron with its self-field", Trans. IEEE of Japan, Vol.115-A, 1105 (1995); in japanese.

[7] V.F.Weisskopf; "On the self-energy and the electromagnetic field of the electron", Phys. Rev. Vol.56, 72 (1939).

Mechanism of Nuclear Reaction and Bose-Einstein Condensation in Solids

Ken-ichi TSUCHIYA

Department of Chemical Science and Engineering, Tokyo National College of Technology,
1220-2 Kunugida, Hachioji. Tokyo 193-0997, Japan
e-mail: tsuchiya@tokyo-ct.ac.jp

Abstract: Many deuterons trapped at void in solids may reach Bose-Einstein condensation (BEC) which would result in nuclear reactions. The present study shows mechanism of the cooperation between BEC and nuclear reactions in solids. The transition temperature of BEC is calculated from the density of deuterons trapped at voids. The nuclear reaction rate is calculated from the wave function of condensed deuterons. In the local space of the deuteron storing metal, BEC induces nuclear reactions, and nuclear reactions restrain BEC. The continuous reactions can be explained by this cooperation.

1 DD reaction rate in solid

In our previous work [1], DD reaction rates in Pd void are calculated by applying the equivalent linear two-body (ELTB) method. [2,3] In the ELTB method, N-body ground state wave function for charged Bose particles is written as

$$\Psi(\mathbf{r}_1, \mathbf{r}_2, \cdots, \mathbf{r}_N) \approx \phi(\rho)/\rho^{\frac{3N-1}{2}}, \tag{1}$$

where ϕ is a solution of the Schrödinger equation under the effective potential and ρ is defined as

$$\rho^2 = \sum_{i=1}^{N} \mathbf{r}_i^2. \tag{2}$$

The equation for ϕ is written as

$$\left(-\frac{d^2}{dx^2} + \sum_{m=2}^{M} A_{N,m} x^{2m-2} + \frac{p}{x^2} + \frac{q'}{x} f_{TF} \right) \phi(x) = \varepsilon \phi(x), \tag{4}$$

where the nondimensional variable x is defined as

$$x = \sqrt{\frac{m\omega}{\hbar}} \rho. \tag{5}$$

In this equation, the second term involving $A_{N,m}$ means attractive interaction between a void and deuterons, and the fourth term involving f_{TF} means screened repulsive interaction between two deuterons. [1] They are defined as

$$A_{N,m} = \frac{K^{2m-4} (3N)!! \left(\frac{\hbar}{m\omega}\right)^{m-2}}{2^{m-2} (m-1)! (3N+2m-4)!!} \tag{6}$$

and

$$f_{TF}(\rho) = 3(N-1) \int_0^{\pi/2} d\theta \sin\theta \cos^{3N-4}\theta \times \exp\left(-k\sqrt{2}\rho \sin\theta\right). \tag{7}$$

Using them, the nuclear reaction rate is written as

$$R = -\frac{2\sum_{i<j} \langle \Psi \mid Im V_{ij}^F \mid \Psi \rangle}{\hbar \langle \Psi \mid \Psi \rangle}, \tag{8}$$

where the imaginary part of Fermi pseudopotential V_{ij}^F [2,3] is written as

$$Im V_{ij}^F = -\frac{A\hbar}{2} \delta(\mathbf{r}_i - \mathbf{r}_j). \tag{9}$$

The short-range interactions of nuclear forces between two Bose nuclei are introduced by using δ function. [2,3] The constant A is given by the Bohr radius r_B and the S factor of the nuclear reaction between two deuterons (110 keVb) as

$$A = 2Sr_B/\pi\hbar. \tag{10}$$

The reaction rate is then rewritten as

$$R = \frac{A \sum_{i<j} \int d\mathbf{r}_1 \cdots \mathbf{r}_N \mid \Psi \mid^2 \delta(\mathbf{r}_i - \mathbf{r}_j)}{\int d\mathbf{r}_1 \cdots \mathbf{r}_N \mid \Psi \mid^2} = \frac{AN(N-1)\Gamma(3N/2)}{2\pi^{3/2}\Gamma(3(N-1)/2)} \frac{\int_0^\infty d\rho \{\phi(\rho)\}^2 / \rho^3}{\int_0^\infty d\rho \{\phi(\rho)\}^2}. \tag{11}$$

Using eq.(11), reaction rates are obtained from the ELTB solutions. The ELTB solution also gives the

critical temperature T_c of BEC by the well known formula which is written as

$$T_c = \frac{h^2}{2\pi m k_B}\left(\frac{n}{\zeta(\frac{3}{2})}\right)^{2/3}, \qquad (12)$$

where n is the local number density of Bose particles and $\zeta(Z)$ is the Riemann's zeta function. The probability of the ground-state occupation is given by

$$\Omega = 1-\left(\frac{T}{T_c}\right)^{2/3} \quad for\ T < T_c\ . \qquad (13)$$

If the ground state occupation for $T<T_c$ is taken into account, the fusion rate is given by $R\Omega$. When $T \geq T_c$, no nuclear reactions occur because $\Omega=0$. The trapped site for a deuteron cluster is shown in Fig.1. The calculated results for T_c and R are listed in Table 1. When $N\geq4$ with using non-linear screening [4,5], T_c is higher than the room temperature. The ELTB solution is plotted in Fig.2 for the case of the 5 deuteron cluster trapped at VacO. In Fig.2, we find a sharp peak of the wave function formed at the potential well.

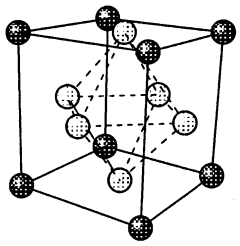

Fig.1 The structure of VacO in fcc lattice. The black and the gray circles represent occupied and unoccupied lattice points, respectively. These defects construct octahedral void, which is called VacO in this paper.

Table 1 The nuclear reaction rate R and the critical temperature T_c for the case of N deuterons trapped at VacO in Pd.

	Thomas-Fermi screening		non-linear screening	
N	T_c [K]	R [10^7sec^{-1}]	T_c [K]	R [10^9sec^{-1}]
3	56	2.1	260	0.3
4	66	3.5	330	0.6
5	76	5.0	400	1.1
6	86	6.7	480	1.6
7	95	8.6	560	2.2

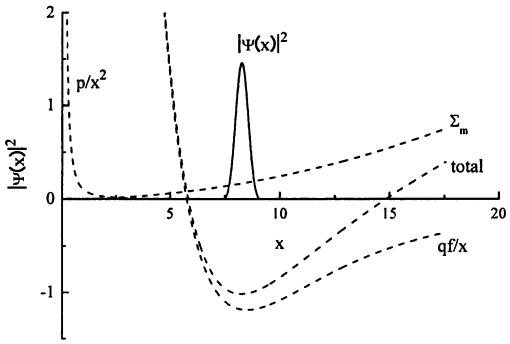

Fig.2 The ELTB solution for the system including 5 deuterons in VacO in fcc Pd. Non-linear screening potential [4,5] is used as the DD interaction. The nondimensional variable x is defined as $x = \sqrt{m\omega/\hbar}\,\rho$, where ω=0.86×10^{14} sec^{-1}. The solid line represents the ELTB solution. The dashed lines represent the potentials normalized by $|\varepsilon|$=|-409|. p/x^2; component divided from the operators for kinetic energy. qf/x; screened DD repulsion potential. Σ_m; the lattice summation for the Coulomb potentials by host Pd ions. (see Ref.1)

In eqs (8) and (9), the imaginary part of the Fermi pseudopotential has an important role for the calculation of the nuclear reaction rate. The short range interactions between nuclei are introduced by the delta function. However, the size of the nuclear-force-effective region should be included in eq.(9) by using $\delta(|\mathbf{r}_i-\mathbf{r}_j|-r_0)$. This process will give more exact reaction rates. This effect will be discussed in the next work.

2 Thermal Conduction

If nuclear reactions occur in solids, heat generated from the reaction center is diffused. In the present work, the thermal conduction from the center of a DD reaction in Pd is estimated. The equation of the thermal conduction in matter is written as

$$\frac{\partial T}{\partial t} = k\nabla^2 T, \qquad (14)$$

where T is the deviation of the temperature from a stationary reference and t is the time from the moment of occurrence of a reaction. The constant k is defined as

$$k = K/C\rho\,, \qquad (15)$$

where K, C and ρ represent the thermal conductivity

(75.5 W/(m·K)), the specific heat (25 J/(mol K)) and the density (12.0 g/cm^3 = 12.0×10^6/166.4 mol/m^3), respectively. The initial condition used for solving eq.(14) is $T=T_0$ in the $d\times d\times d$ cube and $T=0$ for otherwise. In this condition, the parameter d corresponds to the size of the deuteron cluster and the initial temperature is obtained by

$$T_0 = E/CM_0, \tag{16}$$

where E and M_0 represent the energy released by a DD reaction (D+D→^{4}He+ γ +23.8 MeV) and the number of moles in the $d\times d\times d$ cube (=$4/N_A$, where N_A is the Avogadro number), respectively. The periodic boundary condition used for solving eq.(14) is written as

$$X(x) = \begin{cases} 0 & for\ \ 0 \le x < \dfrac{L-d}{2} \\ T_0^{1/3} & for\ \ \dfrac{L-d}{2} \le x \le \dfrac{L+d}{2} \\ 0 & for\ \ \dfrac{L+d}{2} < x \le L \end{cases} \tag{17}$$

and

$$X(x) = X(x+L), \tag{18}$$

where $X(x)$ is the x-dependent component of T under separation of variables;

$$T(x,y,z,t) = X(x)Y(y)Z(z)U(t). \tag{19}$$

A solution using Fourier expansion is written as

$$T = \sum_{n_x,n_y,n_z} C_{n_x} C_{n_y} C_{n_z} \cos(q_x x)\cos(q_y y)\cos(q_z z) e^{-k(q_x^2+q_y^2+q_z^2)t}, \tag{20}$$

where constants are defined as

$$q_i = \frac{2n_i\pi}{L} \quad \text{and} \quad C_{n_i} = (-1)^{n_i}\frac{2T_0^{1/3}}{n_i\pi}\sin\frac{n_i\pi d}{L}. \tag{21}$$

The parameter L represents distance between two neighboring reaction centers. This parameter is obtained by the well known formula for the concentration of Shottky defect in solids. It is written as

$$n/N = e^{-w/k_BT}, \tag{22}$$

where n, N and w represent the number of defects, the number of total atoms and vacancy formation energy (~1 eV), respectively. Assuming a uniform distribution of the trapped sites, the parameter L is obtained by

$$L = \frac{a}{4^{1/3}} e^{w/3k_BT}, \tag{23}$$

where a is the lattice constant of fcc Pd (3.89Å). As the temperature is increased, the concentration of the vacancy is increased and the mean distance between vacancies is decreased. They are shown in Figs 3 and 4. The calculated result for the thermal conduction is plotted in Fig.5, where a rapid relaxation can bee seen.

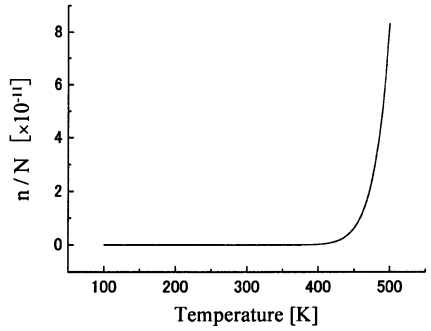

Fig.3 The temperature dependence of the vacancy concentration n/N, where n and N mean the number of the vacancy and the number of the total atom, respectively.

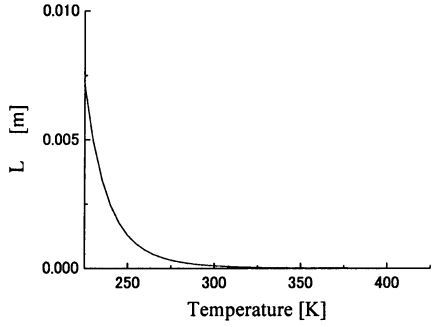

Fig.4 The mean distance between the vacancies as a function of the temperature

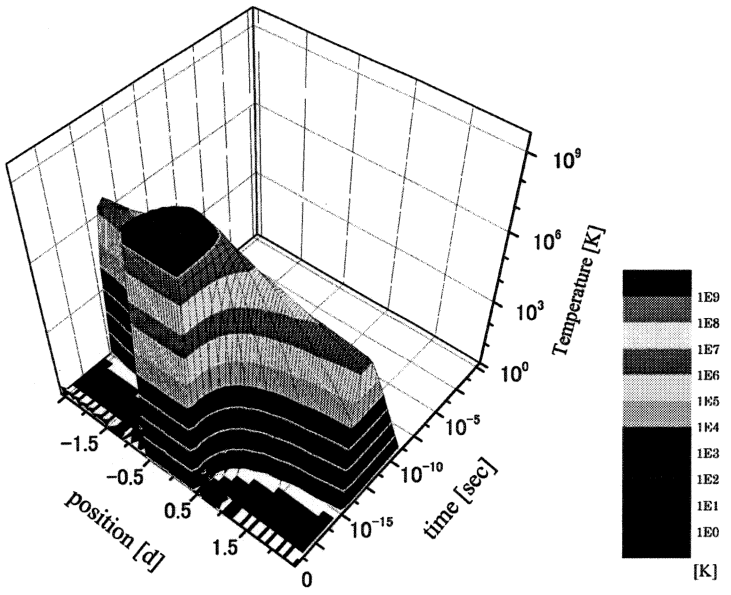

Fig.5 Thermal conduction from a center of a DD reaction.
Position is normalized by the size of a deuteron cluster d. In this case, d=2.45×10^{-10}[m] for 5 deuteron cluster trapped at VacO. This corresponds to the initial temperature T_0=3.85×10^9[K].

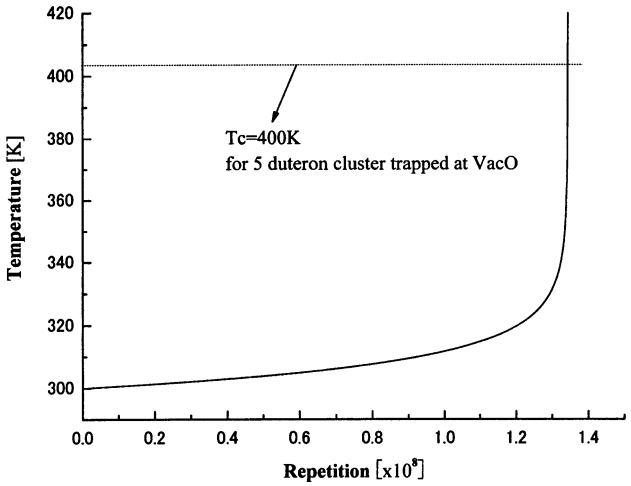

Fig.6 The rise in temperature by repetition of the DD reactions.
In this case, the initial temperature is 300K. For the case of 5 deuteron cluster trapped at VacO, Tc of BEC is 400K (see Table 1), which is shown by the dashed line. After the 1.3×10^8 times repetition of the DD reactions, the temperature becomes higher than Tc and BEC is broken.

3 Conclusions

1. If a DD reaction occurs in a void, temperature of the reaction center becomes extremely high. However rapid recovery from the high temperature is seen, because thermal conductivities of metals are high. For the case of Fig. 5, the recovering time is smaller than 10^{-10} sec. This is smaller than the mean reaction interval, i.e., the inverse reaction rate 1.1×10^{9} sec^{-1}. (see Table 1)
2. If the reactions take place repeatedly, temperature raises slowly. This is shown in Fig. 6. For the case of 5 deuteron cluster trapped at VacO, T_c of BEC is 400K. (see Table 1) Temperature would become higher then T_c after the 1.3×10^{8} times repetition of reactions. After that, local BEC in VacO is broken and DD reactions would no more be possible. This means that nuclear reactions in solid under consideration would not induce thermal explosions.

Acknowledgements

The author wishes to thank Professor Akito Takahashi for helpful discussions.

References

1. K.Tsuchiya, "Quantum States of Deuterons in Pd.", *International Journal of Hydrogen Energy*, **29**,1513 (2004).
2. Y.E.Kim and A.L.Zubarev, "Nuclear Fusion for Bose Nuclei Confined in Ion Trap.", *Fusion Technology*, **37**,151 (2000).
3. Y.E.Kim and A.L.Zubalev, "Equivalent Linear Two-Body Method for Many-Body Problems.", *J. of Phys. B: Atomic, Molecular and Optical Physics*, **33**,3905 (2000).
4. H.Hohenberg and W.Kohn, "Inhomogeneous Electron Gas.", *Phys.Rev.* **136**,B864 (1964).
5. W.Kohn and L.J.Sham, "Self-Consistent Equations Including Exchange and Correlation Effects.", *Phys.Rev.* **140**,A1133 (1965).

Brief Review on Fusion Rates of Bosonized Condensates
Part-I: Basic Theory

Akito Takahashi *1, *2 and Norio Yabuuchi *1
1; High Scientific Research Laboratory, 2: Osaka University
akito@sutv.zaq.ne.jp

Abstract: In Part-I, theoretical basis for formulating fusion rates in condensed matter is summarized. Nuclear strong interaction, S-matrix, T-matrix, fusion rate for steady state dde* molecule as Bosonized condenstate, and fusion rate formula for collision process are briefly given.

1. Nuclear Potential

In general, nuclear reaction is usually theorized and analyzed in three steps; initial state interaction, intermediate compound state and final state interaction. Transition from intermediate state to final state has various, sometimes complex, channels such as the electro-magnetic transition to ground state emitting gamma rays, the particle (neutron, proton, alpha-particle etc.) emission and residual nucleus, which sometimes decay to ground state emitting gamma-rays, and the direct break-up to two or more nuclei like fission. Potential for nuclear strong force and Coulomb force in these cases can be categorized into three cases[1] of Fig.1.

The potential state (I) shows the case that nucleons (neutrons and protons) are trapped in a very deep well of strong force. Stable isotopes of masses less than 60 have this type potential well. Fusion reactions by two light nuclei produce stable isotopes of this type.

The potential state (II) appears for intermediate compound state in general. Radioactive isotope has this kind of potential. Stable isotopes having masses greater than 60 are trapped in these type potentials which are drawn according to the fission channels breaking-up to lighter nuclei. In this case, the depth of trapping potential is deep enough to have very long life time, but positive Q-value for fission channels makes height of potential tail in outer-skirt lower than the depth of trapping well. At ground state, the thickness of potential well is large enough to make the quantum-mechanical tunneling probability of fission "inverse-astronomically" very close to zero.

Therefore, nucleus is regarded as stable isotope. Here, Q-value is obtained by calculating mass defect between before and after reaction, using Einstein's formula $E = mc^2$. However, when the intermediate compound nucleus has high inner excited energy Ex, the thickness of outer wall of trapping potential becomes relatively thin and quantum mechanical tunneling probability for particle emission or fission can dramatically increase. Fission process for uranium and trans-uranium nuclei is induced in this way. Moreover, we may have possibility of fission for lighter nuclei with mass $A < 200$. In some of proposed theories[2-4] in the Condensed Matter Nuclear Science (SMNS), deterministic models of fission for $60 < A < 200$ nuclei have been developed. The potential type (III) is the case for intermediate compound nucleus having very high inner excited energy Ex, such as cases of fusion reactions of hydrogen isotopes. Compound nucleus in this case promptly breaks up to fragment-particles.

2 Strong Interaction

Now we explain very briefly the feature of potential by nuclear strong interaction. The reason why nucleons are trapped within very small spherical space with radius about 5 fm (1 fm = 10^{-15} m) was first solved by the famous Yukawa model of pion exchange. Hideki Yukawa won Nobel Prize by this theory. Later, the theory of strong force has been deepened by the development of QCD[5] based on concept of quark and gluon. However, as the conclusion in recent views of nuclear physics, the strong interaction can be drawn accurately enough by the Yukawa model with charged pions (π^+,π^-) and neutral pion, for relative reaction energy less than about 200 MeV (less than the threshold energy of pion-generation). Especially, for fusion reaction

process, charged pions play role of sticking two (or more) nuclei. Nuclear fusion by strong interaction can be simulated by the catch-ball model of charged pions between nuclei for fusing. Due to the very short range of de Broglie wave length (bout 2 fm) of pion, the strong interaction for fusion becomes very short range force, namely "almost on surface" sticking force. For example, when relatively large (A>6) two nuclei approach closely, fusion force by exchanging charged pions (between neutron and proton for counter-part nuclei) becomes the sticking force near at surface (R=r0). Exchange of neutral pion for scattering (repulsive) force between nucleons of counter-part nuclei also happens relatively near at surface.

Especially, nuclear fusion reactions at very low energy as cold cluster fusion and transmutation, largeness of surface area for exchanging charged pions governs the largeness of reaction cross section. This is specific character of "nuclear reactions in condensed matter".

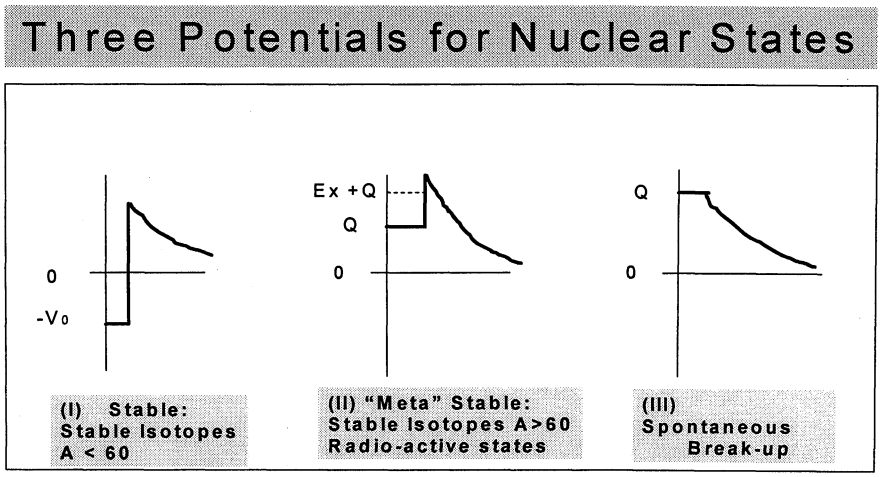

Fig.1: Three potential types for nuclear interaction

3 Optical Potential

Global optical potential[6], written by complex number, is used for nuclear potential of strong interaction for scattering and sticking forces. Image of global optical potential is drawn in Fig.2. The real part, namely deep trapping potential V(r) is a well with rather round shape near at surface of nucleus (Woods-Saxon type) , but is approximated constant value V_0 within in nucleus.

$$U(r) = V(r) + iW(r) \qquad (1)$$

V_0 is about -25MeV for deuteron. V_0 value saturates to about -50MeV for nuclei of A>24. Imaginary part W(r) corresponds to the interaction of charged-pion exchange, and locates near at surface (r = r0) to be approximated by delta-function $W_0\delta(r-r0)$. When we use this delta-function approximation, fusion rate formula becomes simple.

4 T Matrix and Reaction Cross Section

Now we briefly summarize quantum mechanical basis of scattering and reaction process.

Asymptotic wave function[6,7] after scattering is written by Eq.(2).

$$\Psi(r) \approx e^{ikz} + f(\theta)(e^{ikr}/r) \qquad (2)$$

Differential cross section of process is defined by

$$\frac{d\sigma}{d\Omega} = |f(\theta)|^2 \qquad (3)$$

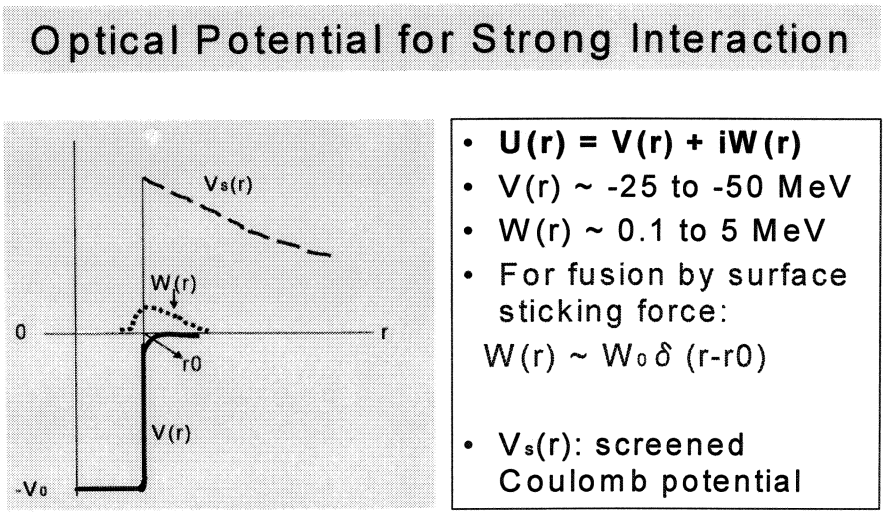

Fig.2: Optical potential for strong interaction

S-matrix is defined by the phase-shift analysis[6,7] as using Legendre polynomial expansion for scattering amplitude $f(\theta)$,

$$f(\theta) = (1/2ik)\sum_{l=0}^{\infty}(2l+1)(S_l - 1)P_l(\cos\theta) \qquad (4)$$

$$S_l = e^{2i\delta_l} \qquad (5)$$

In general reaction process, not only elastic scattering but also absorption, fusion, particle emission processes are taking place as transition. To treat the transition from (α, β) to (α', β') channel, evaluation of T-matrix elements are usually done. T-matrix is defined[7] by the following Lippmann-Schwinger equation,

$$T = U + UG_0T \qquad (6)$$

$$G_0 = (E - H_0 + i\delta)^{-1} \qquad (7)$$

$$H = U + H_0 \qquad (8)$$

Here, G_0 is the Green operator for H_0 Hamiltonian with kinetic energy and spin Hamiltonian only.

Scattering amplitude is defined by,

$$f(\theta;\alpha\beta \to \alpha'\beta') = -(2\pi/h^2)\langle\Psi_{\alpha'\beta'}|T|\Psi_{\alpha\beta}\rangle \qquad (9)$$

If we approximate $T=T^{(0)} = U$, formula (9) becomes the Born approximation.

Lippmann-Schwinger equation can be regarded as an integral type equation of Schroedinger differential equation. The first order approximation of T is given by inserting T=U in Eq(6), and we get $T^{(1)} = U + UG_0U$. The second order approximation is then given as $T^{(2)} = U + UG_0T^{(1)}$, and the n-th order approximation gives $T^{(n)} = U + UG_0T^{(n-1)}$. This successive treatment is known as Neumann series solution[8] of integral equation.

We can treat reaction cross section including transition by evaluating T-matrix elements.

For the optical potential of V + iW type with constant V and W values, formulas of reaction cross section are given in standard text book of nuclear physics (Chapter 9 of Reference-6, for example) for S-wave ($l = 0$).

$$\sigma_{r,0} = \pi\lambda\!\!\!^{-2} \frac{-4kR\,\mathrm{Im}\,f_0}{(\mathrm{Re}\,f_0)^2 + (\mathrm{Im}\,f_0 - kR)^2} \quad (10)$$

$$K = \frac{1}{\hbar}\sqrt{2M(E+V+iW)} \quad (11)$$

$$f_0 = KR\cot KR \quad (12)$$

And relations between S-matrix and T-matrix for Legendre coefficients are:

$$T_\ell = e^{i\delta_\ell}\sin\delta_\ell \quad (13)$$

$$S_\ell = 1 + 2iT_\ell \quad (14)$$

By evaluating T-matrix elements, we can treat reaction with channel transition.

As shown in Figs.3 and 4, X. Z. Li evaluated[9] fusion cross section for dd, dt and d^3He reactions using S-matrix formulas. Fusion cross sections are shown in Fig.3. S-matrix formula and evaluated values of V and W (written as U_{1r} and U_{1i} in Fig.1-4) for dt reaction are shown in Fig.4..

X.Z. Li: ICCF11

Selective Resonant Tunneling ○ & NNDC Data +

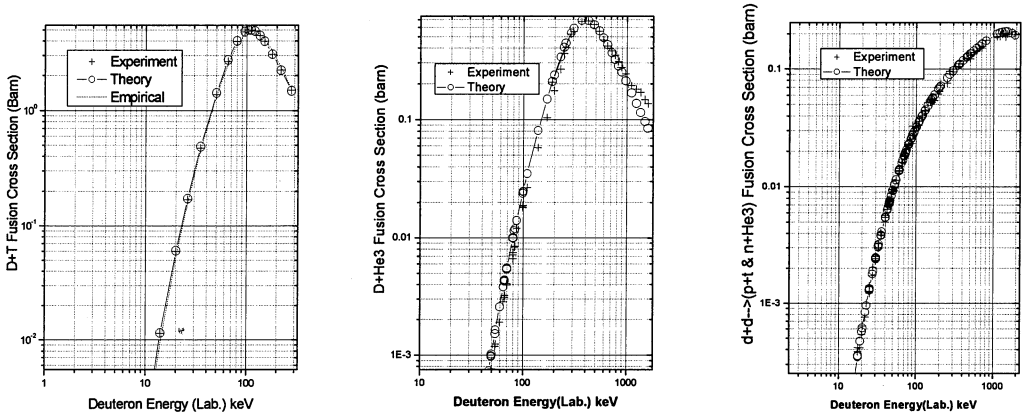

X. Z. Li, H.Hora, et al., *Laser and Particle Beam*, 22 No.4 (2004)

Fig.3: Fusion cross sections for dt, d^3He and dd processes

Li used the reaction cross section formula with S-matrix elements as shown in Fig.4. He obtained averaged values of V and W of optical potential by fitting calculated curves to experimental cross sections.

As explained in nuclear physics text books[6], S-matrix elements by the phase-shift analysis can be used for estimating not only elastic scattering cross section but also total reaction cross section. However, the phase-shift analysis does not give information on out-going channels and products by final state interaction.

5 Imaginary Part of Optical Potential

Now we move to the explanation of physical meaning for the imaginary part W of optical potential. From the conservation of quantum

mechanical probabilistic density flow (a kind of continuity equation), we can take meaning of the imaginary part.
The forward Schroedinger equation is:

$$i\hbar\frac{\partial\Psi}{\partial t}=\left[-\frac{\hbar^2}{2M}\nabla^2+V+iW\right]\Psi \qquad (15)$$

and the backward or adjoint equation is:

$$-i\hbar\frac{\partial\Psi^*}{\partial t}=\left[-\frac{\hbar^2}{2M}\nabla^2+V-iW\right]\Psi^* \qquad (16)$$

Here we used complex conjugate potential for the adjoint (backward) equation.

We multiply Ψ^* on Eq.(15) from the left side, make mutual subtraction to get for the left hand side:multiply Ψ on Eq.(16) from the left side and

$$i\hbar\left(\Psi^*\frac{\partial\Psi}{\partial t}+\Psi\frac{\partial\Psi^*}{\partial t}\right)=i\hbar\frac{\partial\Psi\Psi^*}{\partial t}=i\hbar\frac{\partial\rho}{\partial t} \qquad (17)$$

Here,

$$\rho=\Psi\Psi^* \qquad (18)$$

Li_ICCF11

$$S_0=e^{i2\delta_0} \qquad Cot(\delta^0)=W_r+iW_i$$

$$\sigma_r^{(0)}\approx\frac{\pi}{k^2}(1-|S_0|^2)\equiv\frac{\pi}{k^2}\left\{\frac{-4W_i}{W_r^2+(W_i-1)^2}\right\}$$

Reaction Cross Section

$$\begin{cases}W_r=0\\W_i=O(-1)\end{cases}$$

$$\begin{cases}E=110\ \text{keV}\\\sigma_r^{(0)}=5.01\ \text{b}\end{cases}\qquad\begin{cases}U_{1r}=-47.33\ MeV\\U_{1i}=-115.25\ keV\end{cases}$$

$$a=1.746\times10^{-13}\left(A_1^{1/3}+A_2^{1/3}\right)\ cm$$

Fig.4: Fitting of dt fusion cross sections by. S-matrix formulas, by Li[9)]

And we get for the right hand side:

$$i\hbar\frac{\partial\rho}{\partial t}=-\frac{\hbar^2}{2M}\left[\Psi^*\nabla^2\Psi-\Psi\nabla^2\Psi^*\right]+i[2W\rho]=-i\hbar div\vec{j}+i[2W\rho] \qquad (19)$$

Here we used formulas of quantum mechanical current flow as,

$$\vec{j}=\frac{\hbar}{2im}(\Psi^*\vec{\nabla}\Psi+\Psi\vec{\nabla}^*\Psi^*)=\frac{\hbar}{2im}(\Psi^*\vec{\nabla}\Psi-\Psi\vec{\nabla}\Psi^*) \qquad (20)$$

$$div\vec{j}=\frac{\hbar}{2im}(\vec{\nabla}(\Psi^*\vec{\nabla}\Psi)-\vec{\nabla}(\Psi\vec{\nabla}\Psi^*)) \qquad (21)$$

$$=\frac{\hbar}{2im}(\Psi^*\nabla^2\Psi+(\vec{\nabla}\Psi^*)(\vec{\nabla}\Psi)-\Psi\nabla^2\Psi^*-(\vec{\nabla}\Psi)(\vec{\nabla}\Psi^*))$$

$$=\frac{\hbar}{2im}(\Psi^*\nabla^2\Psi-\Psi\nabla^2\Psi^*)$$

Consequently we obtain the modified continuity equation for probabilistic density flow:

$$\frac{\partial \rho}{\partial t} = -div(\vec{j}) + \frac{2}{\hbar} W\rho \qquad (22)$$

It is obvious that the second term of Eq.(22) corresponds to the absorption rate term of the balance. (We do not have the second term in the continuity equation of fluid.)

Mean free path of particle in the strong force field of optical potential is given as (velocity)x(life-time), namely:

$$\Lambda = (\hbar/2)v/W(r) \qquad (23)$$

6 Fusion Rate for Steady Molecule

Now we move to formulate fusion rate formulas for pseudo-molecule (EQPET molecule)[10-11] of two deuterons and bosonized electrons (quasi-particle) e*(m/m_e,Z). Here, m_e is the electron mass and Z is number charge of quasi-particle.

For deriving the trapping Coulomb potential, we will treat later. Here, we assume an EQPET molecule is trapped in a shielded Coulomb potential similar to the Morse potential[8]. We illustrate the image of shielded Coulomb potential $V_s(r)$ with optical potential in Fig.5. Scales are deformed for easy understanding the feature.

Range of strong nuclear force is very short in several fm region, and concentrated in near surface (r = r0) of nucleus. On the other hand, Coulomb interaction as electro-magnetic force distributes from r0 in several fm to nm long region.

As a result, fusion rate for low energy under the strong interaction at around r=r0 can be treated by adiabatic approximation (namely Born-Oppenheimer approximation in quantum mechanics) to take product of the absorption rate by nuclear optical potential (imaginary part) and the tunneling probability of dd pair at r = r0.

Fusion rate per dd pair is therefore defined as,

$$\lambda_{dd} = Tn\left|\Psi(r0)\right|^2 \qquad (24)$$

$$Tn = (2/\hbar)\left\langle \Psi_f \left| W(r) \right| \Psi_i \right\rangle \qquad (25)$$

Here, $\left|\Psi(r0)\right|^2$ is equivalent to the quantum mechanical tunneling probability of dd pair through the shielded Coulomb potential Vs(r), as given by the WKB approximation[7]. Fusion rate for muonic molecule dde*(208,1) can be approximately given by Eq.(1-25), assuming the life time of muon is long enough. Actually the life time of muon is 2.2 micro-sec, and trapping potential should be regarded as adiabatic.

7 Fusion Rate for Dynamic Process

For more transient and dynamic process than muonic dd molecule, it is better to use formulas (Fermi's second golden rule) for cross section. Especially, for fusion rate calculations of EQPET molecules dde*(2,2), dde*(4,4), dde*(6,6), dde*(8,8), lifetimes of pseudo-molecules are much shorter (on the order of femto-sec) than muonic dd molecule.

Fusion rate is formulated as,

$$\lambda = \sigma v = (1/\hbar) v T^2 \rho(E') \qquad (26)$$

$$T = \left\langle \Psi_f \left| H_{int} \right| \Psi_i \right\rangle \qquad (27)$$

Here v is the relative velocity for d-d interaction, $\rho(E')$ is the final state density, and H_{int} is the effective interacting Hamiltonian as given by the approximate solution of Lippmann-Schwinger equation.

Fusion rate per dd pair is given by $<\sigma v>$. Cross section σ is proportional to the square of T-matrix. To evaluate T-matrix elements, we need to treat many steps of physics as the formation process of EQPET dde* molecule by the consequence of electromagnetic interaction in ordered (or constrained) space in condensed matter – solid state physics calculation of dynamic behavior of deuterons in lattice Bloch potential, atomic physics calculation to evaluate shielded Coulomb potential Vs(r) and strong interactions by global optical potential. After that, we need to evaluate the intermediate compound state with excited energy and

spin-party state. Finally we have to evaluate out-going channels and branching ratios of the final state interaction. In every step, we need to evaluate T-matrix elements.

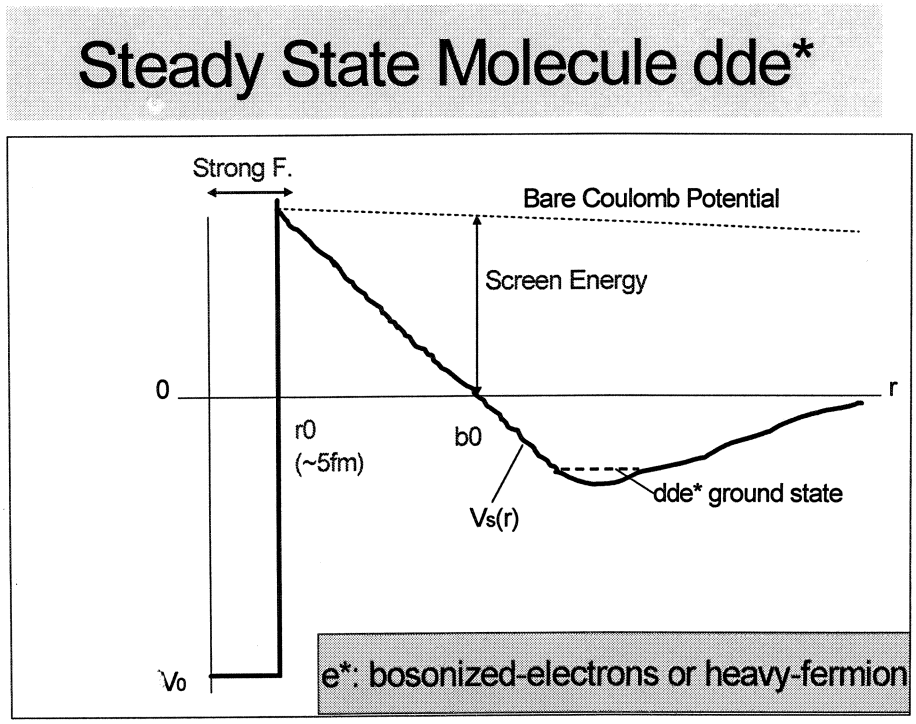

Fig.5: Trapping Coulomb + strong force potential for steady EQPET molecule of dde*

[References]

1): J. M. Blatt, V. F. Weisskopf: **Theoretical Nuclear Physics**, Chapter VIII, Springer-Verlag, 1979

2): A. Takahshi, et al: *JJAP*, 41(2001)pp.7031-7046

3): M. Ohta, A. Takahashi: *JJAP*, 42(2002)pp.645-649

4): A. Takahashi: Theoretical backgrounds for transmutation reactions, ppt slides for Sunday School of ICCF10, see http://www.lenr-canr.org/ Special Collection for ICCF10

5): B. Povh, K. Rith, C. Scholtz, F. Zetsche: **Teilchen und Kerne**, Springer, 1994

6): K. Yagi: **Nuclear Physics (in Japanese)**, Asakura, Tokyo, 1971

7): L. I. Schiff: **Quantum Mechanics**, McGraw-Hill (1955)

8): P. M. Morse, H. Feshbach: **Methods of Theoretical Physics**, McGraw-Hill (1953)

9): X. Z. Li, et al: *Phys. Rev. C*, 61(2000)24610

10): A. Takahashi: Condensed matter nuclear effects, Proc. Int. Meet. Frontiers of Physics, Kuala Lumpur, 25-29 July 2005, *Malaysian J. Physics*, to be published

11): A. Takahashi: Deuteron cluster fusion and related nuclear reactions in metal-deuterium/hydrogen systems, *Recent Res. Devel. Physics*, 6(2005)pp.1-28, ISBN: 81-7895-171-1

Brief Review on Fusion Rates of Bosonized Condensates
Part II: EQPET/TSC Model

Akito Takahashi *1, *2 and Norio Yabuuchi *1
1; High Scientific Research Laboratory, 2: Osaka University
akito@sutv.zaq.ne.jp

Abstract: In Part-II, application for TSC-induced fusion is summarized. Fusion rate formulas for adiabatic approach in EQPET theory are summarized. Final state interaction is briefly discussed. Time-dependent approach for TSC squeezing motion is briefly introduced.

2.1 Tetrahedral Symmetric Condensate (TSC)

As a seed of cold fusion or more extendedly condensed matter nuclear effects, a charge-neutral entity (pseudo-particle) of Platonic regular polyhedron composed with alternative positioning of deuteron (or proton) and electron at vertex of polyhedron has been porposed[1-19]. A representative one is the tetrahedral symmetric condensate (TSC) which is composed of 4 deuterons forming a regular tetrahedron and 4 electron balls also forming a regular tetrahedron. Each particle or ball sits at vertexes of cube. An electron ball at vertex depicts effective electron center of coupled two electrons having opposite spins each other. TSC is a transient pseudo-particle with short life (on the order of 100 fs). Exact place and condition for TSC production are still of open question, but two models were proposed[11-17]. One (Model A) is the transient formation of TSC at T-sites of PdD under D-phonon excitation. The other (Model B) is the resonant coupling of two D_2 molecules at some focal points (corner hole, defect, etc) in near surface of metal-deuteride. TSC can make time-dependent squeezing motion under three-dimensional constraint to condensate at central focal point to become transiently a very small (on the order of 10 fm) charge-neutral pseudo-particle, which will make self-fusion of 4 deuterons within strong interaction (charged-pion exchange) range or will make deuteron-cluster-capture reaction with host metal nucleus[11-17].

Estimation of fusion rate by the TSC squeezing motion has been formulated by evaluating T-matrix elements in three adiabatic steps, as illustrated in Fig.2-1.

The first adiabatic process is for estimating D-cluster formation probability in condensed matter.

$$F_{nd} = \langle \Psi_1^2 \rangle \langle \Psi_2^2 \rangle \langle \Psi_3^2 \rangle \langle \Psi_4^2 \rangle \cdots \langle \Psi_n^2 \rangle \qquad (2\text{-}1)$$

where Ψ_n is the "lattice" wave function for the n-th deuteron. To estimate the D-cluster formation probability F_{nd} is most important for predicting experimental conditions.

The second adiabatic process is for estimating quantum mechanical barrier penetration probability P_B. P_B is approximately given by the WKB method[7] as,

$$P_B = \exp(-n\Gamma_n) \qquad (2\text{-}2)$$

where Γ_n is Gamow integral and given as,

$$\Gamma_n = (\sqrt{2\mu}/\hbar)\int_{r_0}^{b}\sqrt{V_s(r) - E_d}\,dr \qquad (2\text{-}3)$$

Here μ is the reduced mass and r0 and b are given in Fig.1-5. For very low energy fusion reaction, b is approximately given by b_0. Once the adiabatic screened potential, as illustrated in Fig.1-5, is calculated, for example as we show later by the EQPET model[11-19], the Gamow integral can be numerically obtained by Eq.(2-3). The barrier penetration probability for multi-body fusion process is given in Eq.(2-2) by assuming that multi-body interaction takes place as very rapid cascade process of two-body interactions.

The third adiabatic process is for estimating cross section of multi-body strong interaction. Instead of evaluating T-matrix directly, it is more practical to use S-value, the astrophysical S-value, to write fusion cross section by strong interaction only as,

$$\sigma_{strong} = S_{nd} / E_d \qquad (2\text{-}4)$$

Pure theoretical estimation of S-values for multi-body interaction is difficult because of so many-body (exchanging more than 6 charged pions for 3d, 4d, 6d and 8d fusion) problem. We introduce empirical extrapolation as shown later.

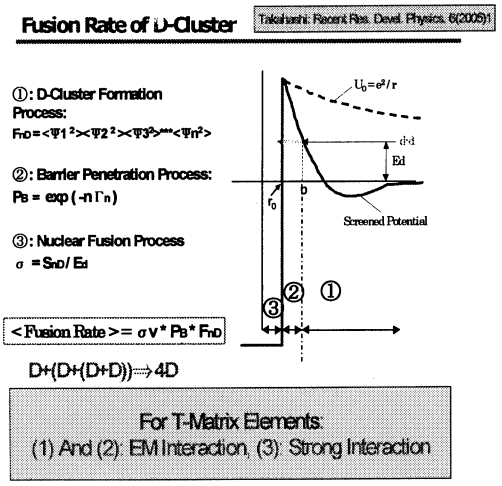

Fig. 2-1: Three adiabatic steps for formulating fusion rate in condensed matter

Model A for TSC formation is illustrated in Fig.2-2. We assume local fulfillment of x=1 for PdDx lattice. We do not necessarily require the X=1 condition (full D-loading) for balk Pd sample. The local x=1 condition may be fulfilled in near surface zone of Pd sample in experiment. Then we assume that D-in lattice is excited to higher phonon energy state by external stimulation. Laser beam irradiation on Pd sample surface may be a stimulation method for phonon excitation. It is known that D in PdDx lattice sits as Harmonic oscillator with $\hbar\omega = 64meV$, and $E0 = 32$meV.

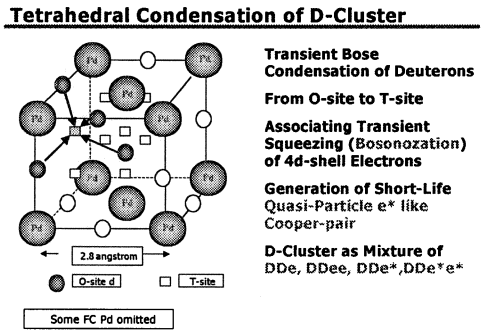

Fig.2-2: Model-A for TSC formation in PdD lattice under D-phonon excitation

As a function of phonon energy, we can estimate D-cluster formation probabilities at central T-sites. However this process is essentially time-dependent (transient), and we have to treat more exactly the process. We may first estimate the D-cluster formation probability within a small time-interval of "deep trapping hole", by treating adiabatically the state (adiabatic dde* state). Then we will make time-averaging for the periodical oscillation process. The adiabatic dde* state is regarded as the most squeezed state (MSS). Numerical calculation for screened potential $V_s(r)$ will be done (shown later) by EQPET.

The example of D-cluster formation probability for Model A, is the treatment[20] with quantum mechanical statistics, which does not include anti-parallel spin configuration for pairing electrons forming electron balls, neither treating the three dimensional constraint of squeezing motion under Platonic symmetry.

Centralized point-symmetric coherence of momentum-vectors for 4 deuterons and 4-electron balls is required to form TSC. This condition can not be expected in random motion of particles in plasma. The squeezing motion under three dimensional constraint (or ordering, or self-organization process) in lattice dynamics can realize that condition.

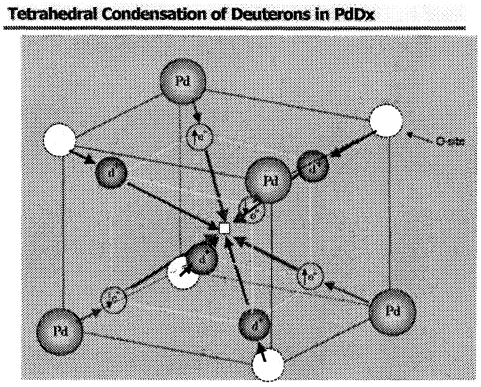

Fig. 2-3: Image of TSC formation in PdD lattice under statistical coherence by phonon excitation

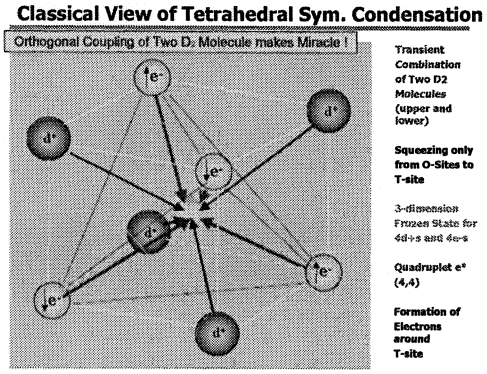

Fig. 2-4: Semi-classical view of TSC (tetrahedral symmetric condensate) for 4 deuterons and 4 electron-balls

The semi-classical image of 4D cluster (TSC) is shown in Fig. 2-4. Pd atom has 10 outer most electrons in 4d-shell. Pd atom is unique atom having largest number of valence electrons among atoms in nature. Electrons in 4d-shell contribute as quasi-free conduction-band electrons in Pd metal lattice.

Transition of physical system happens to realize the system-energy minimum state. The local energy minimum condition is formulated by the variational principle of quantum mechanics[7,8]. Eigen-value problem is led to secular equation.

However, under the ordering process (or self-organization process) in three dimensional constrained motion, the Platonic symmetry (regular polyhedron) for alternative positioning of deuteron (proton) and electron-ball makes obviously the averaged system Coulomb energy zero. Namely TSC realizes minimum system Coulomb energy.

The semi-classical image of TSC is shown in Fig. 2-4. Pair of counter-part two electrons is the combination of anti-parallel spins, combination probability of which can be estimated simply. When momentum vectors of pairing two electrons are 180 degree opposite configuration, the transient Cooper pair e*(2,2) is formed. Moreover, in TSC configuration, two Cooper pairs may couple orthogonally to form the quadruplet quasi-particle e*(4,4). As a general concept, this is the bosonization of electrons. Here, more exact quantum mechanical image for electron-ball is a pseudo-particle of 1/2 of coupling of two electrons with anti-parallel spin each other. More exact image is shown later in the time-dependent problem.

2.2 EQPET model

It is difficult to evaluate directly the total TSC wave function because of so many-body problem. The EQPET (electronic quasi-particle expansion theory) model assumes that the total TSC wave function can be written by the linear combination of partial wave functions for EQPET molecules dde* for e*(2,2) and e*(4,4) and regular molecules dde (D_2^+ ion) and ddee (D_2 molecule).

$$|\Psi_N\rangle = a_1|\Psi_{(1,1)}\rangle + a_2|\Psi_{(2,2)}\rangle + a_4|\Psi_{(4,4)}\rangle + a_6|\Psi_{(6,6)}\rangle + a_8|\Psi_{(8,8)}\rangle \quad (2\text{-}5)$$

Here equation is written for including the case of OSC (octahedral symmetric condensate). For TSC, a_6 and a_8 are zero.

Fusion rate formula for dde* is given[11-19] by,

$$\lambda_{(i,j)} = \nu(S_{2d}/E_d)\exp(-2\Gamma_{(i,j)}) \quad (2\text{-}6)$$

$$\Gamma_{(i,j)} = 0.218\int_0^{\phi(i,j)} \sqrt{V_{s(i,j)}(R_{dd}) - E_d}\, dR_{dd} \quad (2\text{-}7)$$

Here R_{dd} is the inter-nuclear distance between two deuterons in D-cluster.

The modal fusion rate for TSC system is given by,

$$\lambda_N = a_1^2\lambda_{(1,1)} + a_2^2\lambda_{(2,2)} + a_4^2\lambda_{(4,4)} + a_6^2\lambda_{(6,6)} + a_8^2\lambda_{(8,8)} \quad (2\text{-}8)$$

Formulas for screened Coulomb potentials Vs of EQPET molecules were given[11-19] by applying the solution for D_2^+ ion and D_2 molecule, based on the variational method[21], as for dde*,

$$V_{s(i,j)} = \frac{e^2}{R_{dd}} + V_h + \frac{J+K}{1+\Delta} \quad (2\text{-}9)$$

$$V_h = -13.6(e^*/e)^2(m^*/m_e) \quad (2\text{-}10)$$

Here V_h is the virtual binding energy of EQPET atom de*. And,

$$i = e^*/e \quad (2\text{-}11)$$

is the number charge of e*, and

$$j = m^*/m_e \quad (2\text{-}12)$$

The Coulomb integral J is given as,

$$J = (Ze^2/a_B)\left[-\frac{1}{y} + (1+\frac{1}{y})\exp(-2y)\right] \quad (2\text{-}13)$$

The electron exchange integral K is given by,

$$K = (Ze^2/a_B)(1+y)\exp(-y) \quad (2\text{-}14)$$

The non-orthogonal integral is,

$$\Delta = (1 + y + \frac{y^2}{3})\exp(-y) \quad (2\text{-}15)$$

$$y = R_{dd}/(a_B/i/j) \quad (2\text{-}16)$$

Here $aB = a_B/i/j$, and a_B is Bohr radius (52.9 pm).

Fusion rate for multi-body reaction is given approximately by,

$$\lambda_{nd(i,j)} = \nu(S_{nd}/E_d)\exp(-n\Gamma_{(i,j)}) \quad (2\text{-}16)$$

Modal fusion rate of multi-body fusion for TSC is then given by,

$$\lambda_{Nnd} = \sum_i a_i^2 \lambda_{nd(i,i)} \quad (2\text{-}17)$$

Calculated results of screened Coulomb potentials for EQPET molecules are shown in Fig. 2-5.

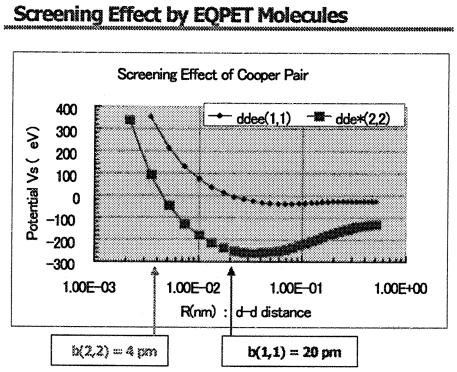

Fig. 2-5: Screened Coulomb potential for ddee (D_2 molecule) and dde*(2,2) (EQPET molecule with Cooper pair)

Screening Energy of EQPET Molecules
$U_s = -e^2/b_0$ for $V_s(b_0) = 0$

	U_s (eV)	U_s(eV)	b_0 (pm)	b_0 (pm)
e*	dde*	dde*e*	dde*	dde*e*
(1,1)	36	72	40	20
(2,2)	360	411	4	3.5
(4,4)	4,000	1,108	0.36	1.3
(8,8)	22,154	960	0.065	1.5
(208,1)	7,579	7,200	0.19	0.20
(6, 6)	9,600		0.15	

Table 2-1: Calculated screening energies by EQPET model

Compared to the bare Coulomb potential, a low

energy d-d pair can come closer to the position b_0 classically and then penetrates quantum mechanically to the point r = r0 of strong interaction range. It is well known that muonic molecule dde*(208,1) realize large dd fusion rate. Shielded Coulomb potential for dde*(4,4) is equivalent to the one for dde*(100,1), and dde*(6,6) has almost the same shielded Coulomb potential as muonic molecule.

Screening energy by e* is estimated by calculating bare Coulomb energy at $r=b_0$. Calculated screening energies are given in Table-2-1.

2.3 Multi-Body Strong Interaction

Now we move to explain the empirical formulas for extrapolating S-values of intrinsic cross section terms of two-body and multi-body strong interaction in fusion reaction process.

Basic measure PEF (pion exchange force) is defined as the scale of effective surface for very short range attractive force, that is the catch-ball of charged pion between neutron-nucleon and proton-nucleon between two fusing nuclei. One PEF is defined as the number of string between n and p.

As discussed in Part-1, sticking force of fusion happens at near surface of fusing nuclei.

The larger is the sticking surface area, the larger is the fusion cross section. Using the PEF measure, PEF = 1 for HD fusion, PEF = 2 for DD fusion and PEF = 3 for DT fusion.

Let us consider fusion reaction of deuteron with heavier nucleus, for example ^{6}Li + d fusion. As drawn by the right figure of Fig.2-6, catch-ball of charged pions is interfered for about half of nucleons in ^{6}Li nucleus due to self-shielding by more front nucleons. As consequence of the self-shielding effect, PEF value would be around 3. For more heavy nuclei, PEF value should saturate to effective PEF values for interacting surface area.

On the contrary, multi-body deuteron fusion under the Platonic polyhedral configuration (regular tetrahedron for 4d fusion), there is no self-shielding effect. We can expect perfect exchange of charged pions among all deuterons of regular tetrahedral configuration as drawn in the left figure of Fig.2-6. PEF =6 is given, for 3d fusion. We can say that effective sticking surface for multi-body fusion becomes very large.

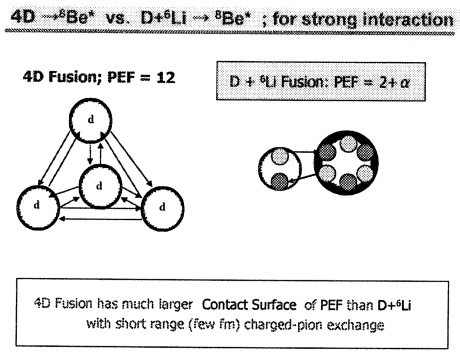

Fig.2-6: Estimation of effective sticking surface for fusion reactions, by the PEF measure for strength of charged pion exchange

Here we recognize that ^{8}Be* is intermediate compound state both for the ^{6}Li + d and 4d reactions. And 4d fusion will have much larger cross section than the ^{6}Li + d reaction.

PEF values, hence fusion cross sections for 6d and 8d fusions in OSC condition may become much larger than 4d fusion.

Using known experimental S(0)-values for boson-related fusions, as pd, dd and dt fusion, we draw plot of S(0) values as a function of PEF value, and extrapolate to multi-body fusion using scaling formula, as shown in Fig.2-7. See also Fig.1-2 of Part-I.

$$S_n(0) \propto T_n^2 \propto (PEF)^N \qquad (2\text{-}18)$$

Using S_{dd} = 100 keVb and S_{dt} = 2E+4 keV, we estimated as scaling exponent N =11.4 and we got S_{4d} = 1E+11 keVb.

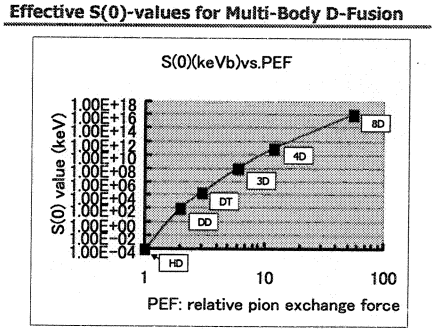

Fig.2-7: Empirical extrapolation of S(0) values as a function of PEF (effective sticking surface of fusion reaction) number, for multi-body fusion

Now we have finished preparation for fusion rate calculation.

2.4 Final State Interaction

Now we briefly summarize on the final state interactions and branching ratios to plural out-going channels.

The out-going break-up channels and branching ratios for dd fusion are very well established, as shown in Fig.2-8.

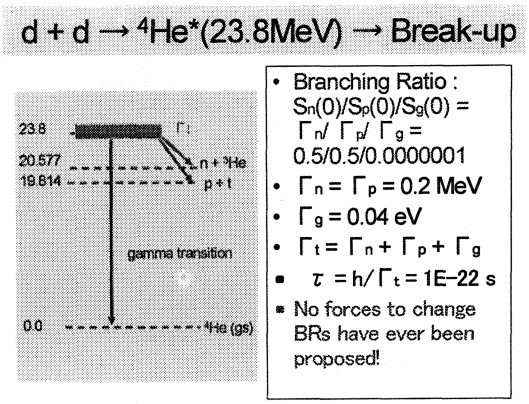

Fig.2-8: Final state interaction and branching ratios for dd fusion

Unless we could change the intermediate excited state ^{4}He*(Ex=23.8MeV) by some external forces putting in, we have no way to change the branching ratios. Namely, major channel for ^{4}He generation never happens otherwise. The electromagnetic interaction (QED, phonon coupling, etc) is too weak to change the intermediate compound state. In the view of author, to put additional charged pion exchange into the d-d interaction is actually possible way to get to the ^{4}He production: however, this idea leads ones automatically to the multi-body (or cluster) fusion process.

In Fig.2-9, the final state interaction for multi-d fusion is drawn. The highly excited state ^{8}Be* can be regarded as a collectively deformed nucleus of two alpha-clusters, because of very hard formation of alpha-cluster (regular tetrahedron of 4 nucleons) in ^{8}Be nucleus. The very high (47.6 MeV) excited energy is therefore rarely redistributed to single nucleon (n or p), or d, or t-cluster for particle emission.

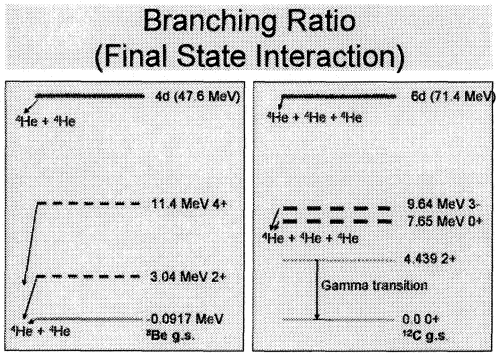

Fig.2-9: Final state interactions for 4d and 6d fusion reactions in condensed matter

We can speculate that all threshold reactions will not open in the final state interaction from 4d fusion, due to collective deformation of two alpha-clusters. Therefore, ^{8}Be* will decay with almost 100% weight to two ^{4}He with 23.8 MeV kinetic energy per ^{4}He, as illustrated in Fig.2-9. The decay channel of 6d fusion by OSC is also shown in the right figure of Fig.2-9, which is break-up to three 23.8 MeV ^{4}He particles.

We know that p + ^{7}Li and n + ^{7}Be channels appear in the ^{6}Li + d beam-target reaction.
We understand that these branches are caused by stripping reactions taking n or p from deuteron approaching to ^{6}Li nucleus. The purely symmetric strong force exchange in the Platonic polyhedral condition, in the case of 4d/TSC reaction in PdD lattice, ignores the stripping process.

2.5 Time-Dependent Approach

Detail of time-dependent analysis is given in Ref-19. Brief feature is illustrated in Fig.2-10. The semi-classical squeezing motion of TSC will get to its minimum size state with about 10 fm diameter in about 74 fs. Calculated effective time-interval for 4d fusion is about 0.04 fs, namely very much short.

The TSC wave function at the starting point (t=0) can be drawn by superposition of 6 D2 molecule wave functions on 6 surfaces of cube, as shown in c) of Fig.2-11. To calculate approximately time-dependent fusion rates, we can use adiabatic dde* potentials, dividing into three time intervals; normal electron state, Cooper pair state and quadruplet state.

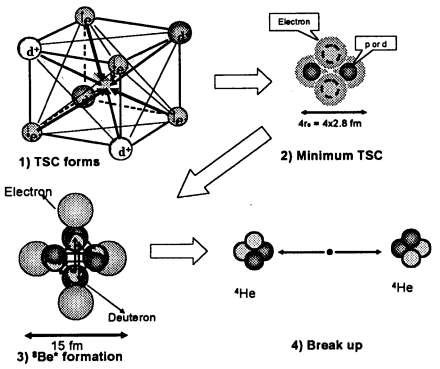

Fig.2-10: Semi-classical view of TSC squeezing motion and self-4d fusion reaction, here electron with spin should be electron-ball of 1/2 of two bosonized electrons in QM view.

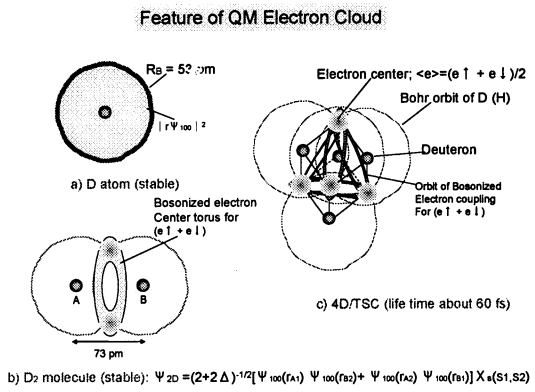

Fig.2-11: Initial state TSC wave function, compared with wave functions of D atom and D_2 molecule.

For more accurate analysis, we need to develop algorithm of molecular dynamics under three-dimensional constraint motion. This is our future task.

Time-dependent squeezing motion of TSC was first treated by the time-dependent EQPET (TDEQPET) model.

$$a_i\Psi_{4D}(r,t) = a_1\Psi_{(1,1)}(r,t) + a_2\Psi_{(2,2)}(r,t) + a_4\Psi_{(4,4)}(r,t) \qquad (2\text{-}19)$$

$$\langle r(t)\rangle = \langle r(0)\rangle - \langle v\rangle t \qquad (2\text{-}20)$$

Because of the three-dimensionally and symmetrically constraint motion with averaged charge-neutrality for total TSC system, there is no force to stop squeezing motion until TSC size gets into the range of strong interaction (range of pion exchange). Therefore, the squeezing motion can be treated by the semi-classical Newtonian motion.

To calculate time-dependent barrier penetration probability, we assumed that time-dependent change of potential can be replaced with three adiabatic potential Vs for D_2 molecule, dde*(2,2) and dde*(4,4) in three time intervals sequentially, according to the change of <r> value comparing with b0-parameters of adiabatic potentials..

Time dependent Gamow integral is defined as,

$$\Gamma(t) = 0.218\int_0^{b(t)} \sqrt{V_s(R_{dd}) - E_d}\, dR_{dd} \qquad (2\text{-}21)$$

Here b(t) is set to <r(t)> for <r(t)> > b_0 parameter in each time interval for assumed adiabatic potential, namely e* state.

Time dependent fusion rate were calculated, as shown in Fig.2-12. Time-averaged fusion rates were obtained as listed in Table 2-2.

Maximum TSC density possibly produced in PdD lattice is on the order of 1E+22 TSC/cm^3. Multiplying this number to cluster fusion rates in Table 2-2, we obtain dd fusion rate which emit neutrons on the order of 3E-3 n/s/cm^3. This level of neutron emission is difficult to detect by usual detectors. On the contrast, we obtain 4d fusion rate as 5.5E+14 α /s/cm^3 which corresponds to 55 kW/cm^3 power level. Thus, neutron free clean fusion reaction producing large heat density and ^{4}He ash, as reported by experiments of Arata, McKubre, de Ninno, Violante, Isobe etc. can be now theoretically explained.

[References]

1): J. M. Blatt, V. F. Weisskopf: **Theoretical Nuclear Physics**, Chapter VIII, Springer-Verlag, 1979

2): A. Takahshi, et al: *JJAP*, 41(2001)pp.7031-7046

3): M. Ohta, A. Takahashi: *JJAP*, 42(2002)pp.645-649

4): A. Takahashi: Theoretical backgrounds for transmutation reactions, ppt slides for Sunday

School of ICCF10, see http://www.lenr-canr.org/ Special Collection for ICCF10
5): B. Povh, K. Rith, C. Scholtz, F. Zetsche: **Teilchen und Kerne,** Springer, 1994
6): K. Yagi: **Nuclear Physics (in Japanese),** Asakura, Tokyo, 1971
7): L. I. Schiff: **Quantum Mechanics,** McGraw-Hill (1955)
8): P. M. Morse, H. Feshbach; **Methods of Theoretical Physics,** McGraw-Hill (1953)
9): X. Z. Li, et al: *Phys. Rev. C,* 61(2000)24610
10): A. Takahashi: Condensed matter nuclear effects, Proc. Int. Meet. Frontiers of Physics, Kuala Lumpur, 25-29 July 2005, *Malaysian J. Physics*, to be published
11): A. Takahashi: Deuteron cluster fusion and related nuclear reactions in metal-deuterium/hydrogen systems, *Recent Res. Devel. Physics*, 6(2005)pp.1-28, ISBN: 81-7895-171-1
12): A. Takahashi: Proc. ICCF9, pp.343-348, see Ref-2
13): A. Takahashi: Mechanism of deuteron cluster fusion by EQPET model, Proc. ICCF10, see Ref-3
14): A. Takahashi: Proc. JCF5, 6, see http://wwwcf.elc.iwate-u.ac.jp/jcf/
15): A. Takahashi: Proc. ICCF11
16): A. Takahashi: Deuteron cluster fusion and ash, Proc. ASTI5 Meeting, see Ref-5
17): A. Takahashi: A theoretical summary of condensed matter nuclear effects, Proc. Siena2005 Workshop
18): A. Takahashi: Time-dependent EQPET analysis of TSC, Proc. ICCF12, Yokohama 2005
19): C. J. Pethic, H. Smith; **Bose-Einstein condensation in dilute gases,** U. Chicago publ. (2001)
20): A. Takahashi, H. Numata, Y. Iwamura, H. Yamada, T. Ohmori, T. Mizuno, T. Akimoto: **"Nuclear Reactions in Solids" (in Japanese),** Kogakusha, Tokyo, 1999
21): S. Shirato: **Atomic Physics-II (in Japanese),** Nippon Rikou Publ. Tokyo, 1984

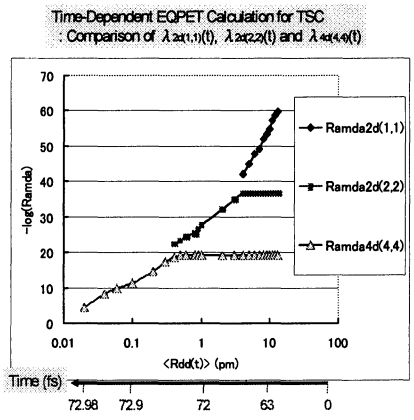

Fig.2-12: Calculated time-dependent fusion rates by TDEQPET model

TDEQPET Cal. For EQPET Molecules

e*(m, Z)	< λ2d> (f/s/cl.)	< λ4d> (f/s/cl.)	λ 2d(0) (f/s/cl.)	λ4d(0) (f/s/cl.)
(1, 1)	4.3E-44	7.8E-63	1.9E-60	7.3E-93
(2, 2)	2.9E-25	2.5E-24	2.4E-37	1.1E-50
(4, 4)	(2.1E-17)*	5.5E-8	(5.5E-22)*	5.9E-20

( )* : virtual value

Table 2-2: Time-averaged fusion rates by TDEQPET model, compared with values at t=0.

POSSIBLE NUCLEAR TRANSMUTATION OF NITROGEN IN ATMOSPHERE OF EARTH (II)

Mikio FUKUHARA, Tohoku University: fukuhara@imr.tohoku.ac.jp

Abstract: Following the pioneering previous work, we propose other possible formation cases of nitrogen in Earth. The first case is nitrogen transmutation by the compression of CO_3 anion in deep seawater over critical depth of 10250 m. The second is transmutation of nitrogen by the double β decay of D atom replaced into calcite Ca_2CO_3 from seawater with heavy water.

Keywords: origin of nitrogen, carbonic acid, deep seawater, nuclear transmutation , double β decay

1. INTRODUCTION

Nitrogen is an origin of all lives. In a previous paper [1], the reason why the Earth's atmosphere has such a high concentration of nitrogen was ascribed to a possible endothermic nuclear transmutation of carbon and oxygen nucleus pairs confined along three [1$\bar{1}$0] directions in a (111) plane of rhombohedral $MgCO_3$ crystals existing in the mantle crust. The nuclear reaction is:

$$^{12}C + {}^{16}O - 2\pi^0 = 2\,{}^{14}N, \qquad (1)$$

based on an assumption which parabolic increase of nitrogen content correlates to abrupt decrease of carbon dioxide one in Archean era (3.8 to 2.5 billion years ago) [2-10]. Actually we got the following formula

$$^{12}C + {}^{16}O + 2e^* + 2\nu \rightarrow 2\,{}^{14}N + {}^{4}He, \qquad (2)$$

with help of the electropionic attraction due to the exited electron capture and neutral pion catalysis. The excited electron e^* was generated by rapid fracture or sliding of carbonate crystals due to volcanic earthquake, and plenty of neutrinos ν were derived from universe, mainly sun. We assumed that the formation of nitrogen and helium had continued for 1.3 billion years in Archean era, until the active volcanism or storm of neutrinos ceases.

Our next interest lies in studying other possibilities of nitrogen formation in other places. Here we propose other possible formation cases of nitrogen.

2. DYNAMIC INTERACTION BETWEEN C AND O ATOMS IN SEAWATER CONTAINING OF CARBONIC ACID IN DEEP SEA

As described in the previous paper [1], the atmospheric composition of carbon dioxide in Archean era parabolic decreases by dissociation into hot sea. The carbon dioxides dissolved in seawater form carbonic acid, H_2CO_3. The carbonic acid has never been isolated, but it undergoes ionization [11], as indicated by eq.(3).

$$CO_2 + 3H_2O \rightleftarrows CO_3^{2-} + 2H_3O^+ \qquad (3)$$

On the other hand, we must consider the following reaction [12] for dissolution of carbon dioxides.

$$H_2O + CO_2 + CaCO_3 \rightleftarrows Ca^{2+} + 2HCO_3^- \qquad (4)$$

However, since there are no sedimentary rocks such as calcium carbonate at the sea bottom of a few thousand meters below the sea level, the calcium carbonate solute is unsaturated in seawater of deep sea [13]. Indeed, the solute content of carbon dioxide in seawater increases with increasing of depth [14]. Thus there is a possibility that CO_2 ions extremely concentrate at deep sea under high pressure. Here we consider two cases in its existence form; 1. replacement of the CO_3 anions to place of H_3O cations in hexagonal water molecules and 2. intercalation of carbon dioxide in hydrates.

2.1 Compression of CO_3 anions in deep seawater

The pressure dependence of specific volume η in liquid carbon dioxide can be expressed as the form [15]

$$\eta = 1.141e^{-0.0011P} \qquad (5)$$

Since the volume at 1 atm is 1.144, we can calculate volume shrinkage ratio of liquid CO_2 at 275 K [16], which is actually temperature near the bottom of deep sea. We use the C-O bond distance of 0.115 nm [17] for gaseous CO_2 at room temperature under ambient pressure. When CO_3 anions in deep sea are hydrostatically compressed at high pressure, the C-O distance decreases according as increase in depth, *i.e.*,

hydrostatic pressure. The pressure dependence of C-O distance for liquid CO_2 at 275 K is shown is Fig.1. From Fig.1, we get the depth, 10250 m, which corresponds to the critical distance, 0.079 nm [1], required for the dynamic nuclear reaction. It is known that Mariana Trench is 10134 m in depth [18].

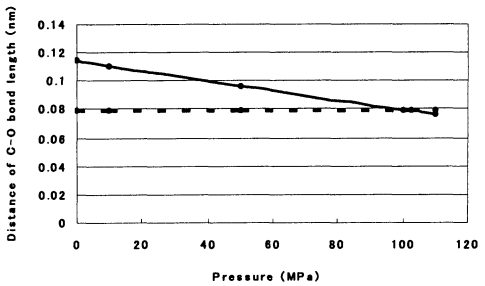

Fig. 1 Pressure dependence of C-O distance for liquid carbon dioxide at 275 K.

2.2 Compression of CO_2 molecules in hydrates at deep sea basin

It has reported that gas hydrates generate only at near-freezing temperatures and under the high pressure over the weight of at least 500 meters below the sea level [19]. The hydrate structure consists of six tetrakaidecahedron and two dodecahedron icy cages that can absorb small gas molecules such as carbon dioxide, methane and hydrogen sulfide [20]. These molecules are intercalated in the cages by electrostatic force. When the cages are hydrostatistically compressed by seawater, the C-O distance decreases according as increase in depth, *i.e.*, hydrostatic pressure, as well as the C-O distance in the previous section. However, since pressure dependence of the C-O distance in carbon dioxide hydrate has not reported yet, we note the pressure dependence of methane hydrate. When the pressure increases, it beguine to crystallize at 0.2-0.3 GPa, then continues the crystalline state to approximately 0.7 GPa, and beguines to decompose to ice VI and fluid methane at 1.5 GPa, and lastly transforme to ice VII and solid methane at 2.3 GPa [21]. Assumed from the behavior, nuclear transformation of nitrogen in dioxide hydrate would not occur, because the water pressure of sea floor in the Earth is not more than 0.1 GPa

3. PHYSICAL ROLE OF HEAVY WATER FOR FORMATION OF NITROGEN

We have already reported the following electropionic reaction [22]

$$e^- + {}^2D \rightarrow \pi^o + \nu + \gamma. \quad (6)$$

From the previous paper [1], it is clear that deuteron D plays important role for formation of nitrogen. The existence of deuteron within reactive zone introduces neutral pions and neutrino, leading to physical catalyses of endothermic nuclear transmutation from carbon and oxygen atoms for formation of nitrogen. Here we note that deuterium in commentary water is enriched by factor of at least 10 relative to the D/H ratio in sea water of the Earth [23]. If an origin of the sea water is water ice in comets or meteorites [24], it is considered that there is a possibility that the primitive sea water, which was abundant in heavy water, played a definitive role for formation of nitrogen. The primitive seawater had also formed D_2CO_3 in absorption of CO_2. Provided that the D_2CO_3 is inserted into calcite lattice under high temperature and high pressure in crust of the Earth, we can assume a configuration and a cross-section of D inserted compound $(Ca,D)CO_3$ [25]. The D atom diffuse other Ca sites. This schema resembles that a nuclear transmutations have been observed on the Pd/complexes which are composed of Pd and CaO thin film and Pd substrate, after subjecting the Pd complexes to D_2 gas permeation [26].

Here we note neutral pion catalysis for nitrogen formation, based on double β decay. Since an addition of neutral pions is equivalent to the addition of two e^- - ν pairs, we reported that the e^- and ν pairs enhances the fusion reaction [27]. The pairs can be also obtained by the double β decay [28]

$$(Z, A) \rightarrow (Z+2, A) + 2e^- + 2\nu, \quad (7)$$

where Z and A are atomic and mass numbers, respectively. From Eqs. (2) and (7), we get the following formula.

$${}^{12}C + {}^{16}O + (Z, A) \rightarrow (Z+2, A) + 2\,{}^{14}N + {}^{4}He, \quad (8)$$

When Z=1, *i.e.*, D, we obtain the next formula from eq.(8),

$${}^{12}C + {}^{16}O + {}^{2}D \rightarrow 2\,{}^{14}N + 2\,{}^{4}He, \quad (9)$$

The double β decay such as ${}^{12}C \rightarrow {}^{12}N$, ${}^{16}O \rightarrow {}^{16}Ne$ and ${}^{40}Ca \rightarrow {}^{40}Ti$ does not occur in nature. High temperature and high pressure accelerates the eq.(9). Eq.(9) is non-equilibrium equation proposed by Prigogine [29]. This is the second

dynamics of the nuclear transmutation of nitrogen formation. It is also reported that emission of charge particle and acceleration of electrical charge make enhance nuclear reaction. This is called as "fractofusion" [30]. In our case, the excited electrons in eq.(7) are generated by rapid fracture and sliding of carbonate crystals. Indeed, it is estimated that the continental crust was often cracked by volcanic earthquake at the Archean era [31]. The detailed reaction was described in previous paper [1]. The Ca is a driving common element for both nuclear transmutations. Especially, there is a possibility that the electrons are derived from calcium element with many electrons such as $3s^2$, $3p^6$ and $4s^2$.

Thus, consumption of deuterium, *i.e.*, formation of nitrogen and helium would continue for 1.3 billion years until content (0.17%) of heavy water in the present sea.

CONCLUSIONS

We studied other possibilities of nitrogen formation in other places in the Earth. When CO_3 anions resolved in deep seawater were hydrostatistically compressed by sea water over critical depth of 10250 m, transmutation of nitrogen would occur. Other possibility is those deuteriums entered into calcite $CaCO_3$ induce transmutation of nitrogen by the double β decay of D atom in primitive Earth's sea enriched by factor of 10.

References:

1) M.Fukuhara, , Nuovo Cimento **27C**, 99 (2004).
2) A.Benlow and A.Meadows, J. Astrophys.Space Sci., **46**, 293 (1977).
3) C.J.Allégre, B.Dupré and O.Brévart,, Philos. Trans. R.London, Ser.**A. 306**, 49 (1982).
4) J.F.Kasting and T.P.Ackerman, Science, **234**, 1383 (1986).
5) P.Warneck,Chemistry of the Natural Atmosphere, 605p, Academic Press, New York, 1998.
6) T.Owen, R.D.Cess and V.Ramanathan, Nature, **277**, 640 (1979).
7) H.Ohmoto, Kagaku, **14**, 360 (1994).
8) J.F.Kasting, Precamb.Res., **34**, 205 (1987).
9) M.I.Budyko,A.B.Ronov and A.L.Yanshin, History of the Earth's Atmosphere, 2, 16 and 128pp,Springer-Verlag, New York,1985.
10) J.-L.Bertaux, in Le Grand Atlas de L'Astromie, edited by J.Andouze and G.Israel 63 p, Encyclopedia Universalis, Japanese language ed., Obunsha, Tokyo,1983.
11) J.J.Lagowski,Modern Inorganic Chemistry, 345p, Marcel Dekker, New York (1973).
12) N.Sasu and T.Asai, Atomosphere and Ocean, 151p, Hoso Daigaku,(1994).
13) T.Akiyama, OceanGraphic Mag., **21**, 53,121pp, 1969.
14) K.Saruhashi, Nihon Kagaku Zashi, **77**, 968 (1956).
15) C.F.Jenkin, Proc. Roy. Sci. London, **A98**, 170 (1920).
16) M.Hoshino, Ocean and Water in Lands, 33p, Tokai University Press,(1956).
17) S.E.Jones, E.P.Palmer, J.B.Czirr, D.L.Decker, J.M,Thorne, S.F.Taylor, and J.Rafelsli, Nature, **338**, 737 (1989).
18) E.Suess, G.Bohrmann, J.Greinert and E.Lausch, Sci.Am.,Nov. 52 (1999).
19) K.Saruhashi, Nihon Kagaku Zashi, **77**, 968 (1956).
20) C.F.Jenkin, Proc. Roy. Sci. London, **A98**, 170 (1920).
21) M.Hoshino, Ocean and Water in Lands, 33p, Tokai University Press, (1956).
22) M.Fukuhara, Fus.Tech., **34**, 151 (1998).
23) D.Bocklee-Morvan,D.Gautier,D.C.Lis,K.Young,J.Keene, T.Phillips,T.Owen,J.Crovisier,P.F.Goldsmith,E.A.Bergin, D.Despois and A.Wootten, Icarus **133**(1),147p. 1998.
24) L.A.Frank,J.B.Sigwarth and J.D.Craven , Geophys. Res. Lett., **13**, 303 (1986).
25) W.L.Bragg,,Proc.Royal Soc.London,Ser.A.,**105**,16 (1924).
26) Y.Iwamura, M.Sakano and T.Itoh, **41**, 4642 (2002).
27) M.Fukuhara, Proc. 6th Meeting of Jpn.Cold Fusion Society, 53 (2005).
28) T.D.Lee and C.S.Wu, Weak Interactions, Ann. Rev. Nucl.Sci.,**5**, 381(1965).
29) I.Prigogine 、Introduction to Thermodynamics of Irreversible Processes, Interscience /Wiley, New York(1968).
30) P.R.Price, Nature, **343**, 542(1990).
31) C.J.Allègre and S.H.Schneider, Sci.Am.,**271**, 44 (1994).

Comments on Role of CaO-Layer in Iwamura Cold Transmutation

Akito Takahashi*1, *2 and Norio Yabuuchi*1
*1 High Scientific Research Laboratory, *2 Osaka University

Abstract: Comments on the role of CaO layer in the MHI transmutation experiments with Pd-complex samples are given. Due to Fermi-level gap in the interface of CaO/Pd layer, additional free electrons from CaO layer will generate transient Cooper pairs with conduction electrons in Pd layer and transient dde*(2,2) quasi-molecules are produced to make 4d/TSC cluster with certain probability. Transmutation reaction by 4d/TSC plus metal-nucleus may be then induced.

1. Introduction

We have proposed a model on nuclear transmutation reaction of 4d/TSC plus metal nucleus system in PdDx surface and lattice focal points[1,2]. Formation of minimum-size "neutral" pseudo-particle of 4d/TSC with about 10 fm diameter is expected to be a seed of nuclear transmutation reaction with host and added metal nuclei. Quantitative estimation of reaction rates are given by the STTBA approximation. Selective transmutations with increment of (mass-8, charge-4), (mass-4, charge-2), (mass-12, charge-6), etc can be treated by the model.

However the role of CaO layer in the Iwamura cold transmutation experiments[3-5] is of open question.

This paper gives a model of TSC formation by combination of two dde*(2,2) EQPET molecules[1,2] which would be generated by localized Cooper pairs (bosonized electron pairs) born at the interface of CaO/Pd layers. Gap of Fermi-levels between CaO and Pd generates "free electrons" from CaO layer with low work-function. These free electrons with momentums may enter the conduction band of Pd layer and form "transient" Cooper pairs e*(2,2). EQPET molecules dde*(2,2) will be then formed at around the interface.

Combination of two dde*(2,2) molecules as transient motion will be happening with some probability there to produce 4d/TSC transient clusters due to stronger condensing force by the change of shielded potentials from the dde*(2,2) state to the dde*(4,4) transient molecular state. Transmuted elements by 4d/TSC plus metal-nucleus reaction, i.e., Pr for instance will diffuse to surface for about 20 nm movement in the MHI Pd-complex samples.

2. Observation of Iwamura Experiments

The structure of Pd-complex samples for deuterium permeation experiments is referred[3] in Fig.1. And typical data for Cs-to-Pr transmutation is referred[4,5] in Fig.2.

We suppose that the transmutation from ^{133}Cs to ^{141}Pr, namely, [mass-8, charge-4]-increased transmutation is the result of ^{133}Cs plus 4d/TSC nuclear fusion (absorption).

From Fig.2, we observe that Pr atoms are detected in the near surface region of 0-30 nm, although Cs-atoms distribute more deeply up to about 100 nm. From Fig.1, the first Pd layer has 40 nm in thickness and the next CaO layer has 2nm in thickness.

As a general view for necessary condition to induce some condensed matter nuclear effect, Iwamura[3-5] suggests that we need high D/Pd loading ratio (we expect x = [D]/[Pd] nearly 1.0, full loading of D in Pd lattice) and high D-flux (more than 1 sccm D-permeation rate). We easily speculate that CaO layers as non-conductive zones may block somehow D-diffusion through the Pd-complex and hence enhance D-concentration in Pd-zones. This is thought to be **the first role of CaO**.

The second important role is speculated as for providing "free electron emission" which may be enhanced in the interface between Pd and CaO layers and may relate to the formation of EQPET dde*(2,2) molecules and 4d/TSC clusters, as we discuss in the next section.

Fig.2 shows that enough Cs atoms existed at around the interface (40 nm depth from the

surface). If we suppose that 4d/TSC is produced near around the interface and makes "metal(Cs) + 4d/TSC" nuclear interaction there, Pr would have been produced also around the interface which located at 40 nm from surface. Since observed Pr atoms distributed in the 0-30 nm depth from the surface, we then have to assume that transmuted Pr atoms diffused toward the surface for about 20 nm distance in average, during the experiment.

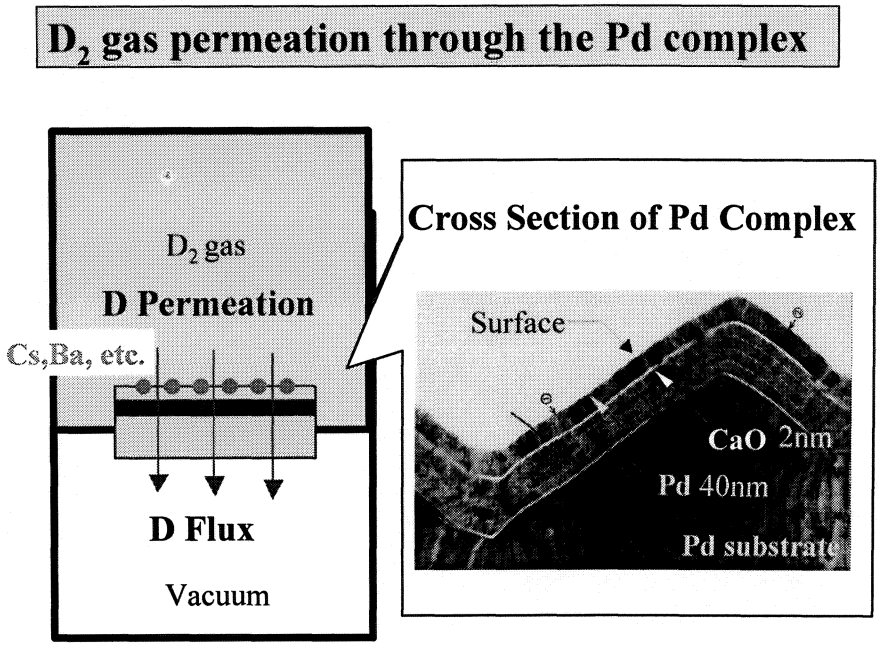

Fig.1: Sample structure of MHI D-permeation and transmutation experiment[3)]

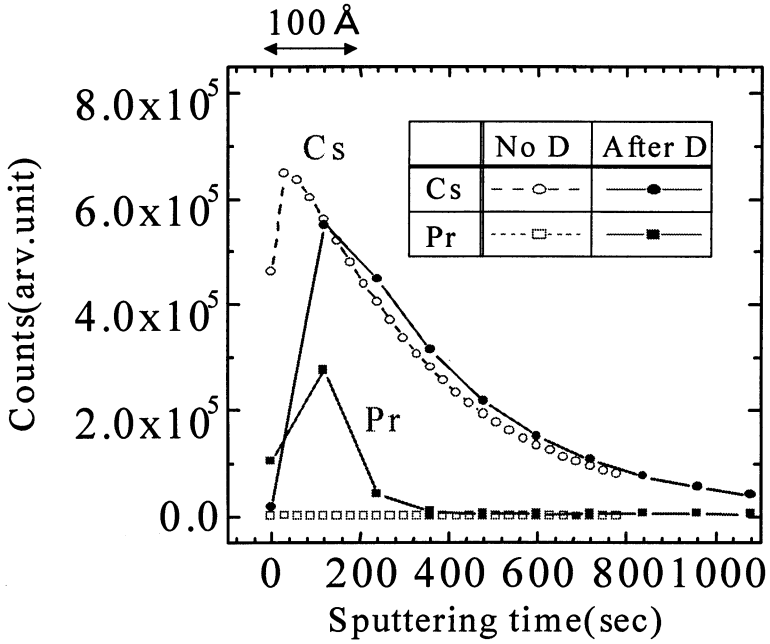

Fig.2: Depth profile of transmuted Pr and original Cs elements[4,5)]

3. The Second Role of Pd/CaO Interface

In addition to the first role as blocking layer for D-permeation, the Pd/CaO interface may have the second role for producing "quasi-free electrons" due to the Fermi-level gap between Pd and CaO. Pd metal is known as electric conductive material. Electron conduction band in the Pd lattice is made by 4d-shell electrons of Pd-atoms and the Fermi-energy (Fermi-level) is high enough to be in the conduction band. On the other hand, CaO is non-conductive material, but its work-function Φw (gap between the lowest level of conduction band and the Fermi-level) is small.

As shown in Fig.3, we may expect emission of "free" electrons from CaO layer into the conduction band of Pd layer, due to the Fermi-level gap at the interface. These free electrons convey meaningful-level of momentums, and may compose local "bosonized" pairs with existing quasi-free electrons in the Pd conduction band. Namely, we expect the generation of "transient" Cooper pairs e*(2,2)'s on the Fermi-level surface of Pd-layer in the zone around the interface. Therefore we may speculate the generation of "local" superconductivity along the interface by these local Cooper pairs, even at room temperature. With respect to the condensed matter nuclear effect, these transient Cooper pairs may stick on deuterium to form dde*(2,2) transient quasi-molecules. Our theoretical interpretation on the results of 3D fusion experiment[6), 2)] by low energy D-beam predicts that the life time of dde*(2,2) would be on the order of 0.1 ms, that is relatively long.

Then we speculate that 4d/TSC may be formed with certain probability by the combination of two dde*(2,2) transient molecules, in orthogonally coupled state with coherence in d-d distance vibration modes at some trapping or focal sites of Pd layer.

This scenario is drawn in Fig.4.

In our past modeling[1,2)], we proposed that dynamic ordering (or constraint) motion of TSC squeezing process in PdDx lattice could enhance very much the formation of minimum-size state 4d/TSC cluster. However, we do have still open question about the detailed mechanism of TSC formation under ordering process in the region around the interface where we need to take into account of Pd lattice, deuterons trapped in Bloch potentials, impurity Cs atoms, CaO lattice, free electrons, transient Cooper pairs, etc, to reach at the more complete modeling for quantitative analysis on TSC formation probability.

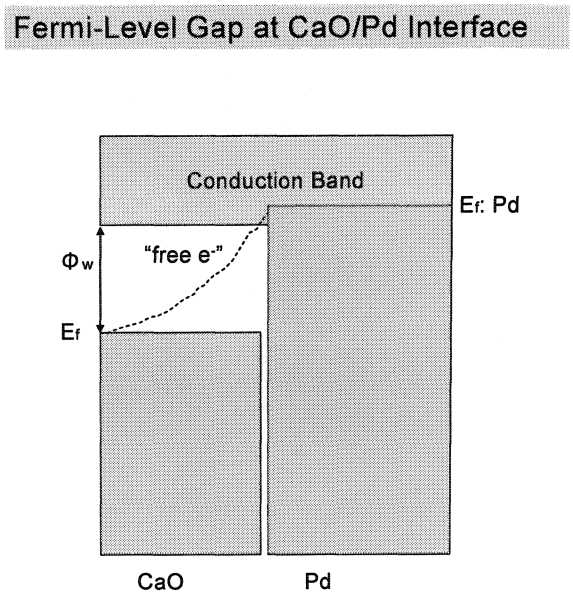

Fig.3: Generation of "free electrons" by the Fermi-level gap at the interface of Pd/CaO layers in MHI Pd-complex sample; Ef denotes Fermi-level.

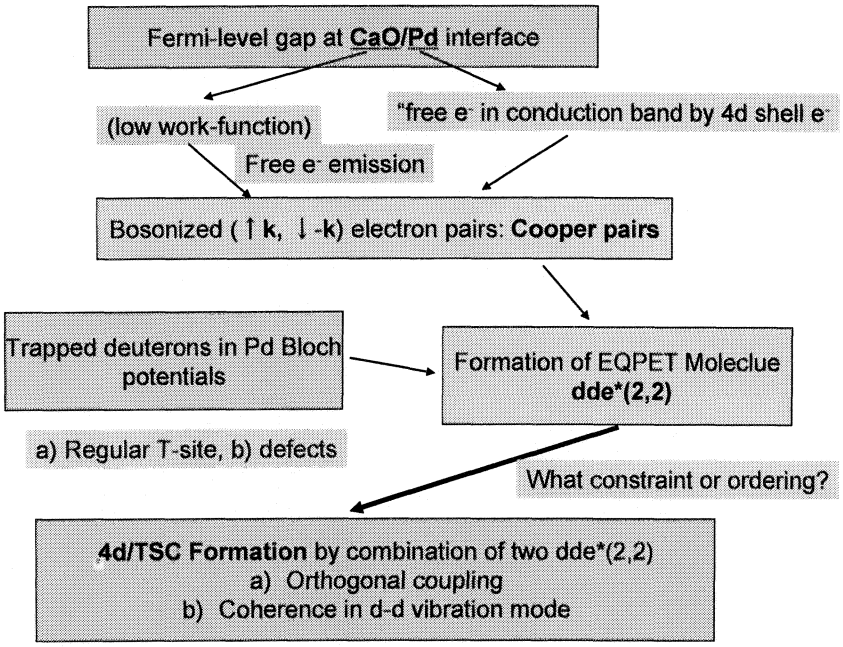

Fig.4: Scenario of Pd/CaO role and TSC production at around interface

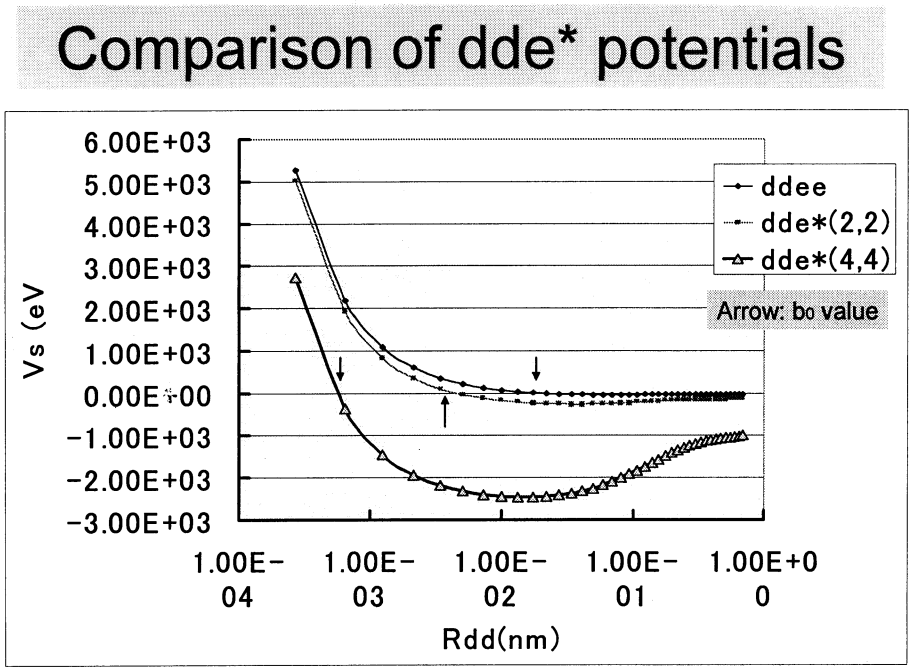

Fig.5: Shielded Coulomb potentials for ddee (namely D_2), dde*(2,2) and dde*(4,4) states with b0-parameters (shown by arrows); Drastic decrease of b0-parameters (see position of arrows) for the change from regular molecule D_2 to dde*(2,2) and then the change from dde*(2,2) to dde*(4,4) corresponds to the deepening of trapping potential depths (negative potential depths), which induce strong condensing force for forming 4d/TSC state.

Around the boundary region of Pd/CaO layer, microscopic transient Cooper pairs e*(2,2) are expected to generate. The transient pseudo molecular state dde*(2,2) will be formed and can have so deeper trapping potential well with smaller b0-parameter (4 pm) for d-d barrier penetration than those (b0 = 20 pm) for usual molecule ddee (namely D_2) that transient condensing force for combining two dde*(2,2) molecules in orthogonal condition can be generated. The formation of 4d/TSC state may have much deeper trapping potential well with much shorter b0-parameter (0.36 pm) to lead to squeezing of 4d/TSC for central condensed state (TSC-minimum) in short time interval (about 80 fs). The change of screened potentials is illustrated in Fig.5, comparing for ddee, dde*(2,2) and dde*(4,4) states.

---

5. Conclusion

Fermi-level-gap with low work-function for CaO layer and Pd conduction band will enhance the generation of transient "bosonized pairs" of electrons around the Pd/CaO interface.

Transient pseudo-molecules dde*(2,2) and its orthogonal coupling 4d/TSC are formed in the region. The minimum-TSC state will cause self-fusion of 4d reaction (two ^{4}He particles are ash of reaction, 23.6 MeV/^{4}He) and transmutation of metal-nucleus + 4d/TSC reactions.

Sample cathode of multi-layers (two to three-dimensional modification) with many Pd/CaO interfaces will be interesting sample for CMNE studies.

References:

1) A. Takahashi: Deuteron cluster fusion and related nuclear reactions in metal-deuterium/hydrogen systems, *Recent Res. Devel. Physics*, 6(2005)pp.1-28, ISBN: 81-7895-171-1

2) A. Takahashi: Brief Theoretical Summary of Condensed Matter Nuclear Effects, Acta Physica et Chemica, Debrecen, Hungary, Vol.38-39, (2005)341-356

3) Y. Iwamura, et al: *JJAP*, 41(2002)4642

4) Y. Iwamura, et al: Proc. ICCF10, World Scientific, pp.435-446 (2006)

5) Y. Iwamura, et al: Proc. ICCF11, World Scientific, pp.339-350 (2006)

6) A. Takahashi, et al: Proc. ICCF10, World Scientific, pp. 657-666 (2006)

Formation of Tetrahedral, Octahedral or Hexahedral Symmetric Condensation by Hopping of Alkali or Alkaline-earth Metal Ion

Hidemi Miura

1-27-6 Tsurugaoka, Izumi-ku, Sendai. 981-3109, Japan

Abstract: When hydrogen/deuterium (H/D) atoms enter into interstitial sites of a transition metal, they expand slightly the interatomic distances of the metal lattice by forming hydrides/deuterides, and then alkali or alkaline-earth metal ions would be able to move easily in it. The probability which alkali or alkaline-earth metal ions move into the other interstitial sites or vacancies overcoming the repulsion potential barrier of the host metal increases, if it is reduced by outer electrical potentials, electromagnetic impulses, etc. While an alkali or alkaline-earth metal ion exchanges positions with one of the H^+/D^+ ions which constitute Tetrahedral Symmetry, Octahedral Symmetry or Hexahedral Symmetry, the other ones are also put back inside the polyhedral symmetry and squeezed by a reaction. Exchanging one phonon of the host metal lattice generates electron transitions of 1s orbital of H/D atoms which are put back inside each polyhedral symmetry, and then electron Cooper pairs and hole Cooper pairs are created, and it occurs for every pair of opposite H/D atoms. The electron Cooper pairs shield the Coulomb repulsion, then H^+/D^+ ions form Tetrahedral Symmetric Condensate, Octahedral Symmetric Condensate or Hexahedral Symmetric Condensate.

1. Introduction

Some models and theories of the nuclear fusion and nuclear transmutation in condensed matter have been advocated. In these, Tetrahedral Symmetric Condensate / Octahedral Symmetric Condensate / Hexahedral Symmetric Condensate (TSC/OSC/HSC) model of protons/deuterons by Takahashi can explain consistently the major experimental results of light/heavy water electrolysis, deuterium permeation and other experiments.[1-2]

We have studied and introduced recently a rough scenario about the formation of TSC/OSC by hopping of alkali or alkaline-earth metal ions into the other sites of the crystal lattice of the host metal.[3]

Making the scenario more in detail, this time, we have studied a mechanism, in which the probability of movement of atoms/ions increases when the repulsion potential barrier of the host metal lattice is reduced by outer electrical potentials, electromagnetic impulses, etc. Moreover, we have studied a mechanism, in which exchanging one phonon of the host metal lattice generates electron transitions of 1s orbital of H/D (hydrogen/deuterium) atoms, and then electron Cooper pairs and hole Cooper pairs are created, and it occurs for every pair of opposite H/D atoms.

2. More Detailed Scenario of Formation of TSC/OSC/HSC

We made the scenario of the formation of TSC/OSC/HSC more in detail:

2.1 Permeation of H^+/D^+ Ions and Formation of Hydride/Deuteride

Figure 1 shows permeation of H^+/D^+ ions and typical infiltration of alkali or alkaline-earth metal ions in the case of electrolysis of water and in a deuterium permeation experiment.

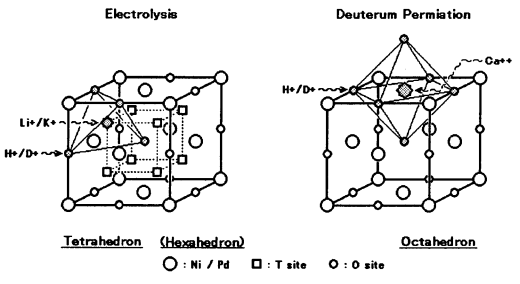

Figure 1. Permeation of H^+/D^+ ions and Infiltration of alkali or alkaline-earth metal ions (typical).

Permeating inside the host metal from the surface of it by electrolytic voltage and gas permeating pressure, and maintaining electrical balances with surrounding free electrons, H^+/D^+ ions (protons/deuterons) move through

interstitial sites corresponding to a concentration gradient or a slope of electrical potential. When the concentration of H/D atoms increases in the host metal, in the case of transition metal, H/D atom is confined to interstitial site, and then a hydride/deuteride is formed by an interaction between 1s orbital of H/D atom and d orbital of the host transition metal.

If the H/D atom content of the host metal is small atomic ratio (Pd: 0.56-1), in the case of fcc crystal lattice such as Ni and Pd, H/D atoms enter into O sites, and if it is large atomic ratio (Pd:1-2), they enter into T sites. Confining H/D atoms to the interstitial sites of the host metal pushes out the surrounding host metal atoms (O site: eight, T site: four) and expand the lattice, and then surrounding interatomic distances and surrounding lattice energies increase.

2.2 Infiltration of Alkali or Alkaline-earth Metal Ion and Formation of TS/OS/HS

Nonmetallic atom such as carbon, nitrogen and oxygen other than H/D, of which the atomic radius referred to the host metal atom which have comparatively large atomic radius (more than 1.3 Å) is less than 0.59, can be enter into the interstitial sites of it.

When H/D atoms enter into the interstitial sites of the host metal, they expand the interatomic distances of the host metal lattice, and then a large radius atom can enter into the interstitial sites of it. An alkali or alkaline-earth metal which ionizes easily can enter into the interstitial sites by ionizing, because its ionic radius is smaller than its atomic radius. In the host metal lattice of fcc, where H/D atoms occupy O sites of it, most of the alkali or alkaline-earth metal ions enter into T sites. Since the space of T site is smaller than that of O site, Li^+ ion which has a small ionic radius and 1 valence favorably enters into T site.

In the host metal lattice of fcc, when H/D atoms enter into O sites or vacancies of it, they form TS (Tetrahedral Symmetry, H/D: four) or OS (Octahedral Symmetry, H/D: six), respectively, and they are located at the vertexes of each polyhedral symmetry centering the alkali or alkaline-earth metal ion. Moreover, when H/D atoms enter into T sites of the host metal lattice, they form HS (Hexahedral Symmetry, H/D: eight). In the host metal lattice of fcc, H/D atoms located at the vertexes of each polyhedral symmetry are pushed out outside the usual interstitial sites due to the alkali or alkaline-earth metal ion of the center of it.

2.3 Hopping of Alkali or Alkaline-earth Metal Ions and Squeezing of H^+/D^+ Ions

Figure 2 shows typical case of hopping of alkali or alkaline-earth metal ions, squeezing of H^+/D^+ ions, recoil and condensation of protons/deuterons.

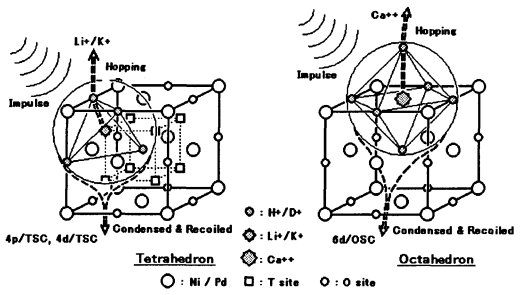

Figure 2. Hopping of alkali or alkaline-earth metal ions, Squeezing of H^+/D^+ ions, Recoil and Condensation of protons/deuterons (typical)

When a slope of electrical potential arises, or when periodic electromagnetic impulses are added, the probability of movement and hopping of the alkali or alkaline-earth metal ion from T site, O site or vacancy to the next sites increases due to the overcoming the reduced repulsion potential barrier of the host metal lattice. While the alkali or alkaline-earth metal ion located at the center of TS, OS or HS moves into the next O sites or T sites of the vertexes of each polyhedron with H^+/D^+ ions, one H^+/D^+ ion confined there is put back inside it exchanging positions with the alkali or alkaline-earth metal ion so that the other ones confined at the other vertexes of it still pushed outside are put back inside it and squeezed by a reaction simultaneously maintaining the spatial symmetry.

2.4 Creation of Cooper Pair by Electron Transitions of 1s Orbital of H/D Atoms

When H^+/D^+ ion is put back inside TS, OS or HS, it draws the 1s orbital electron of H/D atom interacting with the d orbital electrons of the host metal and moves toward the center of it maintaining the spatial symmetry.

Exchanging one phonon of the host metal lattice generates electron transitions, which are 1s orbital drawn electrons of H/D atoms, from the Fermi sheet of H/D atoms located at the space symmetrical vertexes of TS, OS or HS to that of the host metal atom of Ni/Pd, and then electron Cooper pairs and hole Cooper pairs are created, and it occurs for every pair of opposite H/D atoms.

2.5 Condensation of Protons/Deuterons and Nuclear Fusion or Transmutation

The electron Cooper pairs condense and shield the Coulomb repulsion of squeezed cluster H^+/D^+ ions (protons/deuterons) moving toward the center of TS, OS or HS and maintaining each polyhedral symmetry. And then, according to Takahashi's Electronic Quasi-Particle Expansion Theory, four, six or eight protons/deuterons (H^+/D^+ ions) form Tetrahedral, Octahedral or Hexahedral Symmetric Condensation, respectively.[1-2]

When the alkali or alkaline-earth metal ion which has moved to the next O site or T site, having exchanged the position with one of the H^+/D^+ ions (protons/deuterons) confined at the vertexes of TS, OS or HS, further moves to another T sites, O sites or vacancies and hops out from the system of four, eight or twelve atoms of the host metal surrounding each polyhedral symmetry, respectively, four, six or eight H^+/D^+ ions (protons/deuterons) of each polyhedron squeezed into the center of it maintaining the spatial symmetry receives the reaction of hopping of the alkali or alkaline-earth metal ion as a whole.

When the squeezed cluster D^+ ions (deuterons) do not receive the strong recoil from the hopping of the alkali or alkaline-earth metal ion, TSC, OSC or HSC would cause the nuclear fusion of four, six or eight deuterons in the main, respectively, according to Takahashi's TSC/OSC/HSC nuclear fusion theory.[1-2] If TSC, OSC or HSC consists of H^+ ions (protons), no nuclear reaction proceeds.

On the other hand, when the squeezed cluster H^+/D^+ ions (protons/deuterons) receive the strong recoil from the hopping of the alkali or alkaline-earth metal ion, TSC, OSC or HSC would cause the nuclear fusion, nuclear transmutation or nuclear fission related to the collision of four, six or eight protons/deuterons against the other atomic nucleus of the host metal, respectively.

For example, especially in the combination of weak recoil of squeezed cluster D^+ ions (deuterons) the clean nuclear fusion would be caused.

In the case of 4d/TSC:

$$4d/TSC \rightarrow Be^* \rightarrow 2\alpha + 47.6MeV \quad (1)$$

In the combination of strong recoil, much kind of nuclear transmutations or nuclear fissions would be caused.

In the case of 4p/TSC:

$$4p/TSC + M(A, Z) \rightarrow M^*(A+4, Z+4), \text{others} \quad (2)$$

In the case of 4d/TSC:

$$4d/TSC + M(A, Z) \rightarrow M^*(A+8, Z+4), \text{others} \quad (3)$$

In the case of 6d/OSC:

$$6d/OSC + M(A, Z) \rightarrow M^*(A+12, Z+6), \text{others} \quad (4)$$

In the case of 8d/HSC:

$$8d/HSC + M(A, Z) \rightarrow M^*(A+16, Z+8), \text{others} \quad (5)$$

3. Discussions

3.1 Increase of Probability of Movement and Diffusion of Atom/Ion

According to the diffusion theory in which a light atom passes along the interstitial sites of lattice within a metal, when a partial free energy (potential barrier) decreases along with the fall of concentration of the light atoms, and the amount of drop of potential barrier is δG, the increase of probability of overcoming the barrier and the flux of atomic diffusion are given by, respectively:

$$P = \exp(-(G - 1/2 \cdot \delta G)/RT) \quad (6)$$

$$J = 1/6 \cdot \nu c d \exp(-G/RT)\, \delta G/RT. \quad (7)$$

Here G is partial free energy (potential barrier), R is the gas constant, T is temperature, ν is frequency of the host metal atoms, c is concentration of atoms moving in the host metal and d is interstitial distance of the host metal lattice.

3.1.1 Alkali or Alkaline-earth Metals Ion

From equation (6), when a slope of electrical potential arises by electrolytic voltage, gas penetrating pressure, plasma electric discharge, etc., or when a periodic electromagnetic impulses are added by ultrasonic wave, laser, etc., the repulsion potential barrier go down occasionally. Then the probability of movement and hopping of the alkali or alkaline-earth metal ion from T site, O site or vacancy to the next sites would increase because it overcomes the reduced repulsion potential barrier of the host metal lattice.

3.1.2 H^+/D^+ Ions

In movement and diffusion of H^+/D^+ ions inside the host metal, the probability of overcoming by the equation (6) and the flux of diffusion by the equation (7) increase due to the quantum tunnel effect. Therefore, H^+/D^+ ions can move and diffuse inside the host metal quickly. In order that H^+/D^+ ions constitute the stable polyhedron symmetry, and the alkali or alkaline-earth metal ion hops out to cause the condensation of protons/deuterons (H^+/D^+ ions), Pd of a transition metal with fcc lattice structure is most suitable, in which the occlusions of H/D atoms are carried out and hydrides/deuterides are made.

When the alkali or alkaline-earth metal ion located at the center of TS, OS or HS moves into the next O sites or T sites of the vertexes of the polyhedron, exchanging positions with H^+/D^+ ion there, the potential barrier for H^+/D^+ ions which have been pushed out by the alkali or alkaline-earth metal ion, and have formed the hydrides/deuterides with the host metal atoms go down toward the inner side of the polyhedron, and then H^+/D^+ ions are put back inside it by the equation (6).

3.2 Creation of Cooper Pairs

The creation of the electron Cooper pairs which shield the Coulomb repulsion force related to the condensation of H^+/D^+ ions (protons/deuterons) might become important to form TSC, OSC or HSC. However, the size of the electron Cooper pair in type I superconductor (elemental superconductor; about 0 K, large current) is almost 10^4 Å. This electron Cooper pair is created by exchanging one light acoustic phonon of the host metal lattice, which acts as an attractive long-range force binding both electrons generated by the excitation of two pairs of electrons and holes due to the two electron transitions near the Fermi surface of the host metal. This electron Cooper pair is too large to shield the Coulomb repulsion force of the condensed protons/deuterons (H^+/D^+ ions) inside TS, OS or HS which is as large as or smaller than the unit cell of the host metal lattice.

On the other hand, according to the theory of high temperature superconductor (cuprate superconductor; about 100 K, small current), the size of the electron Cooper pair is a few ~ 10 Å.[4] This electron Cooper pair is created by exchanging one heavy optical phonon of the host metal lattice, of which wavelength is as short as the lattice constant of it, which acts as an attractive short-range force binding both electrons generated by the excitation of two pairs of electrons and holes due to the two electron transitions between two Fermi sheets of compounds. This electron Cooper pair is suitable in size to shield the Coulomb repulsion force of the condensed protons/deuterons inside of TS, OS or HS.

3.2.1 Preliminary Trial: Plane Model of TS

Figure 3 shows Square Symmetry (SS) reduced from Tetrahedral Symmetry (TS) which consists of four Ni/Pd atoms and four H/D atoms, and shows its Fermi Surface in which electron Cooper pair and hole Cooper pair are created at (B, B') and (A, A'), respectively.

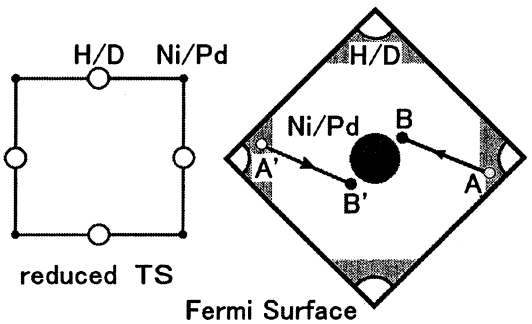

Figure 3. Square Symmetry (SS) reduced from Tetrahedral Symmetry (TS) and its Fermi Surface.

As a preliminary trial, in order to apply the technique of the theory of high temperature superconductor of the two-dimensional plane of YBCO etc. directly to the most simple structure of TS, three dimensional structure constructed with H/D atoms located at vertexes of it and host metal atoms of Ni/Pd surrounding them is reduced to the plane two dimensional structure of Square Symmetry (SS) constructed with the host metal atoms of Ni/Pd located at four vertexes of it and H/D atoms confined at four sides. In this plane model, two dimensional Fermi surface has two sheets illustrated by the electron circle of the host metal atom of Ni/Pd at the center and the small electron hole pockets of H/D atoms at Brillouin boundary. Then, one phonon exchange would create Cooper pair in this condition:

When the alkali or alkaline-earth metal ion located at the center of SS moves to the outside of it exchanging the position with one of H^+/O^+ ions, all of them are put back together inside it and move to the center of it drawing the 1s orbital electrons of H/D atoms interacted with the d orbital electrons of the host metal atom of Ni/Pd, maintaining the spatial symmetry of SS. In SS, an electron Cooper pair and a hole Cooper pair are created by exchanging one heavy optical phonon of the host metal lattice, which has short wavelength and acts as an attractive short-range force binding both electrons generated as the two pairs of electrons and holes due to the two electron transitions, which are the 1s orbital electrons of H/D atoms, from the near spaces (A, A') of small electron hole pockets in the Fermi sheet of H/D atoms to those (B, B') of electron circle in the Fermi sheet of the host metal atom of Ni/Pd.

3.2.2 Future Subjects

After this, we would analyze this SS model more in detail, and try to construct three dimensional TS, OS and HS more precisely using aforementioned SS or other similar plane symmetry. For example, TS would be constructed by the superposition of six SS planes consisting of two-Ni/Pd and two-H/D atoms, intersecting so that each three intersected lines of each two planes were mutually perpendicular. And, OS would be constructed by the superposition of three mutually perpendicular aforementioned SS planes. HS would be constructed by the superposition of six SS planes consisting of four-outer-Ni/Pd and four-inner-H/D atoms, intersecting so that each three intersected lines of each two planes were mutually perpendicular. Each H/D atom of TS, OS or HS would be superposed by three, two or three states on each intersecting planes, respectively. Cooper pairs would be created along the intersected lines of two planes, passing through each H/D atom and the center of each polyhedron.

4 Conclusion

We studied the scenario of formation of TSC, OSC or HSC more in detail, and studied the mechanism in which the probability of movement of an atom/ion increases, and the mechanism in which exchanging one phonon of the host metal lattice creates electron Cooper pair: As a preliminary trial, in order to apply the technique of the theory of high temperature superconductor, we suggested the plane two dimensional SS (Square Symmetry) model reduced the most simple three dimensional structure of TS.

Acknowledgements

The author wishes to thank Professor Takahashi of Osaka University for valuable information and advice.

References

1. A. Takahashi, Deuteron cluster fusion and related nuclear reaction in metal-deuterium/hydrogen systems, Recent Res. Devel. Phys. 6, 1-28 (2005).
2. A. Takahashi, $^3He/^4He$ PRODUCTION RATIOS BY TETRAHEDRAL SYMMTERIC CONDENSATION, Proc. ICCF11, in press, http://www.lenr-canr.org/
3. H. Miura, STUDY ON FORMATION OF TETRAHEDRAL OR OCTAHEDRAL SYMMETRY CONDENSATION BY HOPPING OF ALKALI OR ALKALINE-EARTH METAL ION, Proc. ICCF12, in press, http://www.lenr-canr.org/
4. S. Fujita and S. Godoy, Theory of High Temperature Superconductivity (Kluwer Academic Publishers).

Tetrahedral and cubic forms Ψ and condensate nuclear fusion

Norio YABUUCHI and Akito TAKAHASHI
High Scientific Research Laboratory
2nd Floor, Takano Building, 24-16 Marunouchi, Tsu City, Mie 514-0033, JAPAN
E-mail yabuuchi@kogakken.co.jp, yabu333@lilac.ocn.ne.jp

Abstract:
When theorizing about condensate deuterium fusion reaction, employing a hierarchical model that posits transition to structures having Platonic symmetry (regular polyhedra) enables theoretical development by the same analogy. Strong nuclear interaction in the case of a regular-tetrahedral condensate, and a model of transition between Platonic-structure arrangements are discussed.

1. Introduction

Accomplishment of transmutation in a solid through nuclear fusion unlike any known previously was clearly evidenced by the experiment conducted by Iwamura, et al.[1], and thereafter by the experiment of Kitamura, et al. Kobe University.[2] Accordingly, the arrangement of ions in the atomic nuclei in a solid must have unique properties. Additionally, it has been postulated that a force that attempts to form Platonic structures acts strongly and mutually among the nuclei in addition to condensing force. This formative force, as a medium of electrons in the field of molecular chemistry, is a concept receiving much attention as a self-organizing force[3]. In the area of elementary particles as well, Heisenberg postulated a force that forms elementary particles, borrowing from Platonic and Aristotelian philosophy to name this force a "form;" form theory is developed in his *Physics and Philosophy: The Revolution in Modern Science*.[4] Carl Friedrich von Weizsäcker similarly applied the concept of forms to molecules, atoms, and elementary particles. Platonic structures found success long ago in Kepler's theory of the solar system, and more recently the names of such Platonic polyhedra as the cube and the tetrahedron have become commonplace for structures in molecular chemistry. Professor Matthias Brack of the University of Regensburg, frequently cited by the authors, has succeeded in analyzing atomic structure by means of Platonic polyhedra.[5]

Attacking the final citadel – that is, elucidating the Platonic polyhedral structure of the atomic nucleus – has often been attempted in the past, but further impetus has been added to elucidating nuclear fusion[6,7], and so this paper explores the theory behind it.

2. Basic Concepts

When the wave function in the coordinate representation for a dynamical system composed of n particles is taken to be $\Psi(q_1 s_1 \quad q_2 s_2 \cdots q_N s_N, t)$, its Schrödinger representation is as follows:

$$i\hbar \frac{\partial \Psi}{\partial t} = \left\{ \sum_{j=1}^{N} H_{(qj)} + \sum_{j \neq k}^{M} W_{(qj,\,qk)} \right\} \Psi \qquad (1)$$

$H_{(qj)}=\hbar^2\Delta_j^2/2m + U_{(qj)}$ is the energy operator for the *j*th particle.

For U(qi), refer to Brief Review on Fusion Rates of Bosonized Condensates Parts I and II (JCF7).[8,9]

Here, W indicates the potential of strong interaction, and U indicates the potential of electromagnetic or Coulomb interaction. Deuterium, having a compound nucleus composed of a proton and a neutron, is a boson, and absorption of it in large amounts in a hydrogen-occlusion alloy may lead to a kind of Bose-Einstein condensation. Further, a cluster of deuterium condensed near the thin-film layer boundary of the metal may

exist in a symmetric configuration[10]. Wave motion having the property to arrange the deuterium into a tetrahedral or cubic regular polyhedron forms this configuration. This wave motion acts to arrange the deuterium existing in the wave motion into tetrahedral and cubic regular polyhedra. (In Greek philosophy, a substance which is matter formed into a uniform configuration is termed a "form.")

The potential U(q) of equation 1 is shielded potential when r > r0, as shown in figure 1 (with reference to Fig.1-5 in reference [8]), and the change in depth of the negative component becomes condensing force. Parameter r is the relative distance between deuterium nuclei.

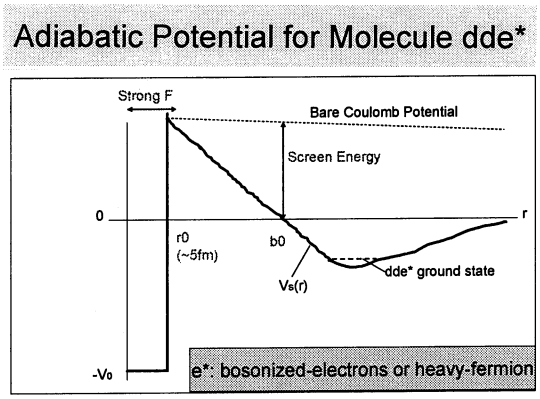

Figure 1. Potential curve for d-d interaction; scale of screening energy, bo value, and depth of negative trapping potential reflect in condensing force for deuteron clusters by the Platonic configuration in condensed matter. Condensation is time-dependent process and its trapping potential is approximated with the adiabatic treatment.

The lower the negative-potential energy, the thinner becomes the Coulomb barrier, the larger grows the tunneling rate, and the better become the conditions facilitating nuclear fusion. The source of the required energy for the tunnel effect in this case is the screening energy at the time of regular-tetrahedral condensation, which is 4 keV (see Table 1 [9]. Next, when a deuteron pair passes through the Coulomb barrier and experience fusion due to strong mutual interaction of the deuterium nuclei, the donor and acceptor forces of the Ψ become formative force that attempt to form a Platonic tetrahedral structure act in combination. This energy, as a result, is sufficient if it exceeds the screening energy of 4 keV for condensing the regular tetrahedron, as shown in Table 2-1 of reference 9. Accordingly, after the passage through the Coulomb barrier, the force of strong mutual interaction by mesons acts additionally, resulting in complete fusion. This means that initially condensing force, subsequently formative force, and finally strong mutual interaction are exerted, resulting in "triple-relay" fusion by these forces.

Table-1: Screening energy Us and bo parameter for dde* molecule

	Us(eV)	Us(eV)	bo (pm)	bo(pm)
e*	dde*	dde*e*	dde*	dde*e*
(1,1)	36	72	40	20
(2,2)	360	411	4	3.5
(4,4)	4,000	1,108	0.36	1.3
(8,8)	22,154	960	0.065	1.5
(208,1)	7,579	7,200	0.19	0.20

3. Strong Interaction and Platonic Symmetry

The tetrahedral structure of helium that is explored below is depicted in Fig.2; Figure 3 depicts the cubic structure of beryllium (see reference [5]).

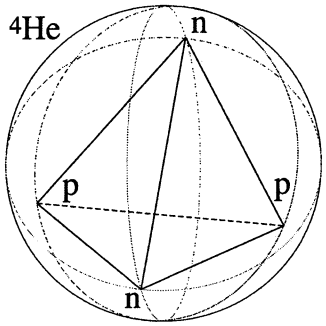

Figure 2. Tetrahedral structure of helium

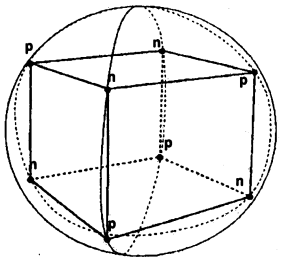

Figure 3. Cubic structure of beryllium-8 as intermediate state

A deuteron is composed of one proton and one neutron, and is believed to exist in a state in which one proton and one neutron are missing from the four nucleons of helium arranged in a tetrahedral form having four apices. When this is expressed as an equation, the regular tetrahedral structure is inscribed within and circumscribed about a sphere, and Ψ_T, taken to be the spherical coordinate, is believed to experience the force of U(qj) and external force and to create a strong mutual interaction with the tetrahedral form (wherein q_1 is the proton and q_2 is the neutron):

$$\Psi_T = \Psi_T (q_{n_1 l_1 m_1 s_1}, q_{n_2 l_2 m_2 s_2}, o, o, t) \quad (2)$$

Although this exists within the probability waves of both the proton and the neutron, Ψt at a given time Δt is believed to yield both Ψ_{T1} and Ψ_{T2}:

$$\Psi_{T1} = \Psi_{T1}(q_1 s_{1/2}, q_2 s_{1/2}, o, o, \Delta t),$$
$$\Psi_{T2} = (o, o, q_3 s_{-1/2}, q_4 s_{-1/2}, \Delta t) \quad (3)$$

Here, q_3 represents the proton and q_4 the neutron.
In Eq.3, to become ^{4}He in a mutually tetrahedral form, for example by action in which Ψ_{T1} attempts to accept q_3 and q_4 from Ψ_{T2}, Ψ_{T2} attempts to donate q_3 and q_4 to Ψ_{T1}. As this self-organizing force, the donor and acceptor forces are normally exerted in the phenomenon of chemical bonds[10], as donor of proton or electron, and so are applied analogously. This yields:

$$\Psi_{T1+2} = a^*a^* \Psi_{T1}(q_1 s_{1/2}, q_2 s_{1/2}, o, o, \Delta t)$$
$$+ aa \Psi_{T2} (o, o, q_3 s_{-1/2}, q_4 s_{-1/2}, \Delta t)$$
$$= \Psi_{T1+2} (q_1 s_{1/2}, q_2 s_{1/2}, q_3 s_{-1/2}, q_4 s_{-1/2}, \Delta t) \quad (4)$$

(Here, a*a* represent the acceptor operators and a a the donor operators.) Accordingly, this yields the results shown in Fig. 4.

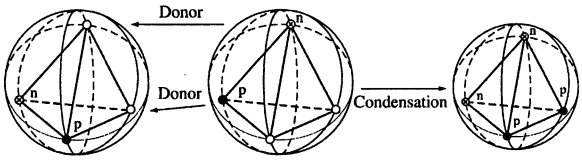

Figure 4. Process by which two deuterium nuclei condense into a helium nucleus

Expressed using Schrödinger's equation, this yields:

$$i\hbar \frac{\partial \Psi_{T1+2}}{\partial t} = \left\{ \sum_{j=1}^{4} H_{(qj)} + \sum_{j \neq k}^{6} W_{(qj, qk)} \right\} \Psi_{T1+2}$$
$$H(qj) = \hbar^2 \Delta_j^2 / 2m + U(qj)$$
$$(Ex = 23.8 \text{ MeV}) \quad (5)$$

Note, however, that the interaction by the donor and acceptor due to the formative force does not arise from deuterons or other particles, but rather the force due to Ψ that forms Platonic structures, and is therefore represented by operational calculus.
A phenomenon similar to that in equation 4 occurs in the Bose-Einstein condensation, yielding:

$$\Psi_{T3+4} = \Psi_{T3+4} (q_5 s_{1/2}, q_6 s_{1/2}, q_7 s_{-1/2}, q_8 s_{-1/2}, \Delta t)$$
$$(Ex = 23.8 \text{ MeV}) \quad (6)$$

In equations 4 and 6, in terms of the states of nuclear physics, the occurrence of collective excitation results in an extremely unstable nuclear structure, causing a transition toward cubic-form ^{8}Be, which has an even higher energy value. (That is to say, ^{4}He* + ^{4}He* → ^{8}Be*). Here the collective excitation is a mode of nucleus excitation by deformed oscillation and rotation (see p.122 of the text book[11]).

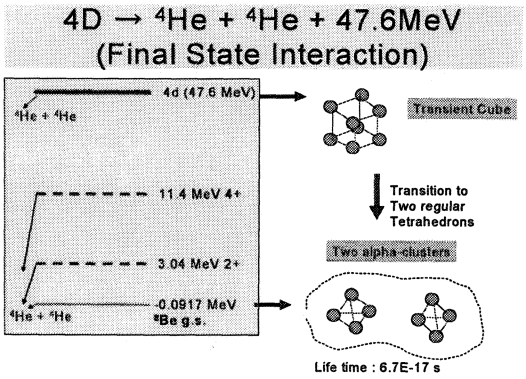

Figure 5. Platonic transition from cube to tetrahedron for 4D fusion break-up

Accordingly, this yields:

$$\Psi_{C1} = \Psi_{C1}(q_1 s^{1/2}, q_2 s^{1/2}, q_3 s^{-1/2}, q_4 s^{-1/2}, o, o, o, o, \Delta t) \quad (7)$$

$$\Psi_{C2} = \Psi_{C2}(o, o, o, o, q_5 s^{1/2}, q_6 s^{1/2}, q_7 s^{-1/2}, q_8 s^{-1/2}, \Delta t) \quad (8)$$

Here 0 denotes zero.

In equations 7 and 8, mutual fusion of the cubic-form Ψ_{C1} and Ψ_{C2} creates Ψ_{C1+2}, as follows:

$$\Psi_{C1+2} = a^* a^* a^* a^* \Psi_{C1}(q_1 s^{1/2}, q_2 s^{1/2}, q_3 s^{-1/2}, q_4 s^{-1/2}, o, o, o, o, \Delta t) + a\,a\,a\,a\,\Psi_{C2}(o, o, o, o, q_5 s^{1/2}, q_6 s^{1/2}, q_7 s^{-1/2}, q_8 s^{-1/2}, \Delta t) = \Psi_{C1+2}(q_1 So, q_2 So, q_3 So, q_4 So, q_5 So, q_6 So, q_7 So, q_8 So, \Delta t)$$

(Ex = 47.6 MeV) (9)

This can be expressed with Schrödinger's equation as follows:

$$i\hbar \frac{\partial \Psi_{C1+2}}{\partial t} = \left\{ \sum_{j=1}^{8} H(qj) + \sum_{j \neq k}^{12} W(qj, qk) \right\} \Psi_{C1+2} \quad (10)$$

However, because Ψ_{C1+2} is in the collective-excitation energy state of nuclear physics, it is unstable and experiences transition in which it splits into its original state of Ψ_{T1} and Ψ_{T2} (alpha clusters), as shown in figure 5. That is to say, the ^{8}Be* degenerates to two ^{4}He nuclei. Ultimately, two stable (ground state) ^{4}He nuclei are produced.

$$\Psi_{C1+2} \rightarrow \Psi_{T1+2} + \Psi_{T3+4} = \Psi_{T1+2}(q_1 s^{1/2}, q_2 s^{1/2}, q_3 s^{-1/2}, q_4 s^{-1/2}, \Delta t) + \Psi_{3+4}(q_5 s^{1/2}, q_6 s^{1/2}, q_7 s^{-1/2}, q_8 s^{-1/2}, \Delta t)$$

(^{4}He, K_E = 23.8 MeV) (11)

Meanwhile, in the two-body DD reaction, the intermediate compound nucleus ^{4}He* (Ex = 23.8 MeV) is believed to change greatly from the tetrahedral structure, becoming as shown in Fig. 6. As a result, an n or p branch is truncated, and break-up to to an n + ^{3}He or p + t exit channel occurs.

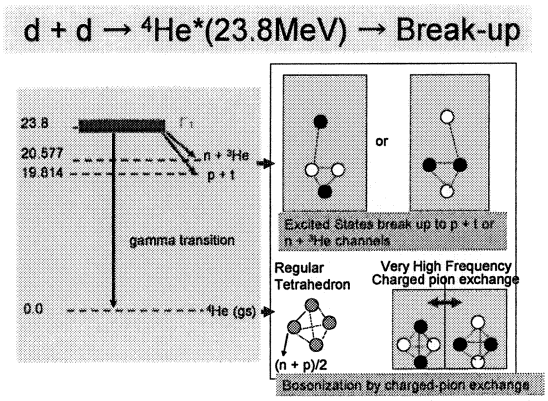

Figure 6. Break-up channels of 2D fusion; deformed excited states of ^{4}He*, compared with regular tetrahedron for ^{4}He ground state

References:

1) Iwamura, Y. et al: JJAP, 41(2002)1456

2) Kitamura, A. et al: this meeting

3) Kunitake, T., et al: Self Organization, NTS, 2004

4) Heisenberg W.: Physics and Philosophy, Harper & Row, New York, 1958

5) Brack, M.: Metal clusters and Magic Numbers, Scientific American, December 1997

6) Yabuuchi N. Cold Fusion, Issue No. 12, May 1995, USA

7) Yabuuchi N. Cold Fusion, Issue No. 17, May 1996, USA

8) Takahashi A, Yabuuchi N. Brief review on fusion rates of bononized condensates, Part I. Proceedings JCF7, Kagoshima, April 27-28, 2006

9) Takahashi A, Yabuuchi N. Brief review on fusion rates of bononized condensates, Part II. Proceedings JCF7, Kagoshima, April 27-28, 2006

10) Takahashi, A., Yabuuchi, N.: Comments on role of CaO-layer in Iwamura cold transmutation, ibid.

11) K. Yagi: Nuclear Physics, p.122, Asakura, Tokyo, 1971